

**THE 1918 AND 1957 VANCOUVER ISLAND EARTHQUAKES**

by

**JOHN FRANCIS CASSIDY**

B.Sc.(Honours Physics), The University of Victoria, 1982

**A THESIS SUBMITTED IN PARTIAL FULFILLMENT OF**

**THE REQUIREMENTS FOR THE DEGREE OF**

**MASTER OF SCIENCE**

in

**THE FACULTY OF GRADUATE STUDIES**

**Department of Geophysics and Astronomy**

We accept this thesis as conforming

to the required standard

**THE UNIVERSITY OF BRITISH COLUMBIA**

November 1986

©John Francis Cassidy, 1986

In presenting this thesis in partial fulfilment of the requirements for an advanced degree at the University of British Columbia, I agree that the Library shall make it freely available for reference and study. I further agree that permission for extensive copying of this thesis for scholarly purposes may be granted by the head of my department or by his or her representatives. It is understood that copying or publication of this thesis for financial gain shall not be allowed without my written permission.

Department of Geophysics and Astronomy

The University of British Columbia  
1956 Main Mall  
Vancouver, Canada  
V6T 1Y3

Date November 25, 1986

## ABSTRACT

The oceanic Juan de Fuca and Explorer plates are subducting beneath the continental America plate west of Vancouver Island. The Nootka fault zone, which separates these oceanic plates, experiences left-lateral shear due to the different rates of subduction for the Juan de Fuca (4 cm/yr) and the Explorer (<2 cm/yr) plates. Since 1918, six significant earthquakes ( $M = 5.3 - 7.2$ ) have occurred in the region where the projection of this fault zone intersects central Vancouver Island. In this study two of the largest events are examined; the 1918 ( $M_s \simeq 7$ ) and the 1957 ( $M_s \simeq 6$ ) earthquakes. Prior to this research, no comprehensive studies of these events had been carried out. A total of 46 seismograms from 24 stations worldwide were obtained for the 1918 earthquake, and 138 seismograms from 46 stations were obtained for the 1957 earthquake.

The preferred epicentre for the 1918 earthquake is  $49.47^\circ\text{N}$ ,  $126.24^\circ\text{W}$ , with an estimated uncertainty of  $\pm 30$  km. The preferred focal depth of 15 km indicates that this was a crustal earthquake. Magnitude estimates are  $M_s = 6.9 \pm 0.3$ ,  $m_b = 7.2 \pm 0.4$  and  $M_I = 7.0$ , in agreement with previous studies. Surface wave analysis suggests this is a predominantly strike-slip earthquake occurring along either a NNW or an ENE striking fault. A seismic moment of  $7.40 \times 10^{25}$  dyne-cm and a stress drop of 122 bars, indicative of an intraplate event, are estimated.

The preferred epicentre for the 1957 earthquake is  $49.65^\circ\text{N}$ ,  $127.02^\circ\text{W}$  with an uncertainty of  $\pm 20$  km. The estimated focal depth of 30 km suggests this event occurred in the subducting oceanic plate. Magnitude estimates are  $M_s = 5.9 \pm 0.2$ ,  $m_b = 6.3 \pm 0.3$  and  $M_I = 5.7$ . Surface wave and P-nodal analyses indicate that this is a predominantly strike-slip earthquake; either dextral along a NNW striking fault, or sinistral along a

ENE striking fault. The seismic moment is estimated to be  $8.14 \times 10^{24}$  dyne-cm, and the stress drop to be 36 bars, which is indicative of an interplate event.

The quality of these data does not allow for an unambiguous interpretation of these earthquakes in terms of seismotectonic models. However, the results of this study indicate that these earthquakes do not have normal or thrust mechanisms. The 1918 earthquake appears to be a crustal, intraplate event resulting indirectly from the complicated interaction of the Explorer, Juan de Fuca and America plates. The preferred epicentre, depth and stress drop for the 1957 earthquake are consistent with left-lateral motion between the Juan de Fuca and Explorer plates along the Nootka fault zone where it is being subducted beneath Vancouver Island. Uncertainties in the above parameters however, do not rule out the possibility of this being a crustal earthquake along a NW striking fault.

## TABLE OF CONTENTS

|   |     |
|---|-----|
| ABSTRACT . . . . .  | ii  |
| LIST OF TABLES . . . . .  | vi  |
| LIST OF FIGURES . . . . .                                       | vii |
| ACKNOWLEDGMENTS . . . . .                                       | x   |
| CHAPTER I INTRODUCTION . . . . .                                | 1   |
| 1.1 Tectonic setting . . . . .                                  | 1   |
| 1.2 Seismicity . . . . .  | 3   |
| 1.3 Seismotectonic models . . . . .                             | 7   |
| 1.4 Previous studies of the 1918 and 1957 earthquakes . . . . . | 9   |
| 1.5 Thesis outline . . . . .                                    | 15  |
| CHAPTER II DATA ACQUISITION AND ANALYSIS TECHNIQUES             | 17  |
| 2.1 Data collection . . . . .                                   | 17  |
| 2.2 Analysis techniques . . . . .                               | 19  |
| 2.2.1 Locating earthquakes . . . . .                            | 19  |
| i) Teleseismic techniques . . . . .                             | 19  |
| ii) Local techniques . . . . .                                  | 20  |
| 2.2.2 Magnitude determination . . . . .                         | 21  |
| 2.2.3 Focal mechanism studies . . . . .                         | 23  |
| i) P-nodal method . . . . .                                     | 23  |
| ii) Surface wave method . . . . .                               | 23  |
| CHAPTER III THE DECEMBER 16,1957 EARTHQUAKE - RESULTS           | 27  |
| 3.1 Introduction and intensity . . . . .                        | 27  |
| 3.2 Epicentre location . . . . .                                | 29  |
| 3.2.1 Teleseismic methods . . . . .                             | 29  |
| 3.2.2 Local methods . . . . .                                   | 35  |
| 3.2.3 Felt area information . . . . .                           | 41  |
| 3.2.4 Epicentre summary . . . . .                               | 42  |
| 3.3 Focal depth . . . . .                                       | 43  |
| 3.4 Magnitude . . . . .   | 44  |
| 3.5 Source mechanism . . . . .                                  | 46  |
| 3.5.1 P-nodal technique . . . . .                               | 46  |
| 3.5.2 Surface wave analysis . . . . .                           | 49  |
| 3.6 Seismic moment, stress drop and aftershocks . . . . .       | 63  |

|              |   |     |
|--------------|---|-----|
| CHAPTER IV   | THE DECEMBER 6, 1918 EARTHQUAKE – RESULTS             | 65  |
| 4.1          | Introduction and intensity . . . . .                  | 65  |
| 4.2          | Epicentre location . . . . .                          | 68  |
| 4.3          | Focal depth . . . . .                                 | 73  |
| 4.4          | Magnitude . . . . .                                   | 75  |
| 4.5          | Source mechanism . . . . .                            | 76  |
| 4.6          | Seismic moment, stress drop and aftershocks . . . . . | 87  |
| CHAPTER V    | SUMMARY AND CONCLUSIONS . . . . .                     | 89  |
| BIBLIOGRAPHY | . . . . .   | 96  |
| APPENDIX A   | Regional earth models . . . . .                       | 100 |
| APPENDIX B   | Data for the December 16, 1957 earthquake . . . . .   | 101 |
| APPENDIX C   | Data for the December 6, 1918 earthquake . . . . .    | 127 |

## LIST OF TABLES

|      |   |    |
|------|---|----|
| I.   | Significant central Vancouver Island earthquakes . . . . .    | 5  |
| II.  | Results of previous studies of the 1918 earthquake . . . . .  | 10 |
| III. | Results of previous studies of the 1957 earthquake . . . . .  | 13 |
| IV.  | Epicentre estimates for the 1957 earthquake . . . . .         | 30 |
| V.   | Local P and S arrival times for the 1957 earthquake . . . . . | 37 |
| VI.  | Epicentre estimates for the 1918 earthquake . . . . .         | 69 |

## LIST OF FIGURES

|     |  |    |
|-----|--|----|
| 1.  | The tectonic setting of western North America . . . . .  | 2  |
| 2.  | Seismicity of southwestern British Columbia . . . . .  | 4  |
| 3.  | Earthquakes of central Vancouver Island . . . . .  | 6  |
| 4.  | Pressure axes of central Vancouver Island earthquakes . . . . .  | 7  |
| 5.  | Previous epicentre estimates for the December 6, 1918 earthquake . . . . .   | 11 |
| 6.  | Previous epicentre estimates for the December 16, 1957 earthquake . . . . .  | 14 |
| 7.  | P-nodal estimates for the 1957 earthquake . . . . .  | 15 |
| 8.  | Isoseismal map for the 1957 earthquake . . . . .   | 28 |
| 9.  | Teleseismic epicentre estimates for the 1957 earthquake . . . . .  | 31 |
| 10. | Stations considered for the 1957 local epicentre study . . . . .   | 36 |
| 11. | Local epicentre estimates for the 1957 earthquake . . . . .  | 38 |
| 12. | Depth studies of the 1957 earthquake . . . . .   | 44 |
| 13. | P-nodal solutions for the 1957 earthquake . . . . .  | 48 |
| 14. | An example of group velocity dispersion curves and spectral<br>amplitude plots for the 1957 earthquake . . . . .                                 | 50 |
| 15. | Best fit surface wave mechanism for the 1957 earthquake . . . . .  | 52 |
| 16. | Observed and theoretical Love wave radiation patterns of the best fit<br>surface wave mechanism for the 1957 earthquake . . . . .                | 54 |
| 17. | Observed and theoretical horizontal Rayleigh wave radiation patterns<br>of the best fit surface wave mechanism for the 1957 earthquake . . . . . | 55 |
| 18. | Observed and theoretical vertical Rayleigh wave radiation patterns<br>of the best fit surface wave mechanism for the 1957 earthquake . . . . .   | 56 |

|     |  |    |
|-----|--|----|
| 19. | Observed and theoretical Love and Rayleigh wave radiation patterns<br>of the top scoring P-nodal solution for the 1957 earthquake . . . . .        | 59 |
| 20. | Observed and theoretical Love and Rayleigh wave radiation patterns of<br>the alternate P-nodal solution (Figure 13b) for the 1957 earthquake . . . | 60 |
| 21. | Observed and theoretical Love and Rayleigh wave radiation patterns of<br>the alternate P-nodal solution (Figure 13c) for the 1957 earthquake . . . | 61 |
| 22. | Comparison of the 1957 P-nodal and surface wave solutions . . . . .  | 62 |
| 23. | Isoseismal map for the December 6, 1918 earthquake . . . . .   | 66 |
| 24. | Epicentre estimates for the 1918 earthquake . . . . .  | 70 |
| 25. | Depth studies of the 1918 earthquake . . . . .   | 74 |
| 26. | “Best” fit surface wave mechanism for the 1918 earthquake . . . . .  | 78 |
| 27. | Observed and theoretical Love and Rayleigh wave radiation patterns of<br>the “best” fit surface wave mechanism for the 1918 earthquake . . . . .   | 79 |
| 28. | Example of the thrust and normal mechanisms considered<br>for the 1918 earthquake . . . . .  | 81 |
| 29. | Observed and theoretical Love and Rayleigh wave radiation patterns of<br>the thrust and normal mechanisms for the 1918 earthquake . . . . .        | 82 |
| 30. | Preferred mechanism for the 1918 earthquake . . . . .  | 83 |
| 31. | Observed and theoretical Love wave radiation patterns of the<br>preferred mechanism for the 1918 earthquake . . . . .                              | 84 |
| 32. | Observed and theoretical horizontal Rayleigh wave radiation patterns<br>of the preferred mechanism for the 1918 earthquake . . . . .               | 85 |
| 33. | Observed and theoretical vertical Rayleigh wave radiation patterns<br>of the preferred mechanism for the 1918 earthquake . . . . .                 | 86 |

34. Cross-section of the Juan de Fuca/Explorer subduction zone  
showing the depth of the 1918 and 1957 earthquakes . . . . . 90

## ACKNOWLEDGEMENTS

*For my grandparents: Alice Hardsand, George Hardsand, Ethyl Cassidy and Joseph Cassidy, with thanks.*

I would like to thank my supervisor, Dr. Robert Ellis for his constant support and guidance. His comments and suggestions have contributed immensely to this thesis. I am also greatly indebted to Dr. Garry Rogers who provided many of the seismograms which were used in this study. In addition, I thank Dr. Rogers for his enthusiasm and his many interesting ideas which have enhanced this research. A special thanks go to those who read my thesis and improved it: Dr. Ellis who removed countless commas and brackets from this manuscript, Dr. Ron Clowes and Dr. Garry Rogers.

This research would not have been possible without the help of Lydia and Susan who typed and posted hundreds of letters requesting data. Thanks also go to my fellow students and the faculty and staff of the Department of Geophysics and Astronomy for making this such an enjoyable place to study. Last but certainly not least, I would like to thank my family. My parents have always supported and encouraged my endeavors, and my wife Lynn has provided an endless supply of love and inspiration.

Financial support for this study was provided by Research Agreements 25/03/85 and 19/03/86 from the Department of Energy, Mines and Resources.

## CHAPTER I

## INTRODUCTION

## 1.1 Tectonic Setting

The major tectonic boundary separating the Pacific and America lithospheric plates lies near the west coast of North America. The San Andreas and Queen Charlotte transform faults dominate this boundary. However, in the region between northern Vancouver Island and northern California, the oceanic Juan de Fuca and Explorer plates lie between the major plates and are being subducted beneath North America (Figure 1).

A study by Riddihough (1977) suggests that the Juan de Fuca and Explorer plates are interacting independently with the continental America plate. Present-day convergence is estimated to be approximately 4 cm/yr in a northeasterly direction for the Juan de Fuca plate and less than 2 cm/yr in a more northerly direction for the Explorer plate (Riddihough, 1977, 1984). It is possible (Riddihough, 1984) that the Explorer plate has stopped subducting in an absolute sense, and is simply being over-ridden by the southwestward moving America plate. The Nootka fault zone separates these two oceanic plates (Hyndman *et al.*, 1979). Its projection intersects the America plate near central Vancouver Island.

A series of spreading ridges and fracture zones off the west coast of Vancouver Island outline the boundary between the Explorer/Juan de Fuca plates and the Pacific plate. Complex triple junctions at the northern end of the Explorer plate and the southern end of the Juan de Fuca plate mark the ends of this subduction zone.

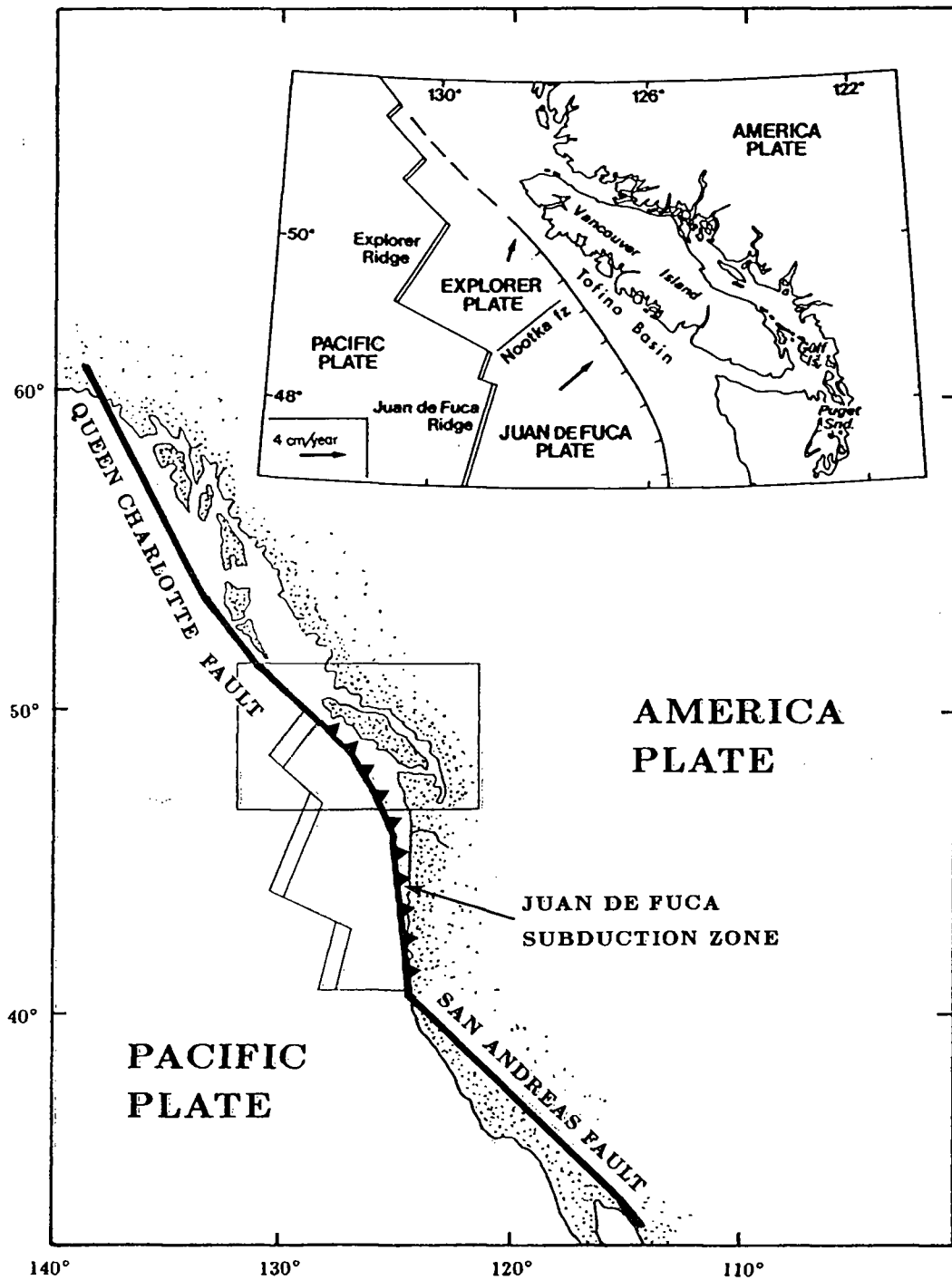


Figure 1. Plate tectonic setting of western North America. The Juan de Fuca subduction zone lies between the large Queen Charlotte and San Andreas transform faults (adapted from Rogers, 1983). Insert illustrates details of the Explorer/Juan de Fuca – America plate interactions off the west coast of Vancouver Island. Arrows indicate direction and rate of subduction (adapted from Spence *et al.*, 1985).

## 1.2 Seismicity

The seismicity of the Explorer/Juan de Fuca subduction zone is not typical of most subduction zones. It lacks a deep ( $> 70$  km) Benioff zone of earthquakes (Rogers, 1983) and there appears to be no shallow thrust seismicity of the type usually found in active subduction zones (Heaton and Kanamori, 1984). There is no record of a major shallow thrust event occurring during historical time ( $\approx 150$  years) which has ruptured the approximately 500 km long subduction zone (Washington Public Power Supply System, 1983). In a recent paper, Heaton and Kanamori (1984) have shown that this region shares many features with other subduction zones which have experienced large thrust events and suggest that this region may represent a major seismic gap.

Seismicity of the Explorer and northern Juan de Fuca subduction zone is shown in Figure 2. The majority of the earthquakes occur near transform faults and fracture zones in the deep ocean to the west of Vancouver Island. Other features visible in Figure 2 are the concentration of continental earthquakes between  $47^{\circ}\text{N}$  and  $49^{\circ}\text{N}$ , and the distinct paucity of events on Vancouver Island north of  $50^{\circ}$  latitude. The Nootka fault zone can also be clearly seen; it is the only concentration of seismicity leading from the offshore earthquakes towards Vancouver Island.

Since 1918 six significant ( $M= 5.3-7.2$ ) earthquakes (see Table I) have occurred in the region where the projection of this fault zone intersects central Vancouver Island. The location, magnitude and focal mechanisms of these events are illustrated in Figure 3. In all cases the previous analyses and interpretations suggest they are crustal events.

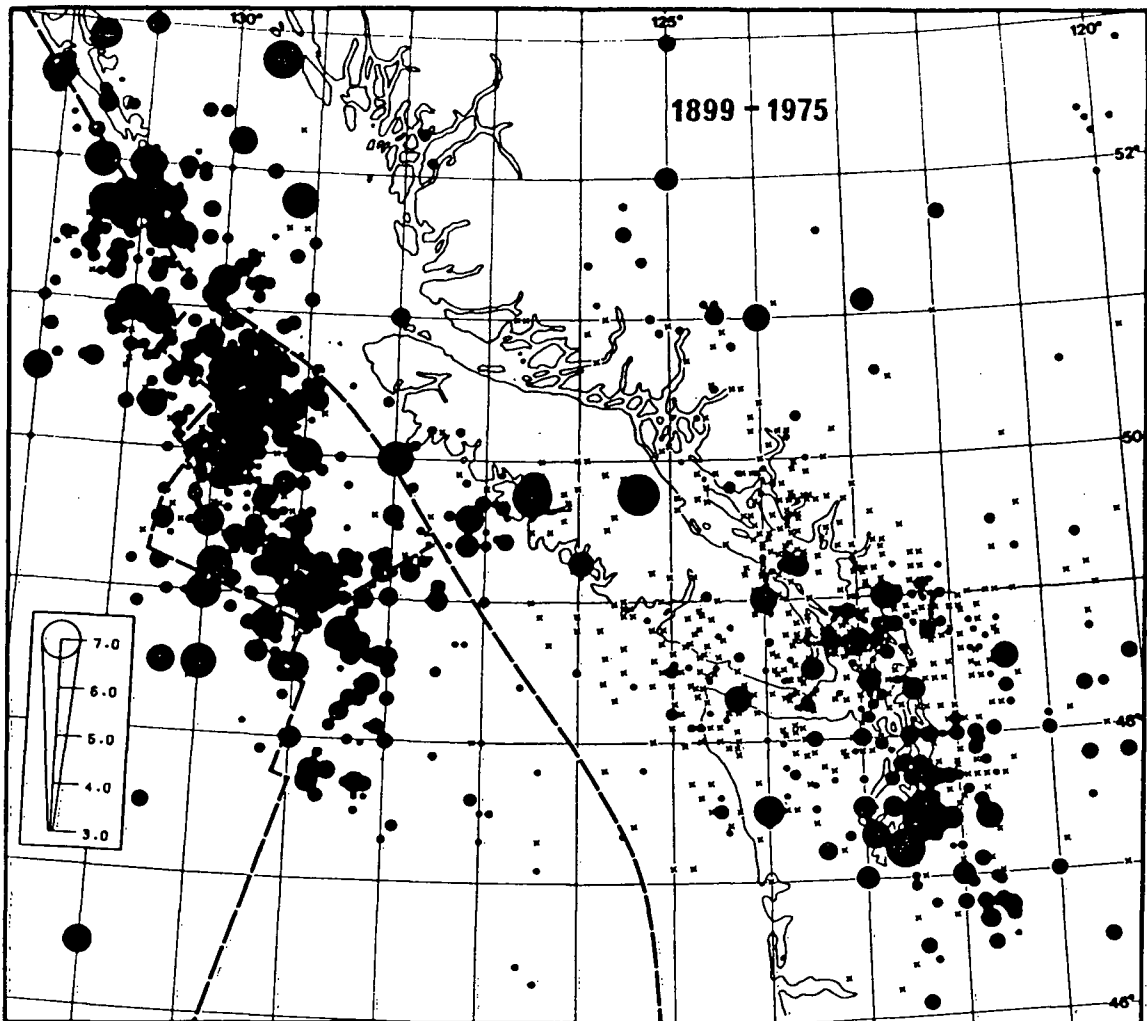


**Figure 2.** Seismicity of southwestern British Columbia (1899–1975). The circle diameters are proportional to the earthquake magnitude. Earthquakes of magnitude less than 3.0 are marked by ‘x’. Note that uncertainties in the epicentres of offshore events may approach 50 km (from Keen and Hyndman, 1979).

The 1946, 1957, 1972 and 1986 events, those closest to the Nootka fault zone, appear to be predominantly strike-slip and have a similar orientation of nodal planes. For each earthquake the motion is dextral on a northwest striking plane, or sinistral on a northeast striking plane. The former was chosen as the preferred fault-plane for

**Table I Significant central Vancouver Island earthquakes**

| DATE          | LOCATION              | DEPTH                | MAGNITUDE                | REFERENCE                          |
|---------------|-----------------------|----------------------|--------------------------|------------------------------------|
| Dec. 6, 1918  | 49.62° N<br>125.92° W | Shallow <sup>1</sup> | $M_s = 7.0$              | Rogers (1983)                      |
| June 23, 1946 | 49.76° N<br>125.34° W | 30 km                | $M_s = 7.2$              | Rogers and<br>Hasegawa (1978)      |
| Dec. 16, 1957 | 49.82° N<br>126.48° W | 0 km                 | $M_s = 6.0$ <sup>2</sup> | Tobin and<br>Sykes (1968)          |
| July 5, 1972  | 49.5° N<br>127.2° W   | 25 km                | $m_b = 5.7$              | Rogers (1976)                      |
| Mar. 31, 1975 | 49.3° N<br>126.0° W   | 18 km                | $M_L = 5.4$              | Rogers (1983)                      |
| June 16, 1986 | 49.4° N<br>127.0° W   | 30 km                | $M_L = 5.3$              | Rogers (personal<br>communication) |

<sup>1</sup> Gutenberg and Richter (1954).

<sup>2</sup> Bureau Central International Séismologique (BCIS) 1957 bulletin.

the 1946 earthquake (see Rogers and Hasegawa, 1978) based on intensity data, water disturbances, calculated ground deformation, and the proximity of the major northwest striking Beaufort fault. Analysis of geodetic data in the epicentral region of the 1946 earthquake (Slawson and Savage, 1979) supports this interpretation. The pressure axes of the 1946, 1957 and 1972 earthquakes, as obtained from P-nodal studies, are nearly horizontal and orientated slightly east of north (Figure 4). The 1975 earthquake, which

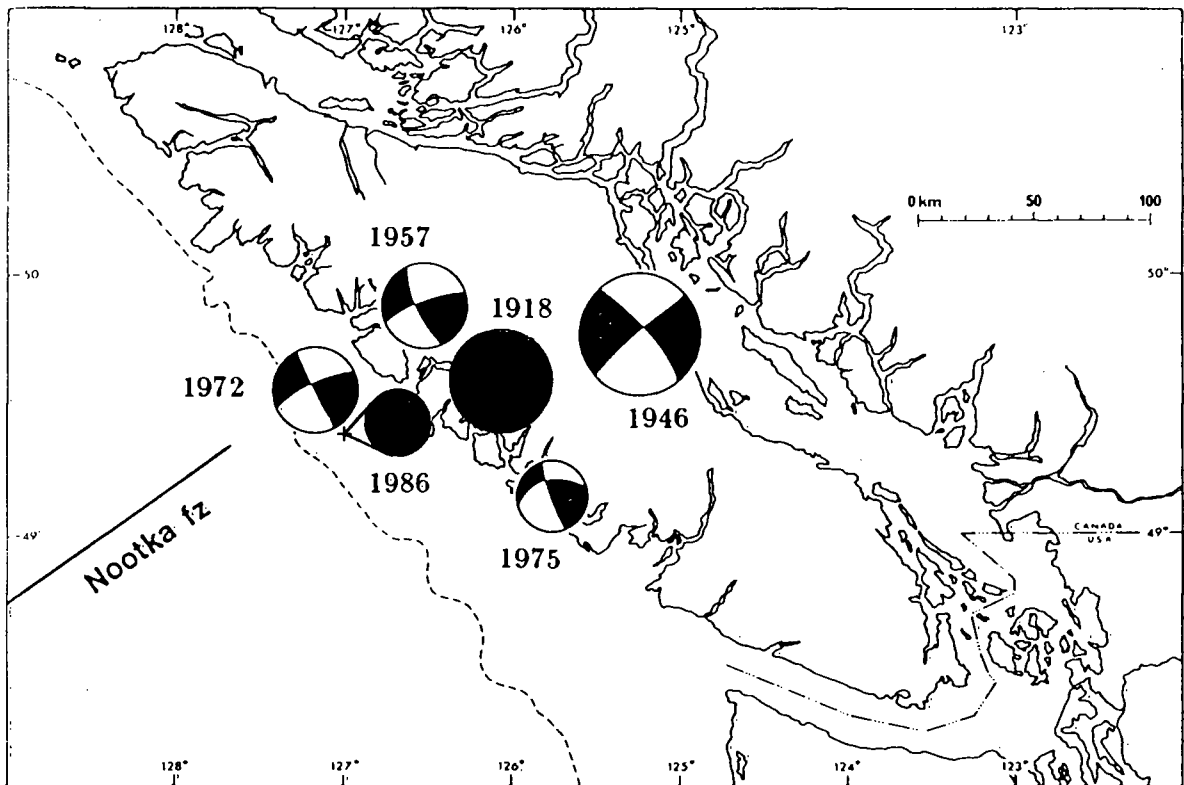


**Figure 3.** Location, magnitude and focal mechanisms for the largest Vancouver Island earthquakes. Circle radius is proportional to magnitude. Solid black circles for the 1918 and 1986 events indicate that no previous estimates for the focal mechanism exist. Dotted line marks the continental margin (adapted from Rogers, 1979).

occurred significantly south of the Nootka fault zone projection, has a pressure axis orientated in a more northeasterly direction (Rogers, 1979).

Although these large earthquakes have occurred near the projection of the Nootka fault zone, it is not obvious how they are related to this fault. Rogers (1983) points out that the continental earthquakes are of a different nature than those occurring offshore: they are larger; there are fewer of them; and they have very few and small aftershocks. He suggests that the central Vancouver Island earthquakes are more characteristic of intraplate events than interplate events.

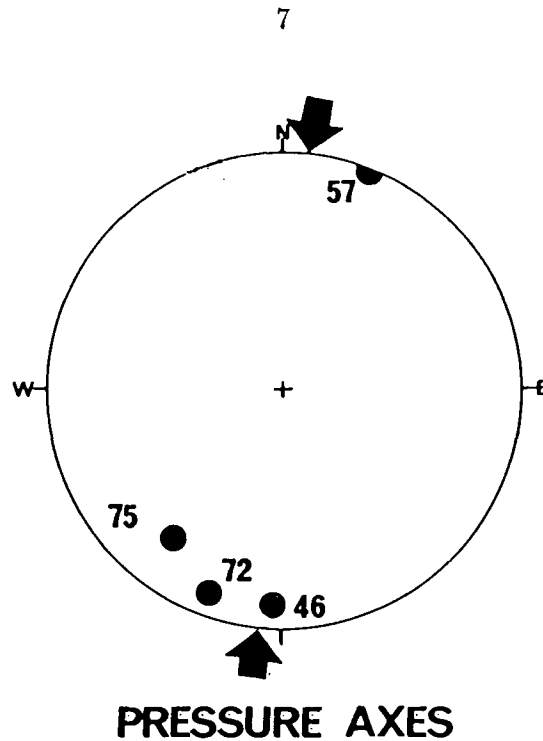


**Figure 4.** Orientation of the pressure axes for the largest central Vancouver Island earthquakes. Symbols are plotted where the axes intersect the lower half of the focal sphere. No previous estimate for the P-axis of the 1918 event exists. Arrows indicate the Explorer–America plate interaction suggested by Riddihough (1977). Numbers indicate the year of occurrence (adapted from Rogers, 1979).

### 1.3 Seismotectonic Models

Rogers (1979) proposed two tectonic models which satisfy the observed characteristics of earthquakes occurring in the continental crust near central Vancouver Island.

1) The movement of the Explorer plate, which Riddihough (1977) suggests has recently (between 1.5 Ma and 0.5 Ma) changed to a northerly direction, is interacting with the America plate at a very oblique angle (see Figure 1). In many regions (e.g. Phillipine Sea, Java) oblique convergence has resulted in strike-slip faulting parallel to the strike of the plate margin. This faulting results from the component of convergence

parallel to the margin, and is likely to occur when the angle of plate interaction becomes more oblique than  $45^\circ$  (Fitch, 1972). The reduced component of convergence perpendicular to the margin may cause normal subduction to temporarily cease until sufficient stress accumulates to produce rupture along the dipping plane. This would result in intense regional compression (Rogers, 1979).

If this type of subduction is occurring at the Explorer–America boundary, it could explain the nearly north–south pressure axes for the large central Vancouver Island events and the predominantly strike-slip faults trending northwest (parallel to the plate margin). This model also favours the intraplate interpretation of these earthquakes, as they would result from intense north–south compression of the continental lithosphere. The distinct lack of seismicity on northern Vancouver Island is expected because, as the northern triple junction is approached, the plate becomes thinner (it is subducting soon after its creation (Riddihough, 1977)) and loses strength. It is assumed that convergence south of the Nootka fault zone is subduction, presently occurring in an aseismic manner (Rogers, 1979).

2) The second model proposes that subduction on either side of the Nootka fault zone is proceeding in an aseismic manner. Differential motion between the Juan de Fuca and Explorer plates (see Figure 1) along the northeast trending Nootka fault zone produces a shear in the overlying continental lithosphere. This results in left–lateral, predominantly strike–slip earthquakes occurring along a northeast trending fault plane. However, this model does not explain the observed north–south compression. Rogers (1979) questions why, if the differential rate of subduction across the Nootka fault zone can produce the large observed events, no typical subduction (thrust) events have been observed on either side of the Nootka fault zone. Recent studies and comparisons with

other subduction zones (Rogers, personal communication) suggest that this may be due to a large recurrence interval (100 – 1300 years) for thrust events along this margin. A thorough study of the 1918 and 1957 Vancouver Island earthquakes, which have not previously been investigated in detail, may provide further information on possible seismotectonic models for this region.

#### 1.4 Previous Studies of the 1918 and 1957 Earthquakes

Of the four largest central Vancouver Island earthquakes which may provide information on the seismotectonics of this region, only the 1946 ( $M_s = 7.2$ ) and 1972 ( $m_b = 5.7$ ) events have been studied in detail (Rogers and Hasegawa (1978), Rogers (1976) respectively). Comprehensive studies of the 1918 ( $M_s \simeq 7$ ) and 1957 ( $M_s \simeq 6$ ) events have not been carried out, although various researchers have looked at some aspects of these earthquakes. Previous studies of these events will be summarized at this point.

*1918* – A summary of the results of previous studies of this earthquake is given in Table II. Previous epicentre estimates are illustrated in Figure 5. The International Seismological Summary (ISS) lists first arrivals from 46 stations for this event, of which 9 have travel-time residuals (based on their epicentre) greater than one minute. The ISS epicentre is likely the least accurate (in 1918 all calculations were done by hand, and only a few stations at various azimuths and distances were used to determine epicentres – see Rogers, 1983, p.16). Denison (1919), using arrival times from Victoria, Ottawa and Saskatoon estimated this event to be on the continental slope, 60 km west of Estevan point (Figure 5). This location was later revised by the Meteorological Service of Canada (1919) using 5 stations and the method of stereographic projection (see Table II).

Table II Results of previous studies of the 1918 earthquake

| SOLUTION                     | ORIGIN TIME | LOCATION             | DEPTH                 | MAGNITUDE                    |
|------------------------------|-------------|----------------------|-----------------------|------------------------------|
| ISS <sup>1</sup>             | 08 41 03.   | 49.0°N<br>124.0°W    | —                     | —                            |
| Denison (1919)               | 08 40 57.   | 49.5°N<br>127.33°W   | —                     | —                            |
| M.S.C. <sup>2</sup>          | —           | 49.53° N<br>127.0°W  | —                     | —                            |
| Gutenberg and Richter (1954) | 08 41 05.   | 49.75° N<br>126.5°W  | shallow<br>( < 60 km) | $M_s^G = 7.0$                |
| Rogers (1983)                | 08 41 05.8  | 49.62° N<br>125.92°W | —                     | $M_I = 7.0$                  |
| Abe (1981)                   | —           | —                    | —                     | $M_s^G = 6.8$<br>$m_b = 7.1$ |

<sup>1</sup> ISS 1918 bulletin.

<sup>2</sup> Meteorological Service of Canada (M.S.C.), 1919.

Gutenberg and Richter (1954) located this earthquake (Figure 5) and classified it as a shallow event (< 60 km). They estimated the magnitude to be  $M_s^G = 7.0$ , where  $M_s^G$  represents the surface wave magnitude derived by Gutenberg (1945) (see section 2.2.2). However, it is unclear how many stations were used. Abe (1981), in re-evaluating Gutenberg and Richter's magnitudes, estimated this event to be  $M_s^G = 6.8$  and  $m_b =$

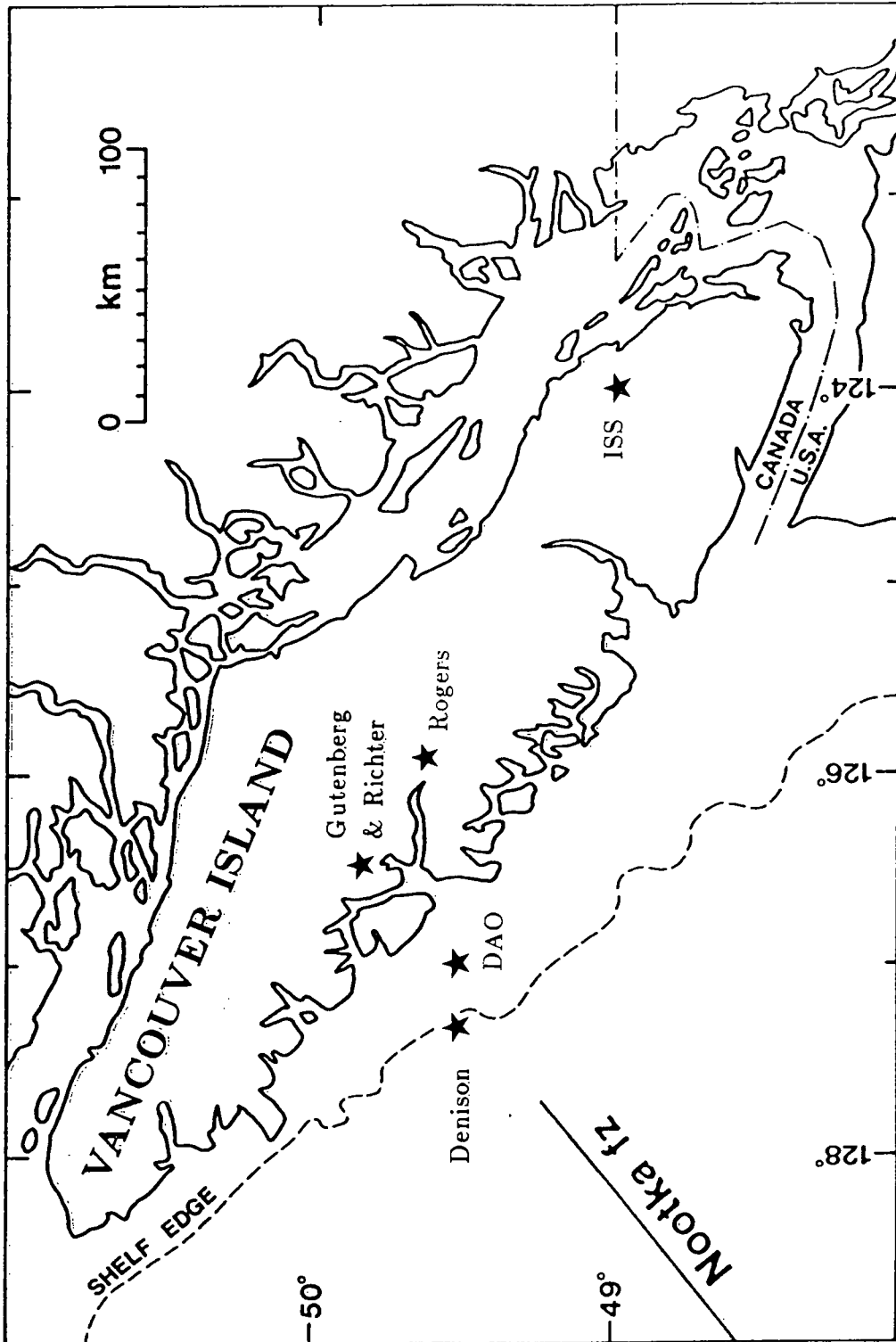


Figure 5. Location of epicentres (discussed in text) for the December 6, 1918 earthquake (adapted from Rogers, 1983).

7.1. The most recent study of this event was by Rogers (1983). Using ISS arrival times he estimated the epicentre to be  $49.62^{\circ}\text{N}$  and  $125.92^{\circ}\text{W}$ , with an uncertainty of  $\pm 50$  km. Using felt area information he estimated a magnitude of  $M_I = 7.0$ , where  $M_I$  represents the intensity or felt area magnitude of Topozada (1975) (see section 2.2.2), in agreement with Gutenberg and Richter's estimate.

To date there have been no estimates of the focal mechanism for this earthquake. Several aftershocks were reported for this event, the largest of which was estimated to be magnitude 4.5 (Rogers, 1979) based on felt reports.

1957 – This earthquake, with a much larger data set than that of the 1918 earthquake has previous estimates of epicentre, depth and focal mechanism. The results of previous studies are summarized in Table III. Epicentre estimates are plotted in Figure 6.

In addition to the epicentre estimates of the ISS (which lists first arrivals from 97 stations for this event) and the Bureau Central International Séismologique (BCIS) (which lists first arrivals from 74 stations for this event), two other studies have been made. Milne and Lucas (1961), using P and S arrivals from local stations only, placed the epicentre at  $49.4^{\circ}\text{N}$  and  $127.2^{\circ}\text{W}$ , about 40 km southwest of Nootka Island (Figure 6). Tobin and Sykes (1968) located this event using teleseismic techniques, as a part of their study of the seismicity and tectonics of the northwest Pacific ocean. They used Jeffreys-Bullen (1940, 1958) travel-time tables and first arriving phases from 105 stations. Their estimate of  $49.82^{\circ}\text{N}$ ,  $126.48^{\circ}\text{W}$  and 0 km depth is given their highest quality rating. The standard error was estimated to be less than 20 km for this epicentre. However, the authors point out that the “accuracy” of the location is more difficult to estimate due to possible azimuthal bias and uncertainty in travel-times in this region.

Table III Results of previous studies of the 1957 earthquake

| SOLUTION                               | ORIGIN TIME | LOCATION             | DEPTH | MAGNITUDE                                 |
|--|-------------|----------------------|-------|---|
| ISS <sup>1</sup>                       | 17 27 51.   | 49.82°N<br>126.59°W  | 12 km | —   |
| BCIS <sup>2</sup>                      | 17 27 47.   | 50.°N<br>127.°W      | —     | 6.3 Tacubaya, 6 Matushiro<br>5 2/3 Moscow |
| Milne and<br>Lucas (1961) <sup>3</sup> | 17 27 46.9  | 49.4° N<br>127.2°W   | —     | —   |
| Tobin and<br>Sykes (1968)              | 17 27 48.7  | 49.82° N<br>126.48°W | 0 km  | —   |

<sup>1</sup> ISS December, 1957 bulletin.

<sup>2</sup> BCIS December, 1957 bulletin.

<sup>3</sup> This study involved local rather than teleseismic data.

The magnitude of this event has not been well defined. The only estimates are those listed in the 1957 BCIS bulletin: 6.3 at Tacubaya; 6 at Matushiro; and 5 2/3 at Moscow.

Rogers (1979) conducted a P-nodal study of this earthquake. Figure 7 illustrates three source mechanisms which satisfy the observed data. The top scoring solution (Figure 7 – left) is predominantly strike-slip and similar to the mechanism of the nearby 1972 event. However, this solution is poorly constrained due to a lack of data from west of the epicentre.

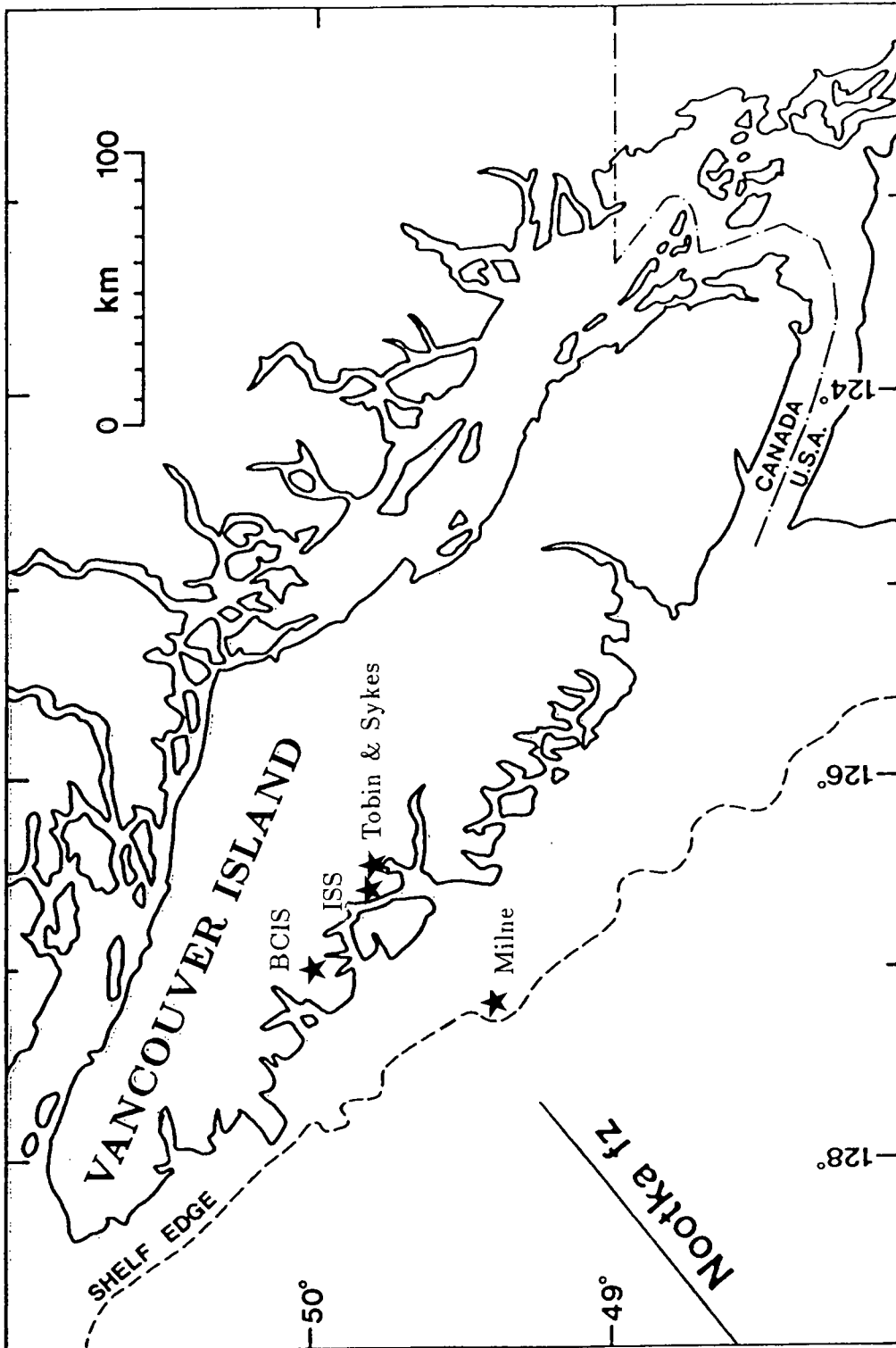


**Figure 6.** Location of epicentres (discussed in text) for the December 16, 1957 earthquake (adapted from Rogers, 1983).

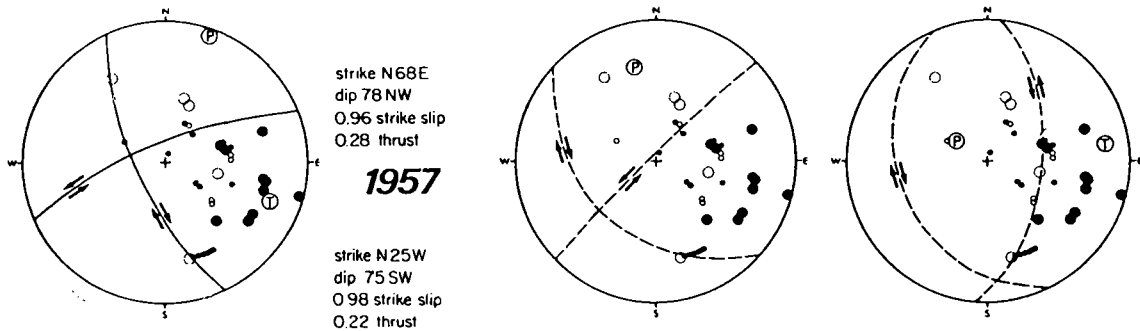


**Figure 7.** Top scoring P-nodal solution (left) and two alternate but lower scoring solutions for the December 16, 1957 Vancouver Island earthquake. Lower half of focal sphere is shown; solid circles are compressional arrivals, open circles are dilatational arrivals, P is the pressure axis and T is the tension axis (from Rogers, 1979).

Only one aftershock was recorded for this earthquake. Its magnitude was estimated to be  $M_L = 2.8$  (Milne, unpublished worksheets).

### 1.5 Thesis Outline

A comprehensive study of the 1918 ( $M_s = 7$ ) and 1957 ( $M_s = 6$ ) Vancouver Island earthquakes was undertaken. The results are compared with previous studies of larger events in this region in order to gain a better understanding of the seismic potential and seismotectonics of central Vancouver Island.

For each earthquake the following studies were made:

- (1) The epicentre was redetermined using teleseismic techniques. In addition, for the 1957 event a local technique was applied. Stability of the solutions was examined by considering various earth models, the effect of station corrections, azimuthal

distribution of stations, "late" picks due to low gain instruments, and the effect of upper mantle structure.

- (2) The depth was estimated using surface wave radiation patterns.
- (3) Felt intensities were examined.
- (4) Body wave, surface wave and felt area magnitudes were determined.
- (5) Source characteristics were determined using both body waves and surface waves. The P-nodal program of Wickens and Hodgson (1967) was used to determine focal mechanisms using first arrivals. The program suite of Herrmann (1978) was used to generate theoretical radiation patterns of Rayleigh and Love waves which were compared to observed radiation patterns. The trial mechanism was varied until a "best" fit was obtained. This analysis provided information on the focal mechanism, depth and seismic moment of these events.
- (6) Aftershock patterns were studied and, when possible, magnitudes of aftershocks were determined.

## CHAPTER II

### DATA COLLECTION AND ANALYSIS TECHNIQUES

#### 2.1 Data Collection

To obtain data for surface wave analysis, written requests were made to stations known to be operating relatively long period instruments in 1918 and 1957. Useful sources of information were Wood (1921) who provides a list of seismograph stations of the world as of 1920 (including a description of instruments in most cases) and Charlier and Van Gils (1953), a similar list for the early 1950's. In addition, seismograms and station bulletins for both the 1918 and 1957 events were purchased from the World Data Centre A - Historical Seismogram Filming Project. As well, records from the Canadian network, the Jesuit network, the United States Coast and Geodetic Survey (U.S.C.G.S.) and the World Data Centre A were provided by Dr. Garry Rogers of the Pacific Geoscience Centre. The goal was to obtain as many records as possible in order to conduct a comprehensive study of these earthquakes.

Seismograms for the 1918 event were requested from a total of 106 stations worldwide, of which only 13 provided records. Many stations did not record this event due to low-gain instruments, others were not operating due to the First World War, and in some cases records had been lost or destroyed. Records from these stations, together with those from 11 stations provided by Dr. Rogers, resulted in a total data set of 46 seismograms from 24 stations for the 1918 earthquake.

Records of the 1957 earthquake were requested from a total of 178 stations, of which 35 provided seismograms. Records from 11 North American stations were provided by Dr. Rogers resulting in a data set of 138 seismograms from 46 stations for this event.

Most of these records were useful for at least one aspect of this study. However, there are many problems encountered when dealing with historical seismograms:

- (i) Timing was often a problem, especially for the 1918 event. Some seismograms had no time indication at all, in some cases there was considerable clock drift and for some records time corrections were not indicated. Drum speeds were typically 15 mm/min and in some cases as low as 8 mm/min. This resulted in uncertainties of 2 – 4 seconds in picking arrival times.
- (ii) For the 1918 event the orientation of the instruments were not indicated in most cases, leading to uncertainty in the polarity of the observed waves.
- (iii) Many records had clipped wave peaks or sections too faint to allow them to be used in surface wave studies.
- (iv) The major problem however, was the lack of calibration data. Magnification, seismometer period, and damping information were not included with most seismograms. In some cases where this information was included, the values were obviously incorrect. For many stations, calibration data were obtained from the previously mentioned directories of seismograph stations. For both earthquakes however, there is a time span of 2–4 years between the earthquake's occurrence and the time when the instrument calibration information was collected. Using information from Wood (1921) or Charlier and Van Gils (1953) therefore involves the assumption that the instrument constants did not change during this time. If damping ratio information could not be obtained, critical damping was assumed. If only the amplitude response was available, the phase response was calculated by applying the Hilbert transform routine of Bolduc *et al.* (1972). For electromagnetic seismometers, response was calculated using the equation of Hagiwara (1958). Coupling between

the seismometer and the galvanometer was assumed to be zero unless otherwise indicated.

## 2.2 Analysis Techniques

### 2.2.1 Locating Earthquakes

Two methods of locating earthquakes are the teleseismic technique, using arrival times from stations 1000 km or more from the epicentre, and the local or regional technique, using arrival times from stations within 1000 km.

The local technique requires a regional earth model as body waves have only traversed the rather inhomogeneous crust and upper mantle. For teleseismic methods however, these waves have penetrated deep into the Earth, allowing an "average" earth model to be employed. For each method, station corrections, which compensate for the effect of geological structure beneath the station, should be applied.

i) *Teleseismic* – The program used for teleseismic location was EPDET, the iterative least-squares program of Weichert and Newton (1970) which uses the first arriving phases only. A trial epicentre and origin time is input. For each station a theoretical arrival time is obtained from a standard earth model and subtracted from the observed arrival time. The sum of squares of these residuals are then minimized in successive iterations. Corrections to the initial epicentre and origin time are obtained from the equation of conditions (Weichert and Newton, 1970).

For a fixed depth these are:

$$t + x \cos \alpha_j \frac{\partial T}{\partial \Delta_j} - y \sin \alpha_j \frac{\partial T}{\partial \Delta_j} = \delta T_j$$

where,  $t, x, y$  are the corrections to origin time, co-latitude and longitude respectively;  $\Delta_j$ ,  $\alpha_j$ , and  $\delta T_j$  are the epicentral distance, the azimuth and the travel-time residual respectively of the  $j^{\text{th}}$  station.

$\delta T_j$  is given by:

$$\delta T_j = A_j - H - T_j - C_j$$

where  $A_j$  is the arrival time at the  $j^{\text{th}}$  station,  $T_j$  is the travel-time to the  $j^{\text{th}}$  station,  $H$  is the origin time of the earthquake, and  $C_j$  is a station correction for the  $j^{\text{th}}$  station.  $T_j$  and  $\partial T/\partial \Delta_j$  are estimated from travel-time tables for P if  $0^\circ < \Delta_j < 110^\circ$  and from PKP if  $110^\circ < \Delta_j < 180^\circ$ .

Stations having a residual greater than 60 seconds are rejected before iterations begin. Stations are then successively culled at three different rejection levels, typically residuals greater than 10.0 sec, 6.0 sec and 4.0 sec.

Earth models considered were Jeffreys–Bullen (1958), Herrin (1968) and Dziewon-ski and Anderson (1981). Station corrections applied were those of Veith (1975) and Dziewon-ski and Anderson (1983).

ii) *Local Techniques* – In this study two programs for locating events using the “local” technique were considered. They are HYPOELLIPSE (Lahr, 1984) and FASTHYPO (Herrmann, 1979). Both are similar to EPDET in that the RMS error of observed – theoretical travel-times are minimized. Both programs use P and S phases and allow weights to be assigned to each arrival. These programs determine depth as well as latitude and longitude, provided at least four arrival times are used. HYPOELLIPSE has the advantage of allowing the location of an event to be fixed; this permits station corrections to be generated using recent events in the region of study.

A variety of earth models were used with these programs including the Canadian Standard model (Stevens *et al.*, 1972), the Vancouver Island–Puget Sound model (Rogers, 1983), and the model of McMechan and Spence (1983) with no low velocity zone. These are listed in Appendix A.

### 2.2.2 Magnitude Determination

There are a number of magnitude scales in use today to estimate the “size” of an earthquake. One complication which arises when dealing with historical earthquakes is that magnitude scales have changed over the years as instrumentation has changed.

The magnitude scales used in this study are  $m_b$ , the broad-band body wave magnitude of Gutenberg and Richter (1956);  $M_s$ , the surface wave magnitude of Vanek *et al.* (1962);  $M_s^G$ , the original surface wave magnitude of Gutenberg (1945) which was extensively used for studies of early earthquakes by Gutenberg and Richter (1954); and  $M_I$ , the felt area or intensity magnitude of Topozada (1975). They are defined as follows:

(i)

$$m_b = \log(A/T) + Q(\Delta, h) + S$$

where  $A$  = the maximum ground amplitude (in microns) in the wave group of PZ, PH, PPZ, PPH, or SH,  $T$  = the corresponding wave period (in seconds),  $Q(\Delta, h)$  is the distance, depth correction (Richter, 1958),  $\Delta$  = epicentral distance of earthquake,  $h$  is the depth, and  $S$  is the station correction (Gutenberg, 1945). This equation is valid for  $\Delta \geq 5^\circ$ .

(ii)

$$M_s = \log(A/T) + 1.66 \log \Delta + 3.30$$

where  $A$  = maximum ground amplitude (in microns) of surface waves of period 18 - 22 seconds,  $T$  = corresponding period of waves (in seconds), and  $\Delta$  is the epicentral distance (in degrees). This equation is valid for  $2^\circ < \Delta < 160^\circ$ .

(iii)

$$M_s^G = \log A + 1.656 \log \Delta + 1.818 + s$$

where  $A$  = vector sum of horizontal components of maximum ground motion (in microns) of surface waves having a period of 17 - 23 seconds,  $\Delta$  = epicentral distance (in degrees),  $s$  is the station correction (Gutenberg, 1945). This equation is valid for  $15^\circ < \Delta < 130^\circ$ .

(iv)

$$M_I = -1.88 + 1.53 \log A$$

where  $A$  is the total felt area of earthquake in  $km^2$ . This relation, developed for crustal earthquakes in California and Nevada, relates to the original Richter local magnitude  $M_L$ . This relation appears to be accurate to within  $\pm 1/4$  magnitude unit for Vancouver Island earthquakes (Rogers, 1983).

### 2.2.3 Focal Mechanism Studies

Both body and surface waves generated by an earthquake provide information on the focal mechanism. Body waves provide information on the region of initial rupture, while surface waves, which are emitted from the entire rupture surface, provide information on a larger area of the fault. In this study, both the first motions of P waves, the P-nodal method, and the radiation pattern of surface waves were considered.

i) *P-nodal Method* – The program used to evaluate P-nodal solutions is a modified version of Wickens and Hodgson (1967). This program searches through a parameter space of focal mechanism orientations. It generates theoretical radiation patterns and compares these to the observed first motions. Based on the weight given the observation, the reliability of the theoretical radiation pattern, and statistical considerations, the program chooses a best fit mechanism. In addition to the best fit, the twenty highest scoring solutions are printed and plotted. The extended distance tables used in this program were those of Hodgson and Storey (1953) and Hodgson and Allen (1954a, b). For stations at epicentral distances less than  $20^\circ$ , arrivals were assumed to be  $P_n$  and the take-off angle fixed at  $60^\circ$  for a crustal earthquake (Rogers, 1979). If the earthquake occurred in the mantle (or the subducting plate), take-off angles are more difficult to estimate for these stations (see discussion in Chapter III).

ii) *Surface Wave Method* - The amplitudes of Rayleigh and Love waves generated by an earthquake are sensitive to source mechanism (strike, dip and slip), focal depth and seismic moment ( $M_o$ ). Ben-Menahem and Harkrider (1964) developed a theory of surface wave radiation from dipolar point sources in a multi-layered earth. Given an earth model (velocity–depth and attenuation) which represents the propagation path,

comparison of the observed azimuthal radiation pattern of surface waves with theoretical radiation patterns allows the focal parameters to be determined.

The analysis began by digitizing the seismograms within group velocity windows of 2.5 km/sec to 5.0 km/sec. Once digitized, full-scale plots were made for each record and placed over the original to ensure accuracy.

A series of programs (Herrmann, 1978) were then used to determine the spectral amplitudes of the Rayleigh and Love waves as a function of azimuth about the epicentre.

The first program, EXSPEC, interpolated the digitized records into an equally spaced time series and removed any trend or D.C. offset. This program then transformed the time series into the frequency domain, where instrument response was removed. For horizontal components the E-W and N-S seismograms were rotated to form the radial and transverse components of ground motion. These were then plotted to check that Rayleigh and Love waves had separated properly. Finally, the spectra were corrected for geometrical spreading on a sphere to a reference distance of  $9^\circ$  (1000 km).

The output of EXSPEC, the Fourier transformed ground motion, was then input to the program FILTER. This program applies a narrow band-pass Gaussian filter to the real frequencies of the transformed ground motion. The inverse Fourier transform was then taken and both real and imaginary parts of this inverse transform were used to form the envelope of the filtered signal. This envelope was then searched for local maxima. These reflect the spectral amplitudes of individual modes making up the surface wave signal provided two or more modes do not arrive too close together in time. The peak of this envelope is then multiplied by the factor  $4T_0$ ,  $T_0$  being the centre period of the filter pass-band, so that the result is dimensionally a spectral amplitude. This procedure was repeated for a series of passband filters, typically from 10.0 seconds to 80.0 seconds.

The output of this program is a log-log plot of spectral amplitudes versus period and a tabulated list of spectral amplitudes, group velocity and phase for each filter period.

A plotting program of Bostwick (1984) was applied to this output to form a contour plot of group velocity versus period. Arrivals of equal amplitude were joined by contours. This form of the group velocity dispersion curve allows an easy comparison of the data with theoretical dispersion curves. This provides a good check on the quality of the data, and together with the plot of spectral amplitudes allows one to determine which wave periods will be useful for analysis.

These contour plots were then scanned and the fundamental mode arrival identified. The spectral amplitudes of Rayleigh and Love waves of periods ranging from 10 seconds to 80 seconds were identified. At this point the waves have been corrected for geometrical spreading; however corrections for anelastic attenuation have not yet been applied.

Theoretical spectral amplitudes were calculated using the program suite of Herrmann (1978). An earth model and a selected range of frequencies were the input for the first program SURFACE. Earth models considered in this study were the continental U.S.A. model of Ben-Menahem and Singh (1981) and the Gutenberg earth model. Attenuation values used were the world averaged values given in Tsai and Aki (1970) and those of Herrmann (1978). The program SURFACE solves the Rayleigh and Love wave period equations in order to determine the dispersion curves for group velocity, surface wave amplitude factors and Rayleigh wave ellipticity. The programs REIGEN and LEIGEN were then used to determine the eigenfunctions as a function of depth for Rayleigh and Love waves respectively. The output from these programs could then be used to generate theoretical radiation patterns, synthetic amplitude spectra or synthetic seismograms.

The program QUESTION accepts the observed Rayleigh and Love wave spectral amplitudes and corrects these for anelastic attenuation. The program then scans through a parameter space of focal mechanism orientations and focal depths to determine the source mechanism which produces the best fit between observed and theoretical radiation patterns.

The parameters which determine goodness of fit are (Herrmann, 1978 p. XI-1):

- 1) The correlation coefficient between the observed and theoretical amplitude spectra at all azimuths and periods, for both Rayleigh and Love waves.
- 2) Seismic moment estimated from Rayleigh wave data.
- 3) Seismic moment estimated from Love wave data.
- 4) Sum of squares residuals between observed and theoretical amplitude spectra using the average seismic moment estimate, for both Rayleigh and Love waves.
- 5) Square root of sum of Love and Rayleigh squared residuals.

The best fit has been found (Herrmann, 1978) to be the one with the largest correlation coefficients and for which the two independent seismic moment estimates are as equal as possible. The program FPDPLT is then used to plot the focal mechanism of the best fit solution.

Another useful program of Herrmann (1978) is RADPAT. This program accepts observed spectral amplitudes for Rayleigh and Love waves, an estimate of the seismic moment, a trial focal mechanism (slip, dip, strike), and depth of the earthquake. The observed amplitudes are corrected for anelastic attenuation and plotted azimuthally. The theoretical radiation pattern is superimposed on this plot allowing comparison with the observed data.

## CHAPTER III

### THE DECEMBER 16, 1957 EARTHQUAKE – RESULTS

#### 3.1 Introduction and Intensity

On December 16, 1957 at 17:27 U.T. (9:27 a.m. local time) an earthquake shook central Vancouver Island. Newspapers in Courtenay reported “the tremors were not violent, but were clearly felt inside buildings”. No damage was reported from this event, which in addition to Courtenay, was felt at the Forbidden Plateau lodge, and for about 30 seconds in the central island communities of Campbell River, Alert Bay and Kelsey Bay (Figure 8). In Campbell River it was reported that “the quake was so slight that it was not noticed by a good many people, especially by those who were out in the open”.

Based on this information the intensity in these areas appears to be about a magnitude III on the Mercalli scale. All available newspapers from Vancouver Island and the adjacent mainland coast were searched for local reports of this earthquake. However, due to sparse population few data are available. Figure 8 illustrates this limited data set. In this diagram circles have been drawn around the epicentre to represent the poorly constrained isoseismal lines. It should be noted that there are no newspaper reports of this earthquake being felt in either Powell River or Port Alberni, although these areas did have a significant population in 1957 (Chapman and Turner, 1956). This provides an eastern and southeastern limit on the maximum felt area of this earthquake.

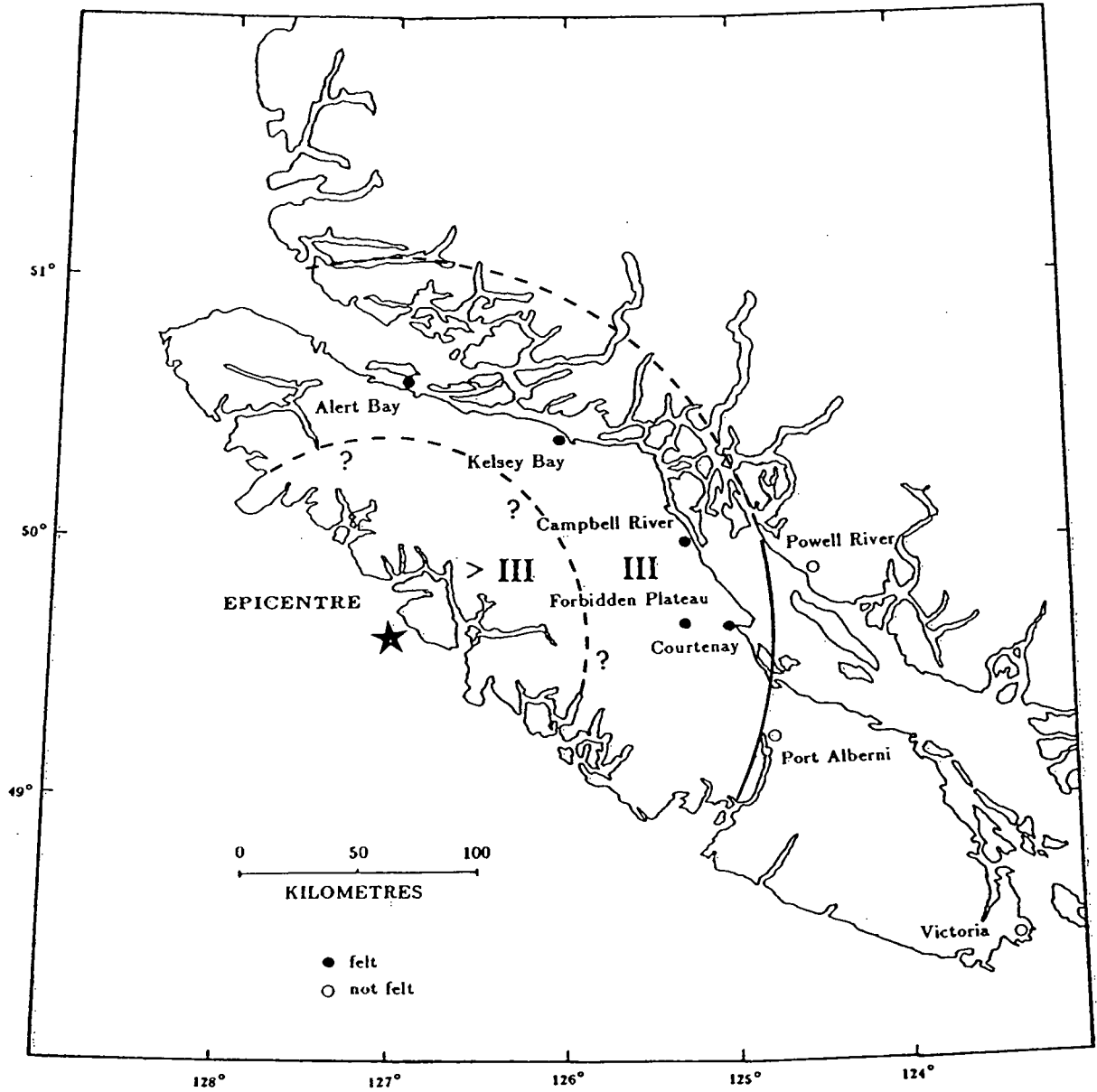


Figure 8. Isoseismal map for the December 16, 1957 earthquake. Solid line indicates the region where the isoseismal curve is better constrained.

### 3.2 Epicentre Location

As described earlier, there are several estimates for the epicentre of this earthquake (Figure 6). In this study the epicentre has been examined by considering teleseismic data, local data and felt information.

#### 3.2.1 Teleseismic Methods

In the following teleseismic epicentre studies it was determined that focal depths of 0–20 km resulted in slightly smaller travel-time residuals than did greater depths. However, epicentres appear to be relatively insensitive to depth. Varying this parameter from 0 to 30 km resulted in epicentre movements of less than  $0.1^\circ$ . For each of the tests described below focal depth was varied from 0 to 60 km, but unless otherwise indicated, the results given are for a fixed depth of 10 km. The arbitrary travel-time residual rejection levels were also varied, but again, unless otherwise stated, results were obtained using limits of 60.0 sec, 10.0 sec, 6.0 sec, and 4.0 sec. It should be noted that most of the seismograms used in this study had a drum speed of 15 mm/min; 4.0 seconds corresponds to a distance of 1 mm on these seismograms.

The first study (Tests 1a, 1b and 1c) involved investigating the effect of earth models and station corrections on the epicentre estimate. For these tests, only the arrival times listed in the December, 1957 ISS bulletin (97 stations) were used with the program EPDET and the following earth models and station corrections; Jeffreys – Bullen (1958) earth model with no station corrections (Test 1a); Dziewonski and Anderson (1981) earth model with Dziewonski and Anderson (1983) station corrections (Test 1b); and the Herrin (1968) earth model with Veith (1975) station corrections (Test 1c). Results from these studies are given in Table IV (see also Figure 9). The solutions obtained are

near Tobin and Sykes (1968) estimate of  $49.82^{\circ}\text{N}$ ,  $126.48^{\circ}\text{W}$ , and not far from the ISS estimate of  $49.82^{\circ}\text{N}$ ,  $126.59^{\circ}\text{W}$ .

Table IV Epicentre estimates

| Test No. | Origin Time | Lat.( $^{\circ}\text{N}$ ) | Long.( $^{\circ}\text{W}$ ) | No. St. | $\sigma$ (sec.) |
|----------|-------------|----------------------------|-----------------------------|---------|-----------------|
| 1a       | 17 27 50.3  | 49.79                      | 126.49                      | 68      | 1.65            |
| 1b       | 17 27 53.0  | 49.77                      | 126.44                      | 71      | 1.89            |
| 1c       | 17 27 53.1  | 49.79                      | 126.40                      | 70      | 1.93            |
| 2        | 17 27 50.3  | 49.81                      | 126.76                      | 78      | 1.40            |
| 3        | 17 27 51.0  | 49.79                      | 126.79                      | 73      | 1.22            |
| 4        | 17 27 49.3  | 49.90                      | 126.88                      | 51      | 1.63            |
| 5        | 17 27 50.8  | 49.79                      | 126.85                      | 69      | 1.40            |
| 6        | 17 27 51.0  | 49.65                      | 127.02                      | 49      | 1.33            |

No. St. = Number of stations included in solution

$\sigma$  = Standard deviation of travel-time residuals.

For the remaining tests all three earth model-station correction combinations were considered; however it was found that in every case the Dziewonski and Anderson earth model with station corrections provided the best fit to the data (the smallest travel-time residuals). Unless otherwise indicated, the following results were obtained using this earth model with station corrections.

Test 2 involved a larger data set (given in Appendix B). This set includes arrival times read from the seismograms of 32 stations, the ISS data, and those data listed in the BCIS but not the ISS. If a difference existed between either a BCIS or an ISS arrival time, and that read directly from a seismogram, the latter was chosen as the

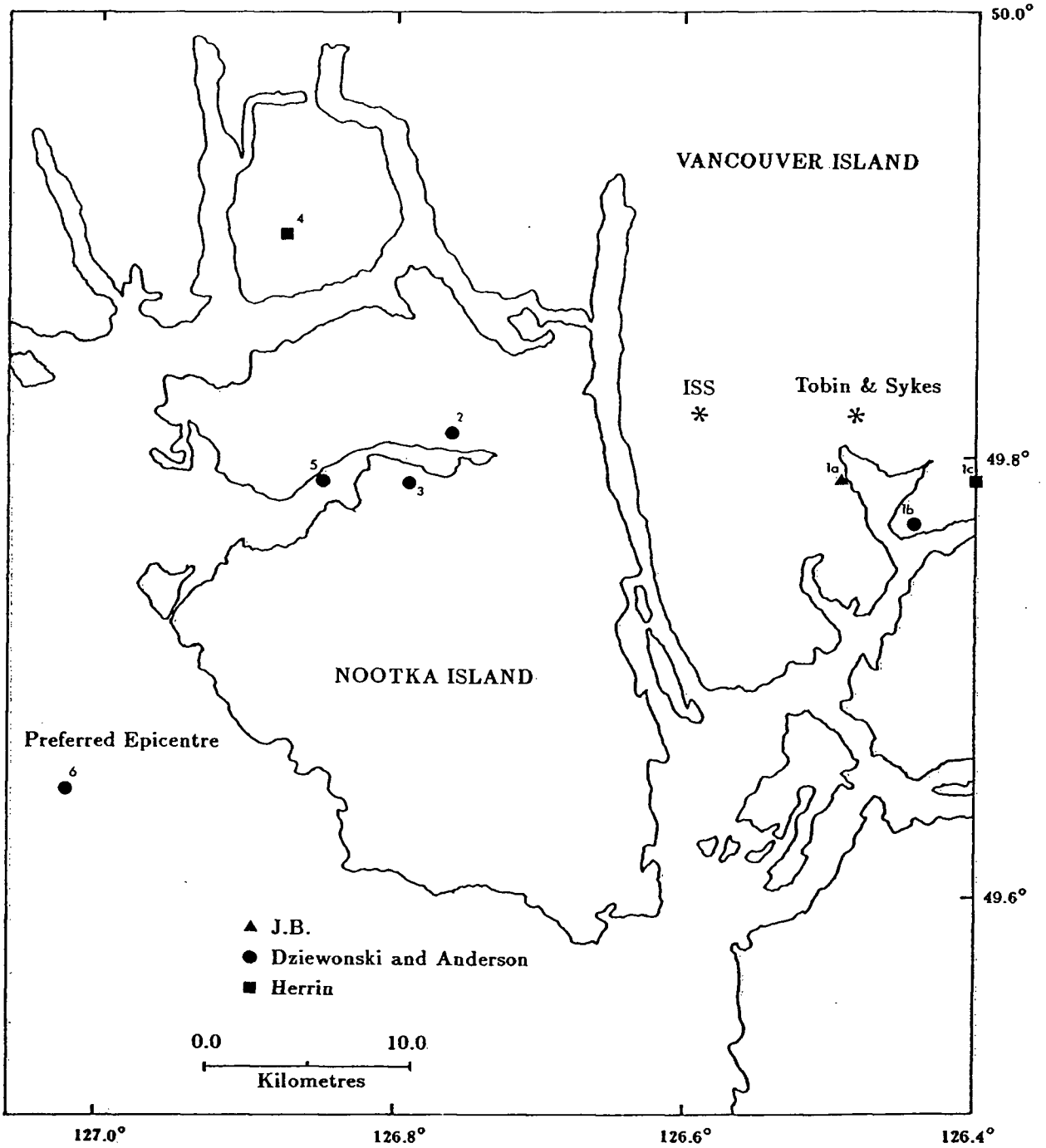


**Figure 9.** Previous teleseismic epicentre estimates, and estimates from this study. Numbers correspond to the tests described in text (section 3.2.1). The symbols represent the earth models used in this study (see legend).

more accurate. In total, arrival times from 113 stations were considered in this study. This is a larger data set than that used in any previous study of this earthquake. The epicentre obtained using this expanded data set is  $49.81^{\circ}\text{N}$ ,  $126.76^{\circ}\text{W}$  (Figure 9).

This solution is significantly different ( $0.32^{\circ}$  longitude) from the previous estimate obtained using the ISS data only (it also has a much smaller standard deviation). Upon comparison of the data used in the final solutions it was noted that of the six arrival times from Japanese stations ( $\Delta = 66^{\circ} - 74^{\circ}$ ), five (SEN, ABU, MTJ, NGS and KYO) had positive residuals close to the 4.0 second rejection limit. If these stations were included in the solution, the epicentre was near  $126.4^{\circ}\text{W}$ . If these were not included, the epicentre was near  $126.8^{\circ}\text{W} - 127.0^{\circ}\text{W}$ . Clearly, determining whether or not these data should be included in the solution is an important consideration in the location of this earthquake.

One possibility is that the residuals are due to a delay introduced along the source-receiver path. The 1972 earthquake, which occurred about 40 km southwest of the 1957 event (Figure 3), provides no conclusive evidence for this. Of the four Japanese stations which recorded this event, two had negative residuals (-0.5 and -3.0 seconds) and two had positive residuals (+7 and +8 seconds).

Another possibility is that these were "late" picks; the body waves may have been so small as to make identifying the first arrival very difficult. Records of this earthquake could not be obtained from these stations. However, of the five Japanese stations having positive residuals of 4.0 - 6.0 seconds, station bulletins were available for two; SEN and ABU. The SEN bulletin indicates that the largest (not necessarily the *first* motion) body wave amplitude was 0.1 mm at a period of 2.5 seconds. The seismometer (Wiechert Z) had a magnification of 105 at this period. The ABU bulletin indicates

that body waves were recorded on two instruments. The maximum amplitude was 1.0 mm at a period of 2.5 seconds (magnification= 600) on a Galitzin vertical, and 0.7 mm at 1.5 seconds (magnification  $\simeq$  7000) on a vertical short period instrument. At each station an emergent first arrival is indicated. Charlier and Van Gils (1953) indicate that three other Japanese stations (KYO, MAT and NGS) have Wiechert instruments with a static magnification of 80. Thus, it is likely that the first arrivals at these stations were also very small. It is interesting to note that three of these stations (KYO, SEN, and NGS) report having some trouble with microseisms (Charlier and Van Gils, 1953). Without seeing the seismograms definite statements cannot be made. However, given the low amplitude arrivals, the emergent character of the arrivals and the possibility of microseisms in December, it is very possible that the first motions were overlooked.

For those stations with small first arrivals, it is more likely that a later arriving phase would be misidentified as the first motion than would noise prior to the actual first arrival be picked. The possible effect of "late" picks can be studied by rejecting all stations having large positive travel-time residuals.

Test 3, using the complete data set with the exception of those stations having a positive residual greater than +2.0 seconds (6 from Eastern Asia, 4 from Europe, 5 from North America and 2 from Antarctica) provides an epicentre estimate of 49.79°N, 126.79°W (Table IV).

A study (Test 4) was made using only North American data (58 stations), as this earthquake was recorded clearly throughout the continent. In addition, seismogram drum speeds were in many cases 30 - 60 mm/min, yielding more accurate arrival times. In this case the Herrin (1968) earth model and Veith (1975) station corrections were used (this earth model was derived primarily for North America). The resulting epicentre is

49.90°N, 126.88°W (Figure 9). The possible bias introduced by using such a restricted azimuthal distribution of stations is discussed at the end of this section.

A data set which should provide for a more accurate epicentre estimate includes only those stations having Dziewonski and Anderson (1983) station corrections. This study (Test 5) resulted in an epicentre estimate of 49.79°N, 126.85°W (Figure 9).

A final experiment (Test 6) involved using only those stations at epicentral distances greater than 20°, and having Dziewonski and Anderson (1983) station corrections. This test should reduce any upper mantle effects on travel-times. For the complicated geological structure of the west coast of North America (e.g. subducting plates and accreted terranes), travel-times through the upper mantle may differ considerably from an "average" earth model. Teleseismic studies of recent earthquakes (1970–1980) west of Vancouver Island (R. Wahlstrom and G. Rogers, personal communication), indicate that by using only stations at epicentral distances greater than 20°, the epicentre is moved significantly southwestward. These solutions appear to be more stable, and in the case of the 1972 earthquake, the teleseismic epicentre is in much better agreement with the well-located largest aftershock (see Rogers, 1976). The result of this study (Test 6) is an epicentre estimate of 49.65°N, 127.02°W (Table IV, Figure 9). This solution is significantly southwest of other estimates. It should be noted that this solution has the smallest travel-time residuals of all tests (except for Test 3, which by definition will have smaller residuals because "late" arrivals – those stations with large residuals, were not included in the data set). This epicentre appears to be stable; changing the data set slightly does not result in large changes to the epicentre. Reducing the travel-time rejection limit from 4.0 seconds to 2.0 seconds, or varying the focal depth from 0 to 60 km results in changes to the epicentre of less than 0.1°.

The final consideration in this study is the azimuthal distribution of recording stations. This earthquake was too small to be recorded in Australia, New Zealand or southeast Asia. As a result there is a distinct lack of data from the quadrant  $180^\circ - 270^\circ$  (only one arrival time is included in the final solution compared to 34 from the quadrant  $0^\circ - 90^\circ$ ). An estimate of the effect of the azimuthal distribution on the solution can be made by considering the 1972 event which was located in the same region as this earthquake. This event was first located using all data (220 stations, including 6 from azimuths of  $180^\circ - 270^\circ$ ). It was then located using a set of stations which matched the 1957 distribution as closely as possible (within  $10^\circ$  azimuth and  $5^\circ$  distance, with the exception of two Antarctic stations which could not be matched). The results indicate only a very slight shift ( $0.06^\circ\text{N}$ ,  $0.03^\circ\text{E}$ ) in epicentre due to the limited data set.

Another experiment was the location of the 1972 earthquake using only North American stations (excluding the Aleutian Islands). This resulted in a shift of  $0.11^\circ\text{N}$ ,  $0.07^\circ\text{E}$  compared to the location obtained using all data. Therefore, although this is a limited study due to the lack of earthquakes large enough to be well recorded worldwide, the results obtained indicate only slight variations ( $< 15$  km) in epicentre due to the limited azimuthal distribution of stations.

### 3.2.2 Local Methods

Arrival times from four local stations – HBC, ALB, VIC and SEA (see Figure 10) – were used in this study (a fifth – LLL had a P-residual of about 10 seconds and was not used). Both P and S arrivals could be picked on the VIC and SEA records, although the S-wave onsets were difficult to determine accurately and are subject to an error of a few seconds. The S arrival time chosen for SEA is about 20 seconds earlier than

that listed in the ISS. Use of the ISS arrival time resulted in a large (18 – 20 second) residual. It is likely that the ISS time corresponds to the  $S_g$  phase rather than the first S arrival ( $S_n$  at this distance of  $\approx 400$  km). The P-arrival time for HBC, and P and S arrival times for ALB were obtained from Milne's original, unpublished worksheets on this earthquake.

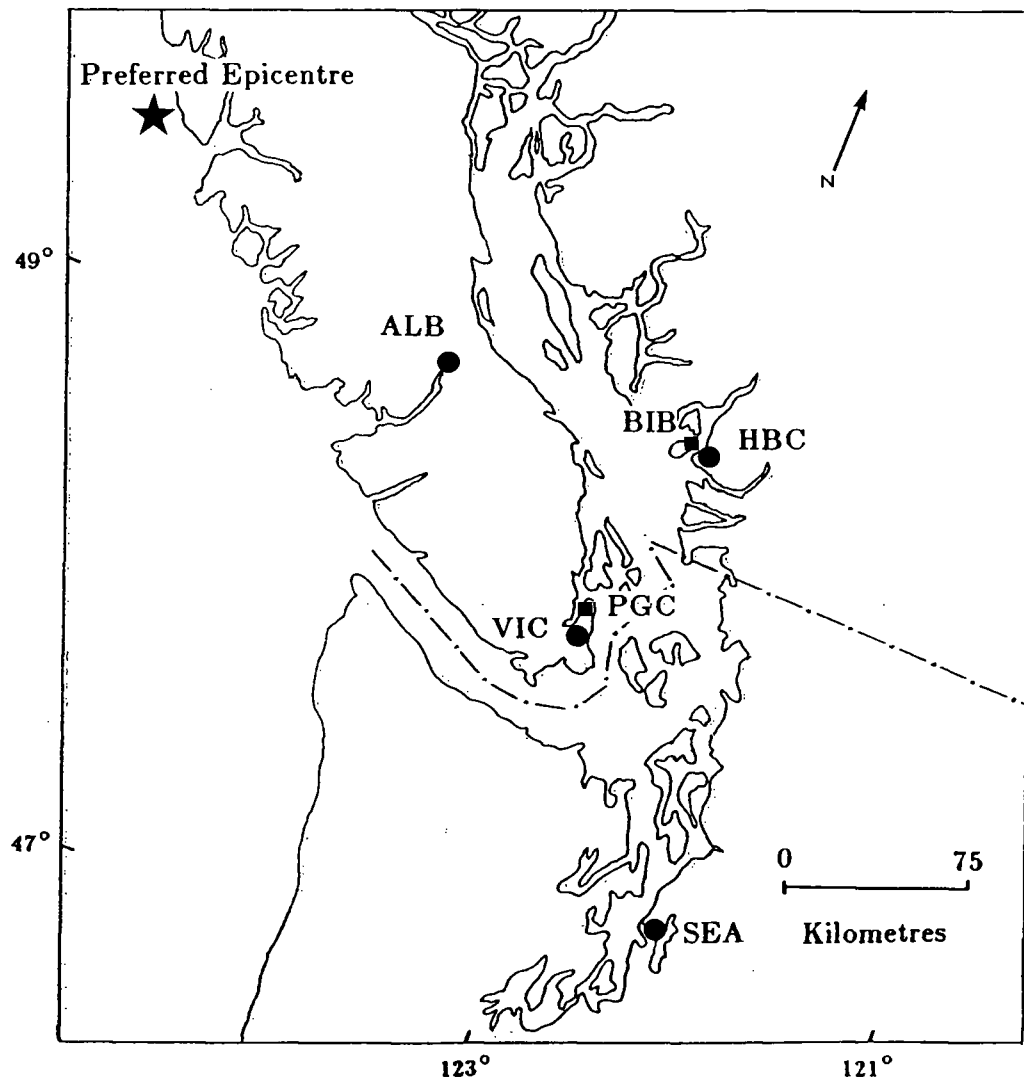


**Figure 10.** Location of stations (dots) used in “local” epicentre studies, and preferred epicentre. Squares represent modern stations used to estimate station corrections (see text) for VIC and HBC.

Table V Arrival Times for Local Stations

| STATION | P-ARRIVAL  | S-ARRIVAL  |
|---------|------------|------------|
| ALB     | 17 28 15.0 | 17 28 33.0 |
| HBC     | 17 28 29.1 | —          |
| VIC     | 17 28 30.2 | 17 29 00.2 |
| SEA     | 17 28 48.0 | 17 29 31.0 |

These data (Table V) were input to the programs FASTHYPO (Herrmann, 1979) and HYPOELLIPSE (Lahr, 1984). Epicentre stability was examined by considering 3 earth models; the Canadian Standard (Stevens *et al.*, 1972); McMechan and Spence (1983) (no low velocity zone); and the Vancouver Island–Puget Sound model (Rogers, 1983). Epicentre stability was also investigated using various combinations of P and S arrival times, assigning weights to these arrivals based on distance from epicentre and accuracy of arrival time, and by using either fixed depths or allowing the depth to float (a hypocentre determination).

In every case the Vancouver Island–Puget Sound model, with floating depth, produced the best fit to the data (smallest RMS error). Solutions obtained using other models differed from the best fit by up to 15 km. For each of the following studies only the hypocentre obtained using the Vancouver Island–Puget Sound model is indicated.

The first hypocentre estimate (Test 1) was obtained using the program FASTHYPO and all data (Table V) with a weight of 1 for P arrivals and 1/2 for S arrivals. The result (see Figure 11) is 49.64°N, 127.35°W and a depth of 13 km (RMS = 1.37 second).

For Test 2 decreasing weights are assigned to the arrivals as distance from the epicentre increases (ALB P=1, ALB S=1/2, VIC P=3/4, HBC P=3/4 and SEA P=1/2).

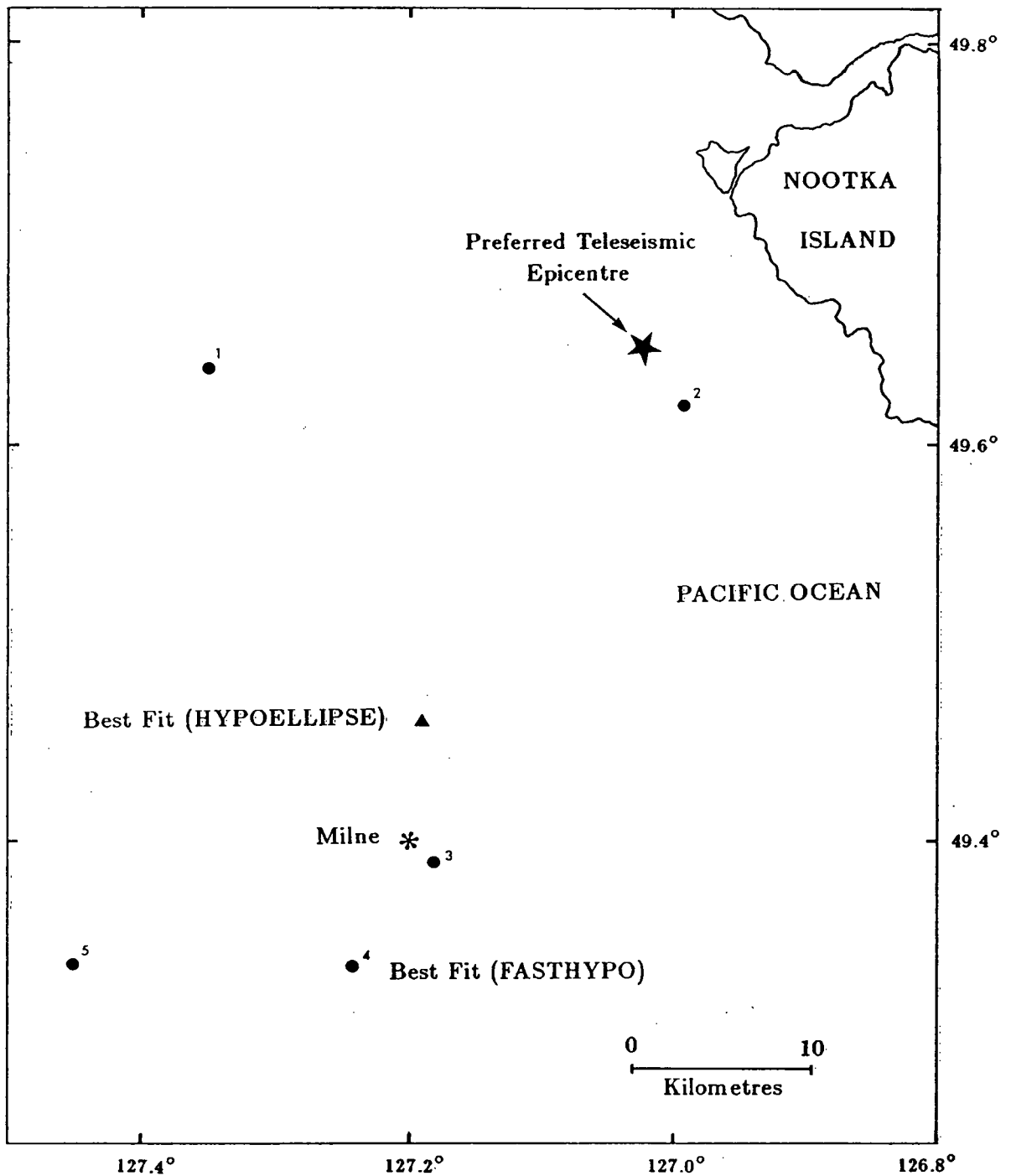


**Figure 11.** Epicentre estimates using local data only. Numbers correspond to the tests described in text (section 3.2.2). Hypocentres are at depths ranging from 0 to 25 km (see text).

This results in an estimate of  $49.62^{\circ}\text{N}$ ,  $126.99^{\circ}\text{W}$  at a depth of 16 km (RMS = 1.91 seconds).

In an effort to improve upon this data set a recent earthquake (1984) in the epicentral region of the 1957 event was used to generate station corrections for HBC, VIC and ALB. Corrections for HBC and VIC (which are now closed) were estimated by calculating travel-time residuals from the 1984 event for the stations BIB (near HBC) and PGC (near VIC) (see Figure 10). The corrections estimated are; for HBC +2.2 seconds; for VIC +1.6 seconds and for ALB +1.4 seconds. These station corrections are very similar to those that were generated using four 1983 earthquakes in this region (HBC= +2.0 - +2.2, PGC= +1.4 - +1.8, ALB= +1.7) (Rogers, personal communication). S wave corrections of +2.4 seconds for ALB and +2.8 seconds for VIC were estimated assuming a  $V_p/V_s$  ratio of 1.73.

Applying these corrections and repeating the last study (arrivals weighted according to distance from epicentre), the result for Test 3 is  $49.39^{\circ}\text{N}$ ,  $127.18^{\circ}\text{W}$  and a depth of 16 km (RMS = 1.33 seconds) (Figure 11). The major effect of applying the station corrections is to move the epicentre south approximately  $0.2^{\circ}$ , providing a much better fit to the data.

Another study (Test 4) was made using the corrected data with with P weights of 1 and S weights of 1/2 for all stations except SEA. As station corrections could not be estimated for this station, the P weight was assigned 3/4 and the S weight 1/4. The resulting hypocentre is  $49.29^{\circ}\text{N}$ ,  $127.24^{\circ}\text{W}$  at 0 km depth (RMS = 1.18 seconds).

A final study (Test 5) was made of the effect of excluding the ALB S arrival (weights the same as the previous run). The results indicate only a slight westward shift in the epicentre to  $49.31^{\circ}\text{N}$ ,  $127.45^{\circ}\text{W}$  at 7 km depth (RMS = 1.26 seconds).

Of the five tests the best fit to the data is provided by Test 4. This solution (with uncertainties) obtained using FASTHYPO is:

$$49.29^{\circ}\text{N} \pm 0.14^{\circ}$$

$$127.24^{\circ}\text{W} \pm 0.25^{\circ}$$

$$0 \text{ km} \pm 18 \text{ km depth}$$

$$\text{O.T.} = 17 \ 27 \ 49.1$$

Similar experiments with HYPOELLIPSE produced a best fit with the same data set and the Vancouver Island–Puget Sound earth model. The results from this program are:

$$49.46^{\circ}\text{N} \pm 0.16^{\circ}$$

$$127.19^{\circ}\text{W} \pm 0.28^{\circ}$$

$$24.7 \text{ km} \pm 27.2 \text{ km depth}$$

$$\text{O.T.} = 17 \ 27 \ 49.9$$

Epicentre estimates for each of these tests are illustrated in Figure 11.

The local data therefore suggest that this earthquake occurred near  $49.3^{\circ} - 49.5^{\circ}\text{N}$ ,  $127.2^{\circ}\text{W}$ . This is in complete agreement with Milne's solution (Milne and Lucas, 1961) of  $49.4^{\circ}\text{N}$ ,  $127.2^{\circ}\text{W}$  (obtained using arrival times from ALB, HBC and VIC).

Although the very small data set used in this study (all from one quadrant) does restrict the confidence that can be placed in this solution, it is significant that no solutions were observed near the previous teleseismic epicentre estimates of Tobin and Sykes (1968) and the ISS (Figure 9).

### 3.2.3 Felt Area Information

It is possible to evaluate potential epicentres by considering the magnitude–total felt area relationship of Topozada (1975).

Rogers (1983) states that for the few Vancouver Island events which have both a well defined magnitude and felt area, the magnitudes estimated by Topozada's felt area relationship are consistent to within  $\pm 1/4$  magnitude unit. If we assume that this is true for this earthquake, and recalling that there are eastern and southeastern maximum felt limits for this event (Powell River and Port Alberni), it is possible to evaluate potential epicentres.

First, considering the local epicentre estimates near  $49.4^{\circ}\text{N}$ ,  $127.2^{\circ}\text{W}$ , the maximum felt area (obtained by drawing a circle around the epicentre limited by Powell River on the east and Port Alberni on the southeast) is  $95,200 \text{ km}^2$ . Applying Topozada's equation (see section 2.2.2) results in a magnitude of  $M_I = 5.7$ .

Next, considering the previous teleseismic epicentre estimates of Tobin and Sykes (1968), and the ISS (near  $49.8^{\circ}\text{N}$ ,  $126.5^{\circ}\text{W}$ , see Figure 9) a maximum felt area (obtained as described above) of  $61,700 \text{ km}^2$  is estimated. Applying Topozada's equation results in a magnitude of  $M_I = 5.4$ . This is low compared to the best magnitude estimate of 5.9 (section 3.4).

Finally, considering the teleseismic epicentre estimate (Test 6 – section 3.2.1) of  $49.65^{\circ}\text{N}$ ,  $127.02^{\circ}\text{W}$ , the maximum total felt area is  $88,900 \text{ km}^2$ . In this case Topozada's equation yields a magnitude of  $M_I = 5.7$ .

Although these magnitude estimates can only be considered as a "weak" argument due to the poorly defined total felt area (constrained only by Port Alberni to the south-

east and Powell River to the east), this information supports an epicentre which is west of previous estimates by the ISS or Tobin and Sykes (1968).

### 3.2.4 Epicentre Summary

The preferred epicentre is chosen to be the teleseismic solution (Test 6) of  $49.65^{\circ}\text{N}$ ,  $127.02^{\circ}\text{W}$  ( $\pm 20$  km). This epicentre was chosen for a number of reasons:

- 1) this solution is closest to the epicentres estimated using only local data; within uncertainties the solutions agree,
- 2) this estimate has the smallest RMS error of all teleseismic estimates (except Test 3 – see discussion),
- 3) the data set used for this estimate reduces the effect of upper mantle velocity variations and includes only those stations for which station corrections have been generated, and
- 4) felt area information supports an epicentre which is significantly west of previous teleseismic estimates.

The teleseismic epicentre is preferred to the local epicentre estimate because of the much larger data set, and better azimuthal distribution of stations. The local solution is based on arrival times at four stations only, all from one quadrant (Figure 10). Given the relatively small data set (50 stations included in the preferred solution), the quality of the data set, possible variations of  $\simeq 15$  km due to the azimuthal distribution of stations, and the scatter of estimates obtained in this study, an uncertainty of  $\pm 20$  km is estimated for this epicentre.

### 3.3 Focal Depth

The focal depth of the 1957 earthquake is estimated by comparing the observed radiation patterns of surface waves with theoretical patterns generated at various focal depths.

A systematic search of the seismograms was made for the phase pP which is indicative of depth; however this could not be identified on any records.

As described in section 3.2.1, travel-time residuals for the preferred epicentre are insensitive to depth over the range 0 to 60 km. This method therefore, provides no information on focal depth. Hypocentre programs (section 3.2.2) using local data only, consistently yield focal depths of 0 to 25 km (with uncertainties of about  $\pm 20$  km).

Surface wave radiation patterns, especially Rayleigh waves, are very sensitive to depth. Using the best fit surface wave mechanism which was determined (see section 3.5.2), the focal depth was varied from 3 km to 60 km. At each depth the surface wave correlation factor (the product of the Rayleigh and Love wave correlation coefficients between the observed and theoretical spectra for all data) was calculated. The normalized correlation factor is plotted in Figure 12. This diagram shows the good fit to the data over the depth range 25–40 km, with a maximum correlation at a depth of 30 km. The bounds of 25–40 km on the depth must be considered a minimum error estimate, as the effect (on depth) of errors in the surface wave data are difficult to estimate.

The lack of aftershocks for this event (only one was recorded – see section 3.6) also suggests that this earthquake occurred at a depth greater than 20 km. In a study of aftershock depths, Page (1968) determined that well-defined aftershock sequences only occur for shallow (<20 km) earthquakes. The location of this earthquake with respect to the subducting plate will be discussed in Chapter V.

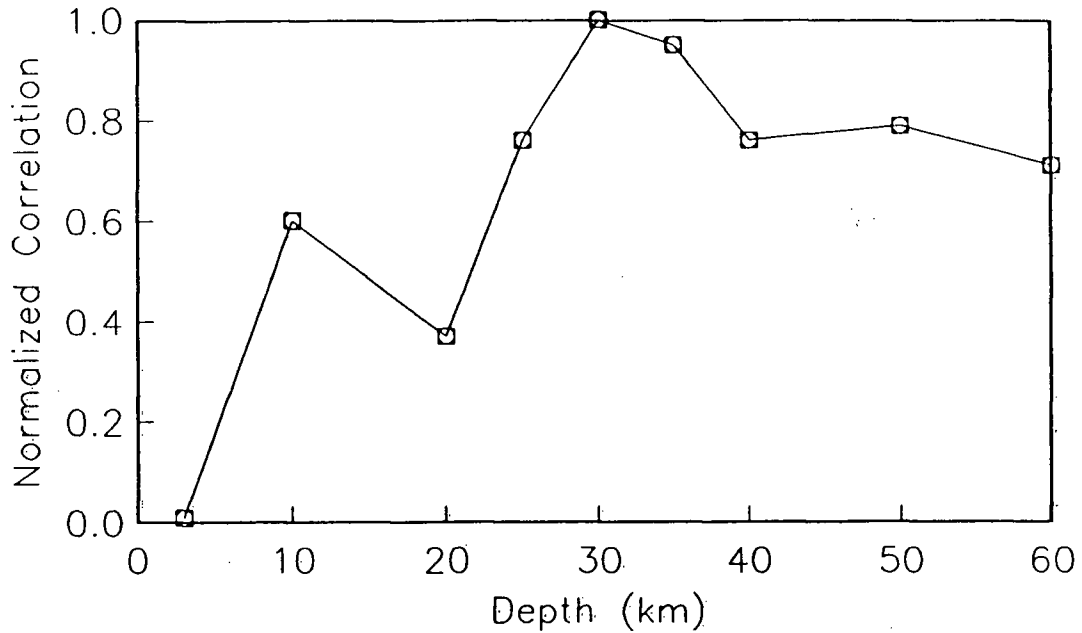


**Figure 12.** Plot of normalized surface wave correlation factor (described in text) as a function of focal depth.

### 3.4 Magnitude

Surface wave (Vanek *et al.*, 1962), broad-band body wave (Gutenberg and Richter, 1956) and felt area (Toppozada, 1975) magnitudes were determined for this earthquake. Seismograph calibration information for all stations considered in this study is given in Appendix B. Both vertical and horizontal components were used in magnitude determinations, with vector addition being applied to form total horizontal amplitudes from the N-S and E-W components. In the few cases for which only one horizontal component was available, the amplitude was multiplied by  $\sqrt{2}$  to estimate the total horizontal amplitude. Body wave magnitudes were calculated using the phases P, PP and SH where possible.

Results of all magnitude estimates are summarized in Appendix B. Using all data (if there is more than one magnitude estimate at a station, the average is taken) the average magnitudes are:

$$M_s = 5.88 \pm 0.21 \quad (22 \text{ stations})$$

$$m_b = 6.30 \pm 0.34 \quad (22 \text{ stations})$$

If only the "best" data is used (i.e. no station bulletin readings, only those stations which provided calibration curves with the seismograms, and those stations for which either a vertical, or both horizontal components were available) the results are:

$$M_s = 5.94 \pm 0.12 \quad (8 \text{ stations})$$

$$m_b = 6.27 \pm 0.44 \quad (6 \text{ stations})$$

The magnitude of this event is therefore,  $M_s = 5.9 \pm 0.2$ ,  $m_b = 6.3 \pm 0.3$ . Applying the equation of Gutenberg and Richter (1956) which relates these two magnitude scales

$$m_b = 0.63M_s + 2.5$$

a magnitude of  $m_b = 6.2$  is obtained using  $M_s = 5.9$ . This is in agreement with the above results.

The felt area magnitude, based on the total maximum felt area estimate of 88,900 km<sup>2</sup>, is  $M_I = 5.7$ .

A Richter (local) magnitude was calculated for Victoria ( $M_L = 5.4$ ) and Seattle ( $M_L = 6.0$ ). These estimates have very large uncertainties ( $\approx 0.4$ ) due to difficulty in

estimating wave periods accurately. In addition, because the instruments were not the standard Wood–Anderson type, the results are likely to be low (Richter, 1958 p. 145).

### 3.5 Source Mechanism

The source mechanism of this earthquake was studied by both the P-nodal technique and the radiation pattern of surface waves.

#### 3.5.1 P-nodal technique

First motion data could be read from seismograms of 27 stations. The quality of these data was in general very good (first motion data are given in Appendix B), however in some cases instrument polarity was not indicated. For these records it was assumed that north, east and up corresponded to the top of the seismogram. First motion data were also available from 10 stations listed in the ISS, 10 were obtained from station bulletins and three were obtained from Milne's original worksheets. There were three stations (SCL, MOR and CRT) for which the station bulletin indicated the opposite polarity to that reported in the ISS. In these cases the station bulletins were assumed to be correct. The complete data set, consisting of 50 readings from azimuths of  $299^\circ$  to  $163^\circ$  is listed in Appendix B. The weights for each arrival were assigned as follows:

|  |     |
|--|-----|
| 1) Bulletin or ISS reading . . . . .                       | 50  |
| 2) Arrivals that were not clear . . . . .                  | 50  |
| 3) Records without instrument polarity indicated . . . . . | 50  |
| 4) Clear arrivals with known instrument polarity . . . . . | 100 |

The results obtained using the modified program of Wickens and Hodgson (1967) (assuming a  $P_n$  take-off angle of  $60^\circ$  for stations at epicentral distances less than  $20^\circ$ ) are illustrated in Figure 13. The three top scoring solutions are very similar to those obtained by Rogers (1979) (see Figure 7). This was expected as the same program was employed and the data sets were very similar. The differences are the addition of 14 readings (12 from the United States and 2 from Europe) in this study, and the reversal of the first motion polarity for three stations (SCL, MOR and CRT) based on the station bulletins of these stations.

The best fit solution (Figure 13a) is predominantly strike-slip, with a fault plane orientated either  $N74^\circ E$  with a dip angle of  $71^\circ$  (from horizontal) in a northerly direction, or  $N24^\circ W$  dipping  $67^\circ$  in a westerly direction. This mechanism is not well constrained due to a lack of data between azimuths of  $180^\circ - 300^\circ$ . The other two mechanisms illustrated have only a slightly lower score than the best fit (91.3 and 90.4 vs 91.4). The preferred focal depth of 30 km suggests that this earthquake may have occurred in the subducting plate (see Chapter V). The take-off angles for those stations at epicentral distances less than  $20^\circ$  are therefore difficult to estimate due to complicated geological structure. Several California stations ( $\Delta = 13^\circ - 18^\circ$ ), and two Alaska stations ( $\Delta = 9^\circ - 19^\circ$ ) define the NNW striking nodal plane of the preferred solution. The uncertainty in the take-off angles for these stations may be about  $\pm 10 - 15^\circ$ . Although this may slightly change the orientation of the NNW striking plane, it does not change the mechanism significantly. These possible mechanisms are examined further using surface wave radiation patterns.

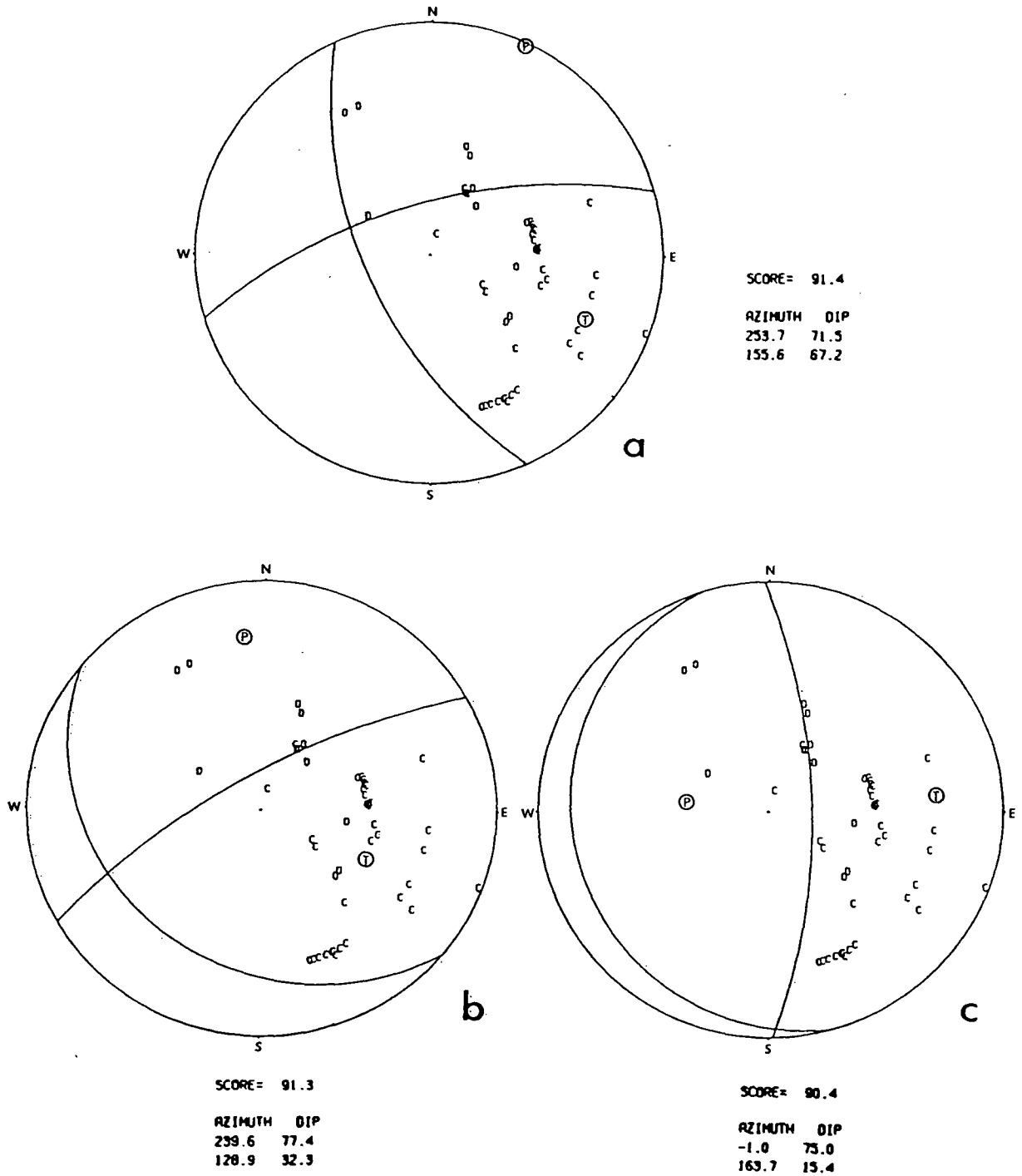


**Figure 13.** Top scoring P-nodal solution (a), and two alternate, slightly lower scoring solutions (b and c). The circles represent the lower half of the focal sphere; C's represent compressional arrivals; D's represent dilational arrivals; P and T represent the pressure and tension axes respectively.

### 3.5.2 Surface Wave Analysis

Surface waves generated by this earthquake recorded at 20 stations with azimuths ranging from  $328^\circ$  to  $163^\circ$  were available for analysis. The digitized surface waves for each station are shown in Appendix B.

For a magnitude 6 earthquake, a point source approximation is valid for surface waves having periods of 10 seconds or more (Tsai and Aki, 1970). Such waves have a wavelength which is long compared to the fault rupture length ( up to 10 km for an event of this magnitude (Acharya, 1979)), and therefore the asymmetry introduced in the radiation pattern by a moving point source can be neglected.

The program suite of Herrmann (1978) (see 2.2.3 ii) was used to calculate the spectral amplitudes of Rayleigh and Love waves for each station. Figure 14 illustrates the Rayleigh and Love wave amplitude spectra and the dispersion curves for the station WES (the quality of these data being typical of most stations). The fundamental Love wave arrival is very clearly defined on the dispersion curve (Figure 14a) from a period of 10 seconds to about 52 seconds. The spectral amplitude plot (Figure 14b) illustrates the near vertical trending noise contaminating the spectra at periods greater than 55 seconds. The fundamental Rayleigh wave arrival (Figure 14c) is not as well defined as the Love wave arrival; this was true for most stations. This arrival is visible from periods of about 15 seconds to 40 seconds. Most stations recorded both Rayleigh and Love waves clearly from periods of 15 – 40 seconds, and a few stations (PAL, PAS and RES) provided data to periods of 70 or 80 seconds. In total 625 spectral amplitudes from periods of 16 – 80 seconds were used in this analysis. These include 264 Love wave amplitudes, 204 horizontal Rayleigh amplitudes and 157 vertical Rayleigh amplitudes.

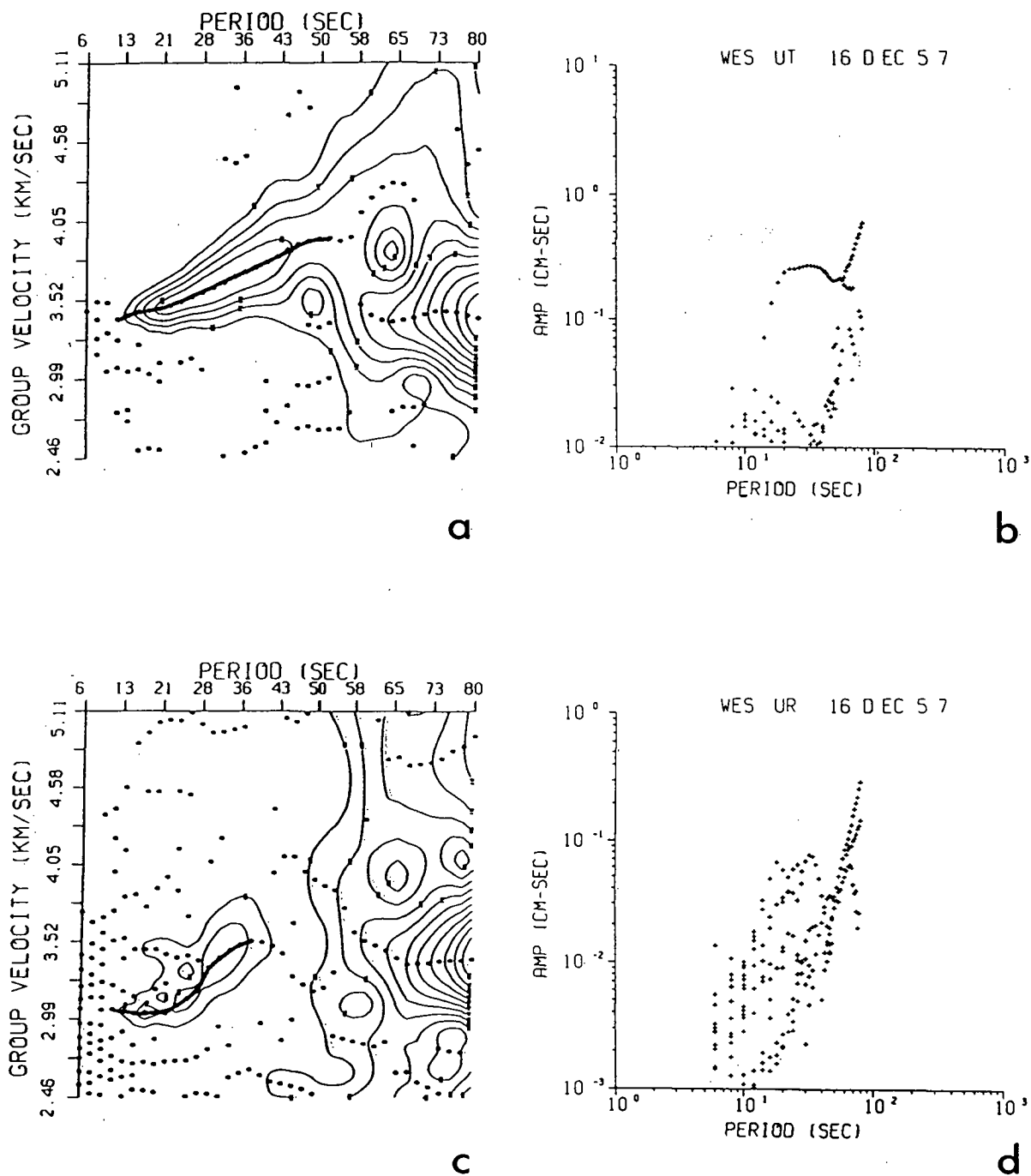


**Figure 14.** Group velocity dispersion curves (a, c) and amplitude spectra (b, d) for the station WES. Upper pair of plots are Love wave data and the lower pair are Rayleigh (horizontal) wave data. Dots (a, c) and crosses (b, d) represent positions of local maxima in the amplitude spectra for various period waves. For dispersion curves contours join arrivals of equal amplitude. The thick solid line represents the amplitude arrivals selected as corresponding to the fundamental mode arrival.

The eight layered earth model of Ben-Menahem and Singh (1981), and the world-wide averaged attenuation values of Tsai and Aki (1970) were used with the 625 observed spectral amplitudes as input for the program QUESTION. A best fit mechanism was determined as described in section 2.2.3 ii. Initially the trial mechanism dip angle was varied from  $0^\circ - 90^\circ$  in  $10^\circ$  steps, the strike was varied from  $0^\circ - 180^\circ$  in  $20^\circ$  steps and the slip angle was varied from  $-90^\circ - 90^\circ$  in  $20^\circ$  steps. Due to the symmetries involved in surface wave radiation patterns, these combinations cover all possible source mechanisms (Herrmann, 1978). The program was run with the focal depth being varied from 3 km to 60 km.

The "best" fit as determined by the program QUESTION is dip=  $80^\circ$ , strike=  $160^\circ$  and slip=  $-30^\circ$ . This solution was obtained at depths of 3 km to 60 km; however, 30 km produced the highest correlation factor. The program was then re-run using a finer grid in the region of the best fit (dip being varied by  $3^\circ$ , strike and slip by  $4^\circ$ ). The best fit mechanism that resulted is dip=  $88^\circ$ , strike=  $154^\circ$  and slip=  $-28^\circ$ . A depth of 30 km again produced the highest correlation factor (Figure 12). This mechanism, with observed first motions superimposed, is shown in Figure 15. This solution is quite similar to the best fit solution obtained by the P-nodal technique. Twelve first motions are inconsistent with the surface wave mechanism. These are four California stations (azimuth=  $160^\circ - 165^\circ$ ), three United States stations (azimuth=  $95^\circ - 135^\circ$ ), two European stations (azimuth  $\simeq 30^\circ$ ), SIT (azimuth=  $328^\circ$ ), RES (azimuth=  $17^\circ$ ) and THU (azimuth=  $20^\circ$ ). Of these data, the three United States stations (dilations) are clearly in the middle of a compressional quadrant; the two European stations have very small first motions which are difficult to pick; and the remaining stations are close

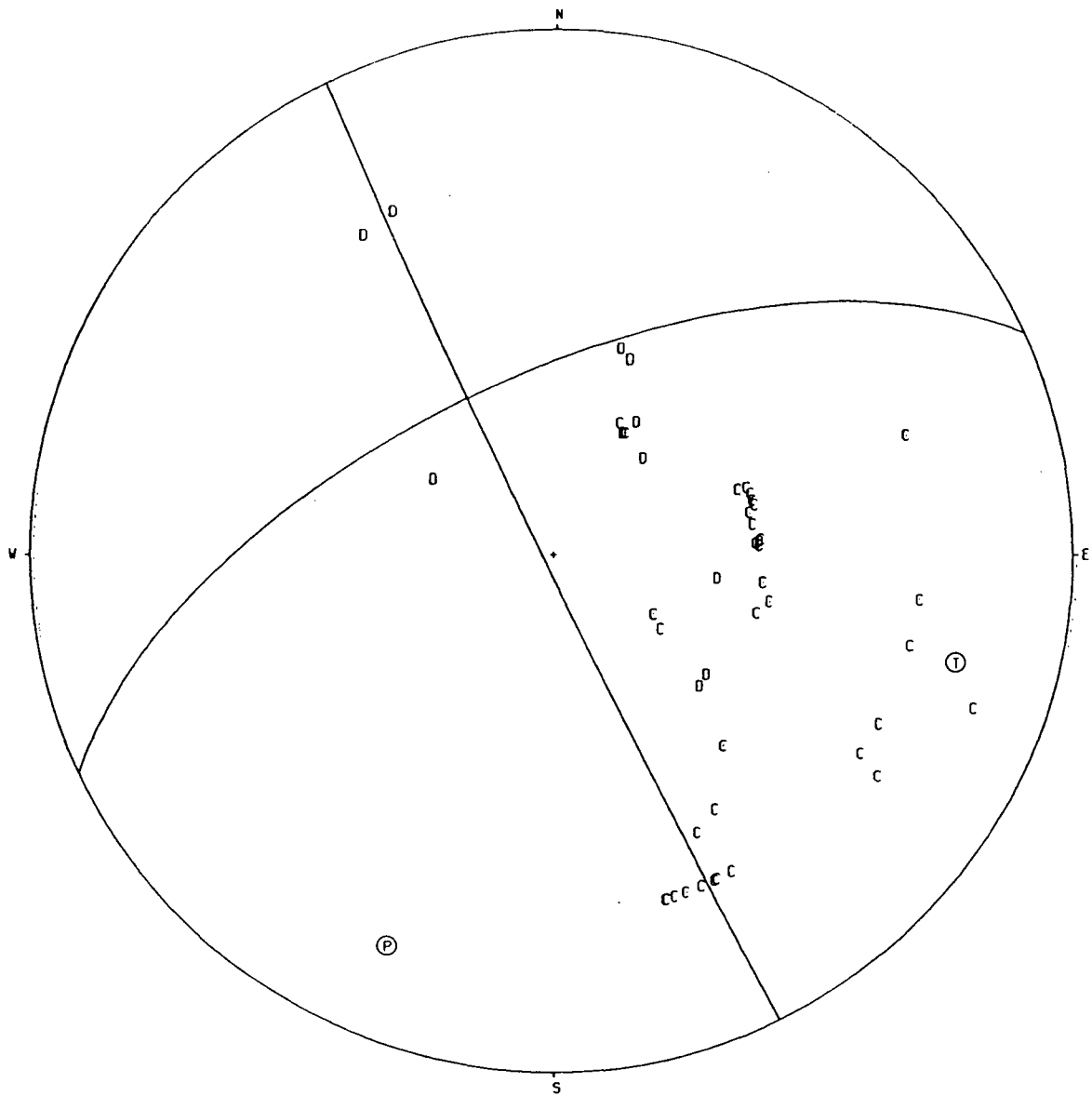


**Figure 15.** Best fit mechanism derived from surface wave analysis. P and T represent pressure and tension axes respectively. Observed first motions have been superimposed on this diagram; C's represent compressional arrivals and D's represent dilatational arrivals.

to nodal lines (which have only been resolved to  $3^\circ - 4^\circ$ ). The surface wave solution provides a good fit to the majority of the first motion data.

Tests were made with a different earth model and attenuation values to determine the effect this might have on the surface wave solution. Applying the Gutenberg earth model resulted in slight changes in theoretical spectral amplitudes ( $\leq 5\%$  over most of the period range 10 – 100 seconds except near 30 – 40 seconds where differences of up to 20% were observed); however this did not change the best fit solution. The attenuation values of Herrmann (1978), which were derived for the stable shield of continental North America (these are between 1.1 and 3 times lower than the values of Tsai and Aki (1970)) were applied to these data. This did not result in a change in best fit mechanism as determined by the program QUESTION but did result in a lower seismic moment estimate ( $5.6 \times 10^{24}$  dyne-cm compared to the previous estimate of  $8.1 \times 10^{24}$  dyne-cm). Therefore, the earth model or attenuation values applied do not appear to have a significant affect on the solution obtained. The world-wide averaged attenuation values of Tsai and Aki (1970) are preferred for this study as all recorded surface waves have crossed major structural boundaries (continental/oceanic boundaries and the cordilleran region). The attenuation values of Herrmann (1978) are likely too low for such travel paths.

Theoretical radiation patterns for Rayleigh and Love waves for the best fit surface wave mechanism (at 30 km depth) were generated and plotted using Herrmann's program RADPAT. Figures 16 – 18 illustrate both the theoretical amplitude patterns (solid curves) for Love waves, Rayleigh horizontal and Rayleigh vertical waves, and the observed spectral amplitudes (corrected for anelastic attenuation and normalized to a reference distance of 1000 km). There is considerable scatter, particularly for Rayleigh

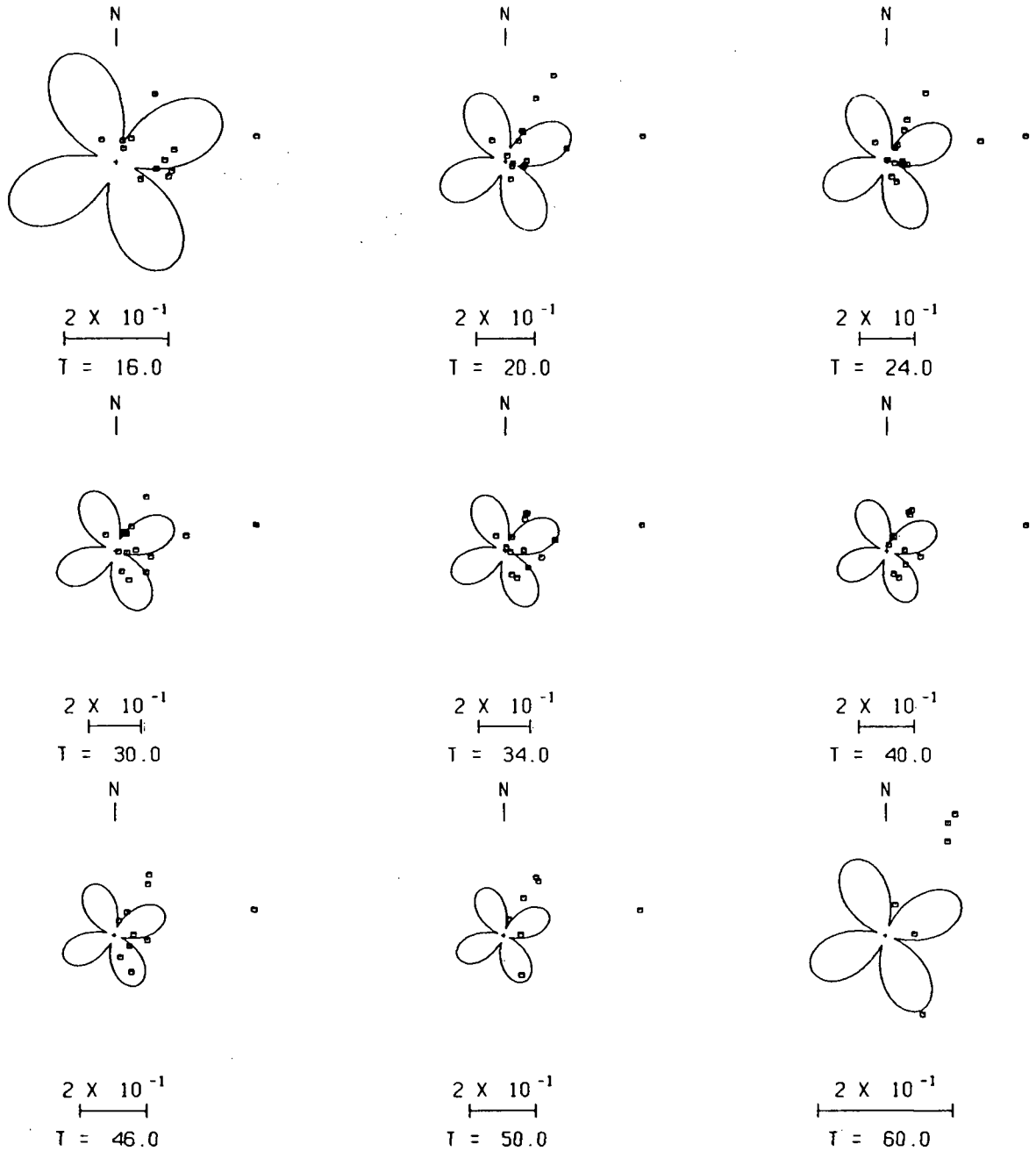


**Figure 16.** Observed (dots) and theoretical (solid lines) Love wave radiation patterns for the best fit surface wave mechanism. Each dot represents a spectral amplitude at a station. The azimuth of the dot represents the station azimuth, and the distance from the centre of the pattern is proportional to the spectral amplitude (normalized to a distance of 1000 km). The period, as well as a scale relating the plot size to units of dyne-cm is written below each pattern.

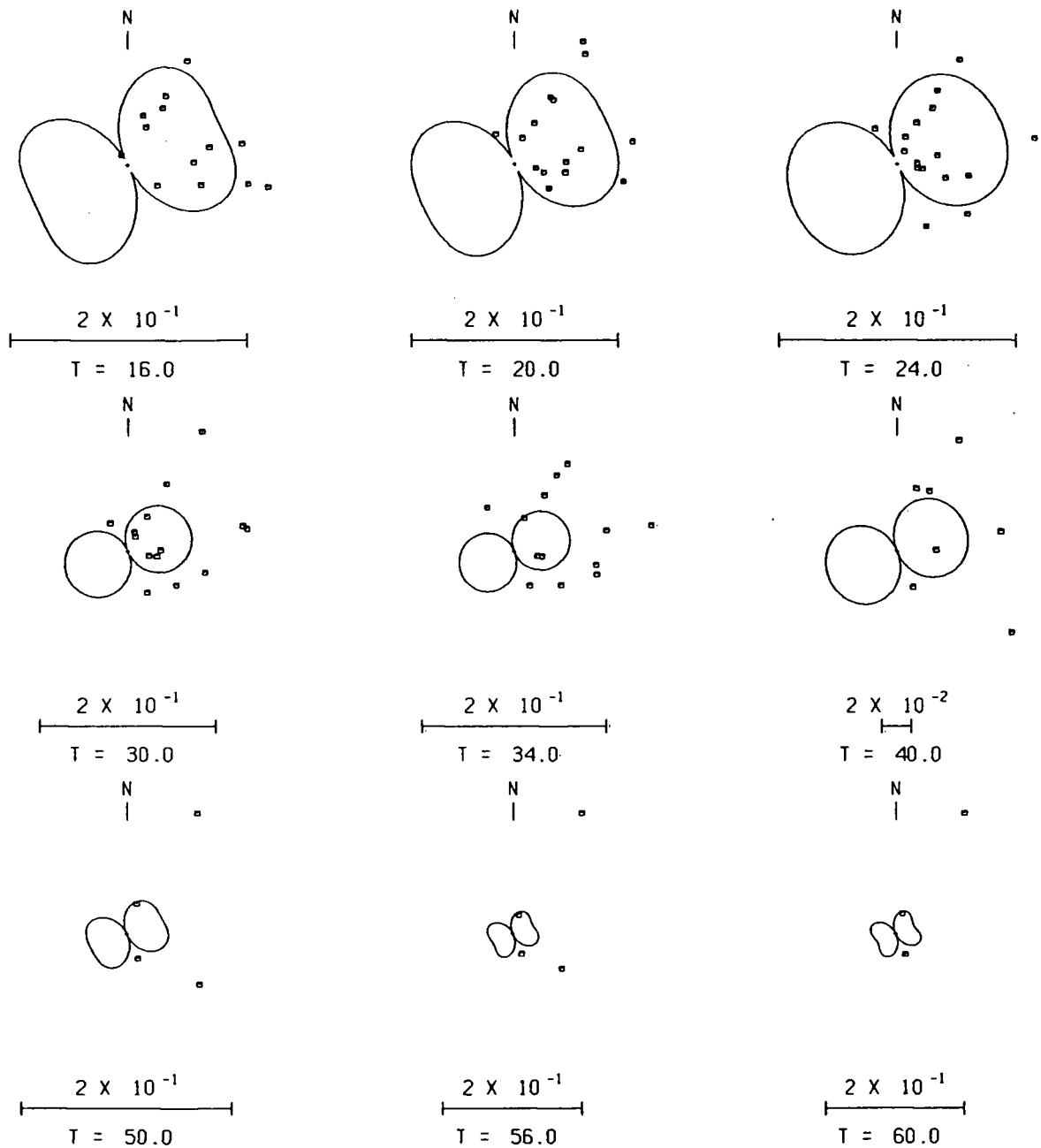


**Figure 17.** Observed (dots) and theoretical (solid lines) horizontal Rayleigh wave radiation patterns for the best fit surface wave mechanism. Each dot represents a spectral amplitude at a station. The azimuth of the dot represents the station azimuth, and the distance from the centre of the pattern is proportional to the spectral amplitude (normalized to a distance of 1000 km). The period, as well as a scale relating the plot size to units of dyne-cm is written below each pattern.

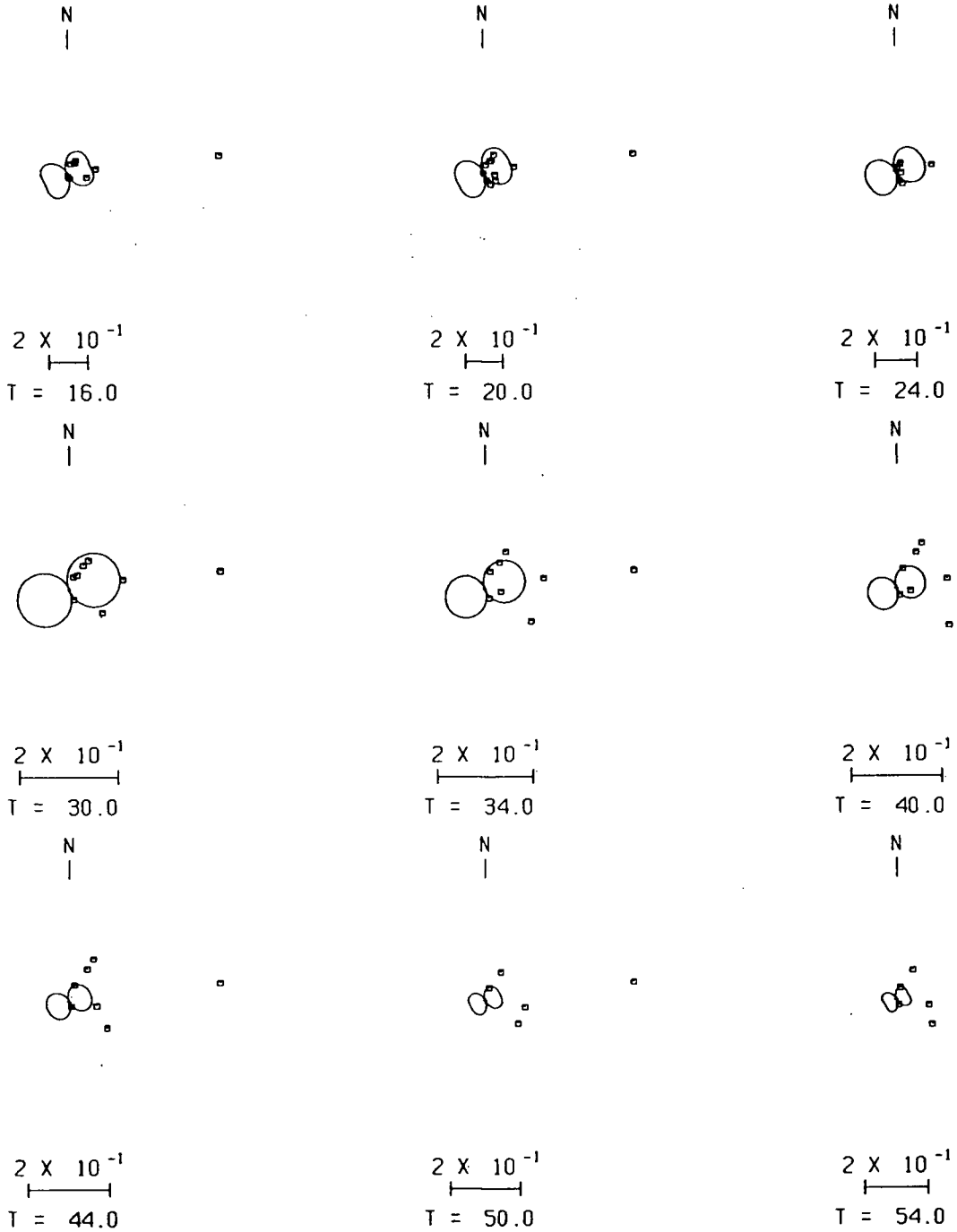


**Figure 18.** Observed (dots) and theoretical (solid lines) vertical Rayleigh wave radiation patterns for the best fit surface wave mechanism. Each dot represents a spectral amplitude at a station. The azimuth of the dot represents the station azimuth, and the distance from the centre of the pattern is proportional to the spectral amplitude (normalized to a distance of 1000 km). The period, as well as a scale relating the plot size to units of dyne-cm is written below each pattern.

waves; however the overall fit seems reasonable. The Love waves appear to fit a four lobed pattern while the Rayleigh waves fit a two lobed pattern.

Observed amplitudes for the station WES (azimuth=  $79.3^\circ$ ) appear far too large for all periods of Love and horizontal Rayleigh waves. However, the magnification of this instrument was not accurately known (the seismograms were marked "magnification = 3000 ?" – and no other information can be located). Other stations which are not in close agreement with the theoretical radiation patterns are SIT (azimuth=  $328^\circ$ ) and the California stations PAS and BRK (azimuth  $\approx 163^\circ$ ). It should be noted that for these stations surface waves from this earthquake have travelled along the continental/oceanic boundary. It is likely that these waves have been refracted or the energy has been partitioned in some way (i.e. mode conversion (see Gregersen and Alsop, 1976)) by this boundary. Figures 16 and 17 indicate that the long period waves ( $>50$  seconds) are in better agreement with the theoretical pattern than are the short period waves. This would be expected as long period waves, having a long wavelength, are less affected by shallow (10 – 35 km) boundaries. Vertical Rayleigh waves at the station PAS provide a better fit than do horizontal Rayleigh or Love waves (Figure 18). This also might be expected as the radial (Rayleigh horizontal) and transverse (Love) waves were obtained by rotating the E–W and N–S seismograms, assuming a straight line source – receiver path. In the case of refraction this is not true and will result in additional error in spectral amplitude determinations.

Observed spectral amplitudes at the four European stations (azimuth=  $18^\circ - 25^\circ$ ) also provide a poor fit to the theoretical patterns. Most notably, the Love waves at these stations have a larger amplitude than the theoretical pattern predicts. Surface waves observed at these stations have traversed several continental/oceanic boundaries.

In addition, due to large epicentral distances ( $\approx 60^\circ - 70^\circ$ ) these stations are subject to the largest errors due to the uncertainty in anelastic attenuation values. Therefore, the stations which deviate the most from the best fit mechanism radiation patterns are those which would be expected to have the largest errors. Considering the uncertainties in the magnification of most of the instruments, the mixed travel-paths which the surface waves have traversed and the uncertainty in attenuation values, these data provide a reasonable fit to the theoretical radiation patterns.

As a further check of possible mechanism solutions, the theoretical radiation patterns of the best fit P-nodal, and the two alternate but slightly lower scoring solutions are plotted in Figures 19 – 21. The top scoring P-nodal mechanism provides a good fit to the Love waves, however the Rayleigh waves are a poor fit (Figure 19). The two-lobed pattern at periods of 30 – 40 seconds appears to be rotated by approximately  $90^\circ$  from the observed data. This drastic change in radiation patterns, by what appears to be a relatively minor difference in focal mechanism (between the best fit P-nodal solution, and the best fit surface wave solution (Figure 22)) is due to the pressure axis azimuth being rotated by  $180^\circ$  in the surface wave solution relative to the P-nodal solution. It should be noted that the orientation of the pressure axis determined by the surface wave data is in good agreement with the orientation of pressure axes of other events in this region (Figure 4). The second highest scoring P-nodal solution provides a poor fit to both Rayleigh and Love waves (Figure 20). The third possible P-nodal solution provides a reasonable fit to the observed Rayleigh waves but does not fit the Love waves (Figure 21).

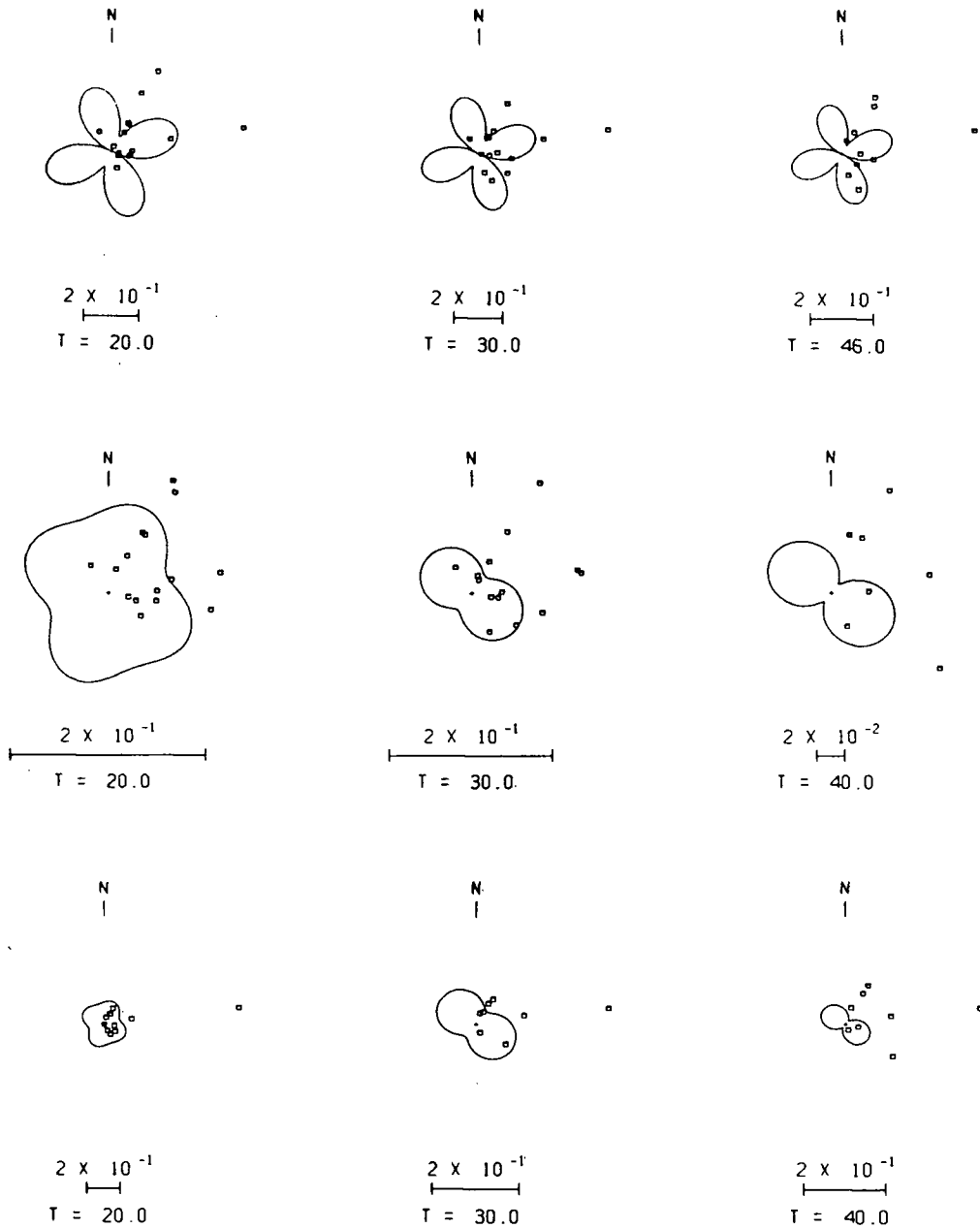


**Figure 19.** Observed (dots) and theoretical (solid lines) Love wave (top), horizontal Rayleigh wave (middle) and vertical Rayleigh wave (bottom) radiation patterns for the top scoring P-nodal solution (Fig. 13a). Each dot represents a spectral amplitude at a station. The azimuth of the dot corresponds to the station azimuth, and the distance from the centre of the pattern is proportional to the spectral amplitude (normalized to a distance of 1000 km). The period, as well as a scale relating the plot size to units of dyne-cm is written below each pattern.

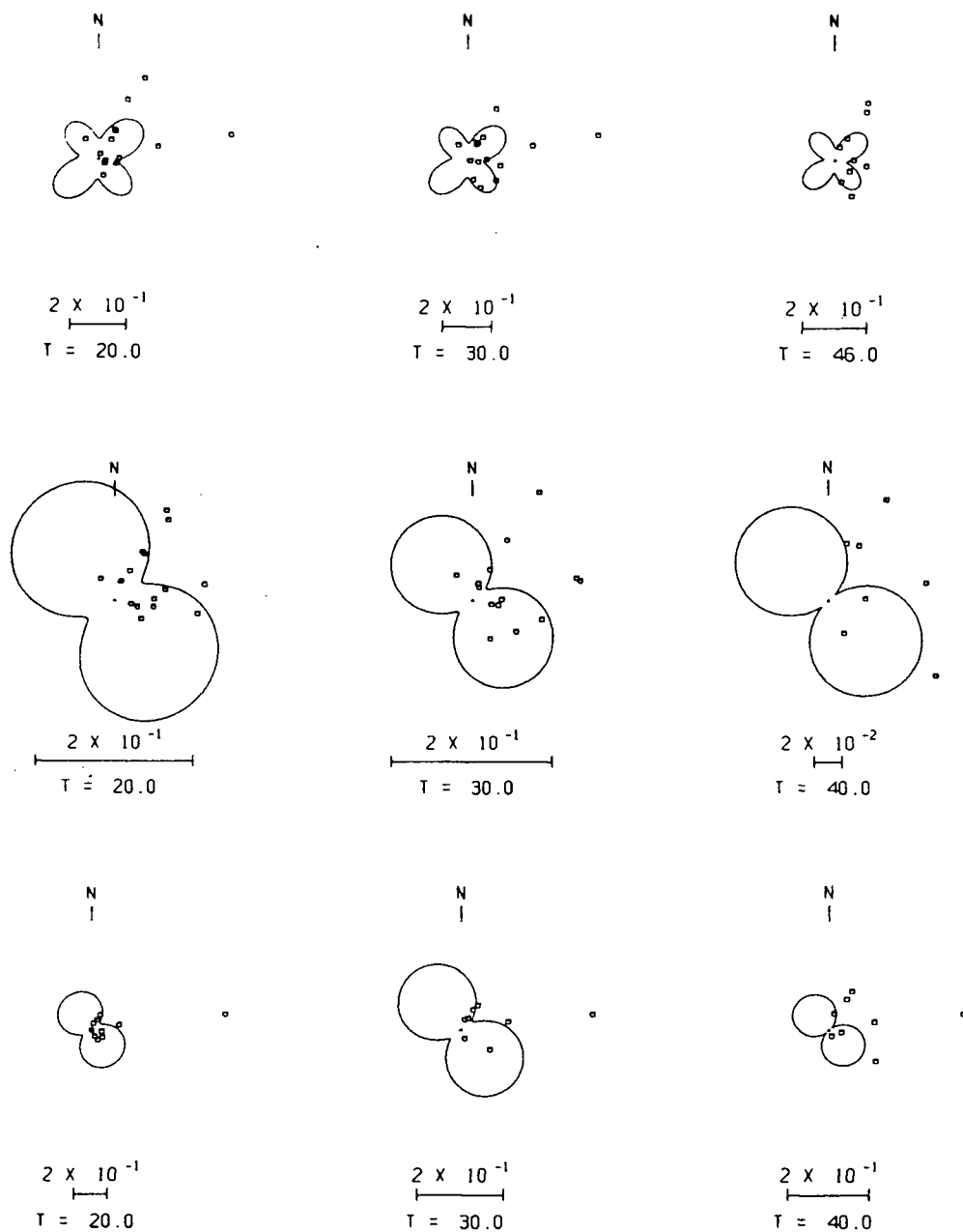


**Figure 20.** Observed (dots) and theoretical (solid lines) Love wave (top), horizontal Rayleigh wave (middle) and vertical Rayleigh wave (bottom) radiation patterns for the alternate P-nodal solution (Fig. 13b). Each dot represents a spectral amplitude at a station. The azimuth of the dot corresponds to the station azimuth, and the distance from the centre of the pattern is proportional to the spectral amplitude (normalized to a distance of 1000 km). The period, as well as a scale relating the plot size to units of dyne-cm is written below each pattern.

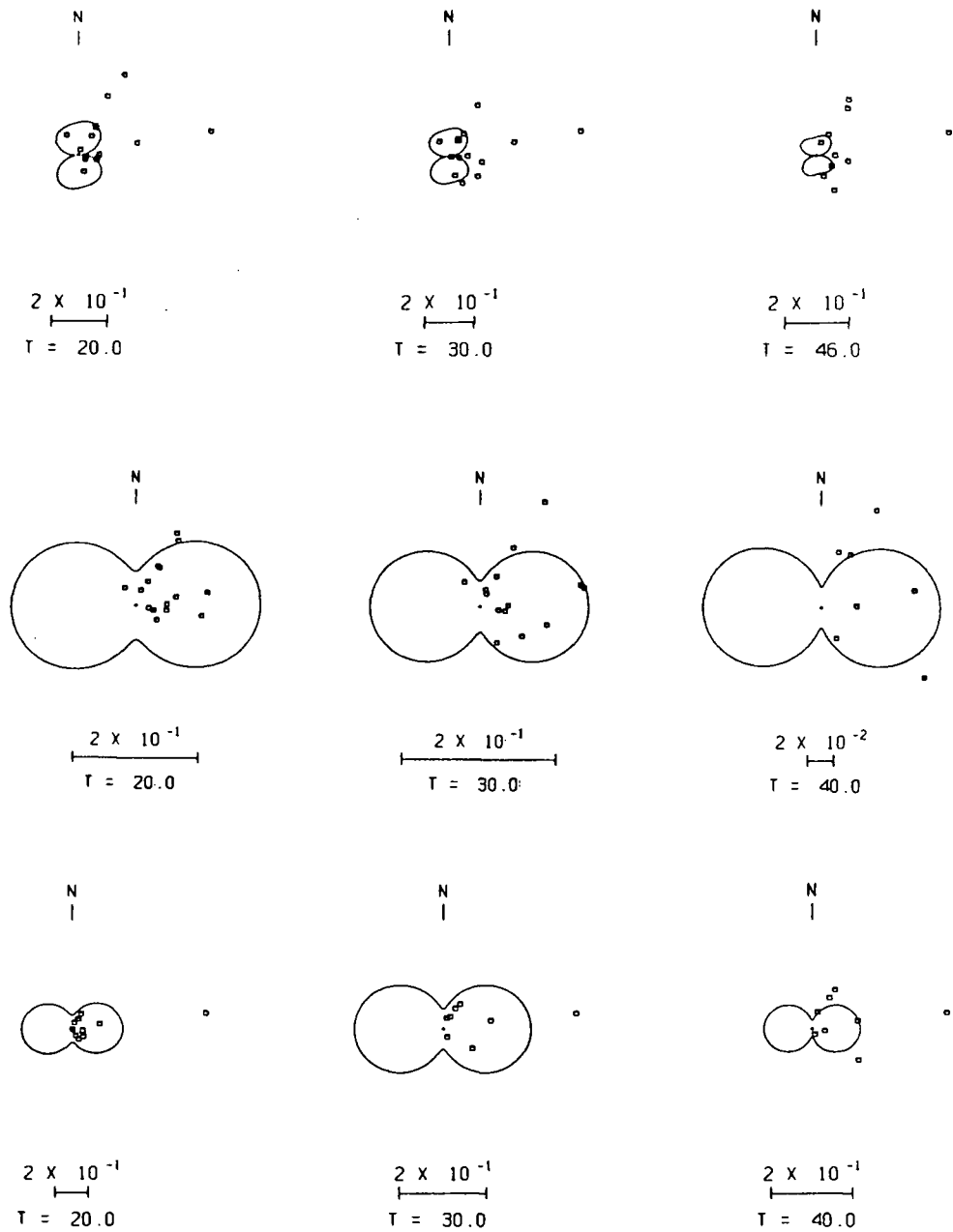


**Figure 21.** Observed (dots) and theoretical (solid lines) Love wave (top), horizontal Rayleigh wave (middle) and vertical Rayleigh wave (bottom) radiation patterns for the alternate P-nodal solution (Fig. 13c). Each dot corresponds to a spectral amplitude at a station. The azimuth of the dot represents the azimuth of the station, and the distance from the centre of the pattern is proportional to the spectral amplitude (normalized to a distance of 1000 km). The period, as well as a scale relating the plot size to units of dyne-cm is written below each pattern.

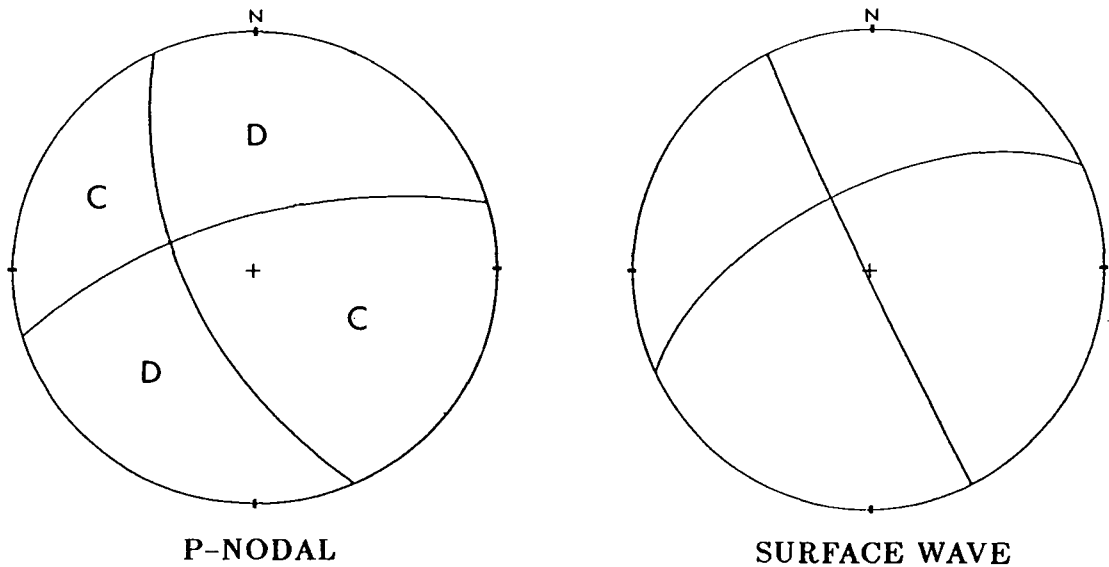


**Figure 22.** Comparison of the top-scoring P-nodal solution with the best fit surface wave solution for the 1957 earthquake. The lower hemisphere projection of the focal sphere is shown.

In summary, the best fit surface wave mechanism is similar to the best fit P-nodal solution (see Figure 22) in that it suggests a predominantly strike-slip earthquake. The P-nodal method suggests either left-lateral motion along a fault striking  $N74^{\circ}E$  and dipping  $71^{\circ}$ , or right-lateral motion along a fault striking  $N24^{\circ}W$  and dipping  $67^{\circ}$ . The surface wave analysis suggests either a fault striking  $N65^{\circ}E$  and dipping  $62^{\circ}$ , or a fault striking  $N26^{\circ}W$  with a dip of  $88^{\circ}$ . The surface wave mechanism has been resolved to  $3 - 4^{\circ}$ , and likely has a total uncertainty of about  $\pm 10^{\circ}$ .

It is possible that the differences between the P-nodal and surface wave mechanisms are real. Body waves provide information on the point of initial rupture. However, surface waves, having a longer wavelength, provide information over a larger region of the fault. If the mechanism did not change during the rupture, then the surface wave mechanism is the preferred solution. The radiation pattern of the top scoring P-nodal solution provides a very poor fit to the observed Rayleigh wave spectral amplitudes

(Figure 19). The surface wave mechanism however, provides a good fit to the first motion data (Figure 15). In addition this mechanism has a pressure axis orientated near  $200^\circ$ , in agreement with other earthquakes in this region (see Figure 4).

### 3.6 Seismic Moment, Stress Drop and Aftershocks

The seismic moment of this earthquake is estimated using Herrmann's program QUESTION. This calculates the seismic moment independently from the Rayleigh and Love waves and averages the two estimates. From the best fit solution at a depth of 30 km the average seismic moment estimates are  $M_o = 8.16 \times 10^{24}$  dyne-cm (Love),  $M_o = 8.11 \times 10^{24}$  dyne-cm (Rayleigh) with the average  $M_o = 8.14 \times 10^{24}$  dyne-cm. This estimate is subject to errors involving:

- 1) focal depth – varying this from 25 to 40 km results in variations of up to 20% in seismic moment.
- 2) attenuation values – use of Herrmann (1978) attenuation values reduces the seismic moment by 35%. These attenuation values, derived for the shield region, are not entirely valid for travel paths considered in this study. Uncertainties in seismic moment due to the lack of accurate attenuation values are likely closer to  $\pm 20\%$ .
- 3) intrinsic error in the surface wave data – the effect of this on moment estimates cannot be estimated.

Therefore, uncertainties in the seismic moment estimate of about 40% (or more) are possible.

Applying the Kanamori and Anderson (1975) relation between seismic moment and surface wave magnitude results in a stress drop estimate of 36 bars for this earthquake. This is close to the stress drop of  $\approx 30$  bars they suggested for interplate earthquakes.

The seismic moment estimate is also subject to large uncertainties. Given the uncertainty of  $\pm 40\%$  in the seismic moment estimate, and the uncertainty of  $\pm 0.2$  in  $M_s$ , stress drops ranging from 20 bars to 90 bars are possible.

Applying the seismic energy- magnitude relation of Gutenberg and Richter (1956)

$$\log E_s = 1.5M_s + 11.8$$

yields an energy of  $E_s = 5.3 \times 10^{20}$  erg.

This earthquake had only one recorded aftershock. It occurred on December 17 at 07 46 15.4 and was recorded at ALB only. Milne (unpublished worksheets) estimated the distance to be 150 km from this station, and the magnitude to be  $M_L = 2.8$  (the lowest detectable magnitude at this time was  $M_L = 2.3$  (Rogers, 1979)). Gibowicz (1973) determined a relation between the stress drop of an earthquake and the difference between the magnitude of the earthquake ( $M$ ) and that of its largest aftershock ( $M_1$ ). For events having  $M - M_1 > 1.2$ , the stress drop of the main shock was determined to be higher than average. Based on this work, and the value of  $M - M_1 = 3.6$  for the 1957 earthquake; Rogers (1979) postulated that this event had a larger than average stress drop, and may be an intraplate event. The stress drop estimated from the seismic moment in this study does not support this interpretation, as intraplate events have a stress drop of 100 bars or more (Kanamori and Anderson, 1975).

## CHAPTER IV

## THE DECEMBER 6, 1918 EARTHQUAKE – RESULTS

## 4.1 Introduction and Intensity

“City Shaken By Quake – People Awakened From Sleep By Rattling of Furniture – People, Panic-stricken, Rush In Night Attire Into Streets Fearing Buildings Would Fall”; this headline, in the December 6, 1918 edition of the Vancouver Sun, describes how one of British Columbia’s largest recorded earthquakes was felt in Vancouver. This earthquake occurred at 08 41 U.T. (00 41 local time) and was felt throughout Vancouver Island, as well as in Vancouver, Seattle and possibly (see discussion below) the Okanagan Valley community of Kelowna, approximately 470 km from the epicentre.

Due to sparse population, no injuries and little damage resulted from this earthquake. Other than broken dishes and some instances of cracked plaster on central Vancouver Island, the only damage reported was to the Estevan Point lighthouse. The steel reinforced concrete of the 110 foot tower cracked its full length in several places, and parts of the glass lens were smashed, temporarily rendering the lighthouse inoperable.

Felt information (Figure 23) was obtained from newspaper reports from communities throughout British Columbia and northern Washington state, and from information collected and published by Denison (1919). The latter, which is very comprehensive, provided most of the information for this study. Due to sparse population the isoseismal lines are poorly constrained; circles have simply been drawn around the preferred epicentre to separate the observed intensity data.

The earthquake was felt most severely at Estevan Point, where damage indicative of intensity VI – VII on the modified Mercalli scale occurred. Throughout central

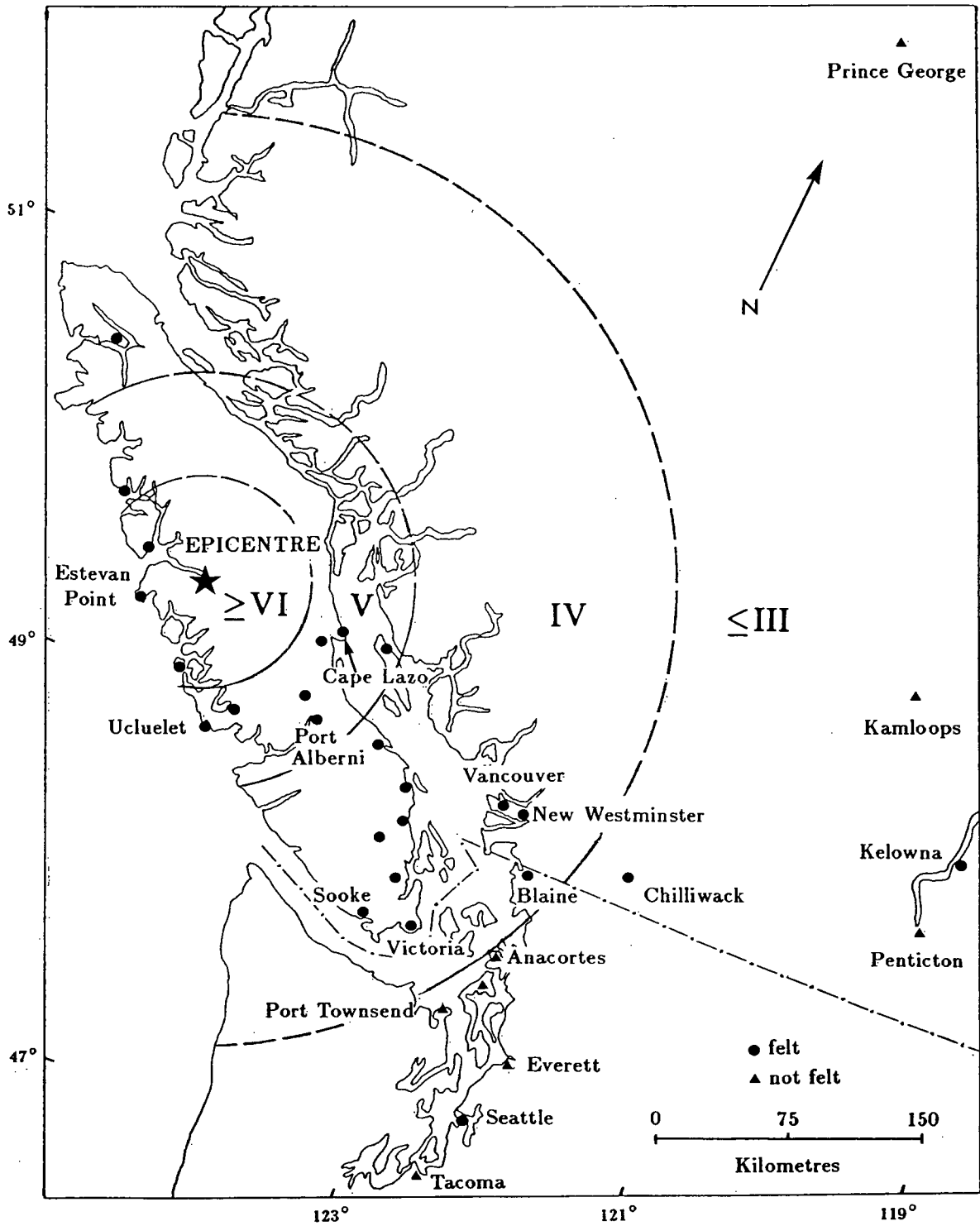


**Figure 23.** Isoseismal map for the December 6, 1918 earthquake. Solid lines indicate regions where the isoseismal curves are better constrained.

Vancouver Island the intensity appears to be V based on numerous reports of windows rattling, pendulum clocks stopping, pictures and dishes falling to the floor and some instances of cracked plaster. Other reports from this region include Ucluelet, where several weak wharf pilings were broken, and Port Alberni where "one house rocked so much that chairs appeared to rock six inches out of the vertical" (Denison, 1919).

In Vancouver the intensity also appears to be V based on reports of clocks stopping and light objects falling to the floor. This high intensity may be due in part to soil conditions or simply the large population (more observers and therefore a better chance of the earthquake being noticed); it should be noted that in the surrounding areas this earthquake was felt as intensity IV or less. In New Westminster, 20 km east of Vancouver, many people slept through the earthquake, and in Blaine, 40 km south of Vancouver, the shaking did not awaken the majority of the people. In Victoria it was felt as intensity IV, while in Sooke, 25 km west of Victoria, only 2 people out of 15 interviewed after the earthquake felt it.

This earthquake shook furniture and rattled dishes in downtown Seattle for about 90 seconds. In the outlying areas however, again it was not felt as severely. Newspapers in Everett, Tacoma, Anacortes and Port Townsend (Figure 23) contain no local reports of this earthquake being felt. In Kelowna, about 470 km from the epicentre, several pendulum clocks stopped, several people heard a noise but felt no shaking, and one person felt a building on a wharf sway. However, there are no reports of this earthquake being felt in other interior communities (Penticton, Kamloops, Prince George), so the possibility of the Kelowna shaking being caused by a small local tremor, or some other phenomena cannot be ruled out. If the Kelowna reports were a result of the Vancouver

Island earthquake then the total felt area, obtained by drawing a circle around the epicentre and limited in radius by Kelowna, is approximately 690,000 km<sup>2</sup>.

#### 4.2 Epicentre Location

The epicentre of this event was examined by the teleseismic method. In the following studies it was found that the Dziewonski and Anderson (1981) earth model with Dziewonski and Anderson (1983) station corrections provided both the largest number of stations in the final solution and the smallest travel-time residuals. A depth of 0 km usually provided the smallest residuals, although these varied only slightly (<0.1 sec) over the focal depth range 0–30 km. Epicentre estimates are also insensitive to variations of 0–30 km in focal depth, moving less than 0.1°. Unless otherwise indicated the following results were obtained using the Dziewonski and Anderson earth model and station corrections, a fixed focal depth of 0 km and travel-time residual rejection limits of 10.0 sec, 6.0 sec and 4.0 sec.

Initially this earthquake was located using only the arrival times as listed in the 1918 ISS bulletin (Test 1). This data set includes 46 arrival times, of which 10 have residuals greater than 60 seconds. The solution obtained (Table VI) is 49.61°N, 126.09°W (Figure 24). A larger data set, given in Appendix C, includes the ISS data and three arrival times obtained from seismograms of European stations. Arrival times could be read directly from seismograms of 16 stations, however only two improvements (NRT, EBR) were made to the times listed in the ISS. Using this complete data set (Test 2) resulted in an epicentre estimate of 49.63°N, 126.08°W (Figure 24). Given the poor quality of the data (many first motions were of low amplitude), the travel-time residual rejection limits were increased to 20.0 sec, 15.0 sec and 10.0 sec to determine the possible effect

on the epicentre estimate (Test 3). This allowed four additional stations to be included in the final solution and resulted in an epicentre slightly ( $0.1^\circ$ ) south of the previous estimate (Figure 24).

Table VI 1918 Epicentre estimates

| Test No. | Origin Time | Lat. ( $^\circ$ N) | Long. ( $^\circ$ W) | No. St. | $\sigma$ (sec.) |
|----------|-------------|--------------------|---------------------|---------|-----------------|
| 1        | 08 41 07.9  | 49.61              | 126.09              | 21      | 2.36            |
| 2        | 08 41 07.6  | 49.63              | 126.08              | 25      | 2.25            |
| 3        | 08 41 08.3  | 49.53              | 126.06              | 29      | 3.51            |
| 4        | 08 41 07.2  | 49.63              | 126.00              | 20      | 1.93            |
| 5        | 08 41 07.6  | 49.68              | 126.03              | 15      | 2.12            |
| 6        | 08 41 07.1  | 49.61              | 126.24              | 14      | 2.03            |
| 7        | 08 41 06.2  | 49.47              | 126.24              | 9       | 1.95            |

No. St. = Number of stations included in solution

$\sigma$  = standard deviation of travel-time residuals.

As there is such a small data set for this earthquake, the stability of the epicentre was examined as individual stations were excluded from the solution. The only station which, when not included in the solution, had a significant ( $> 0.05^\circ$ ) effect on the epicentre was HON. Excluding the HON arrival time from the data set resulted in an epicentre movement of  $0.15^\circ$  east. This however, may be a result of the azimuthal distribution of stations (only two stations – including HON, are in the azimuthal range  $180^\circ - 320^\circ$ ). This effect will be discussed at the end of this section.

Another study involved eliminating the possible effect of “late” picks (as described in the previous chapter). Test 4 includes all data except those stations having a positive

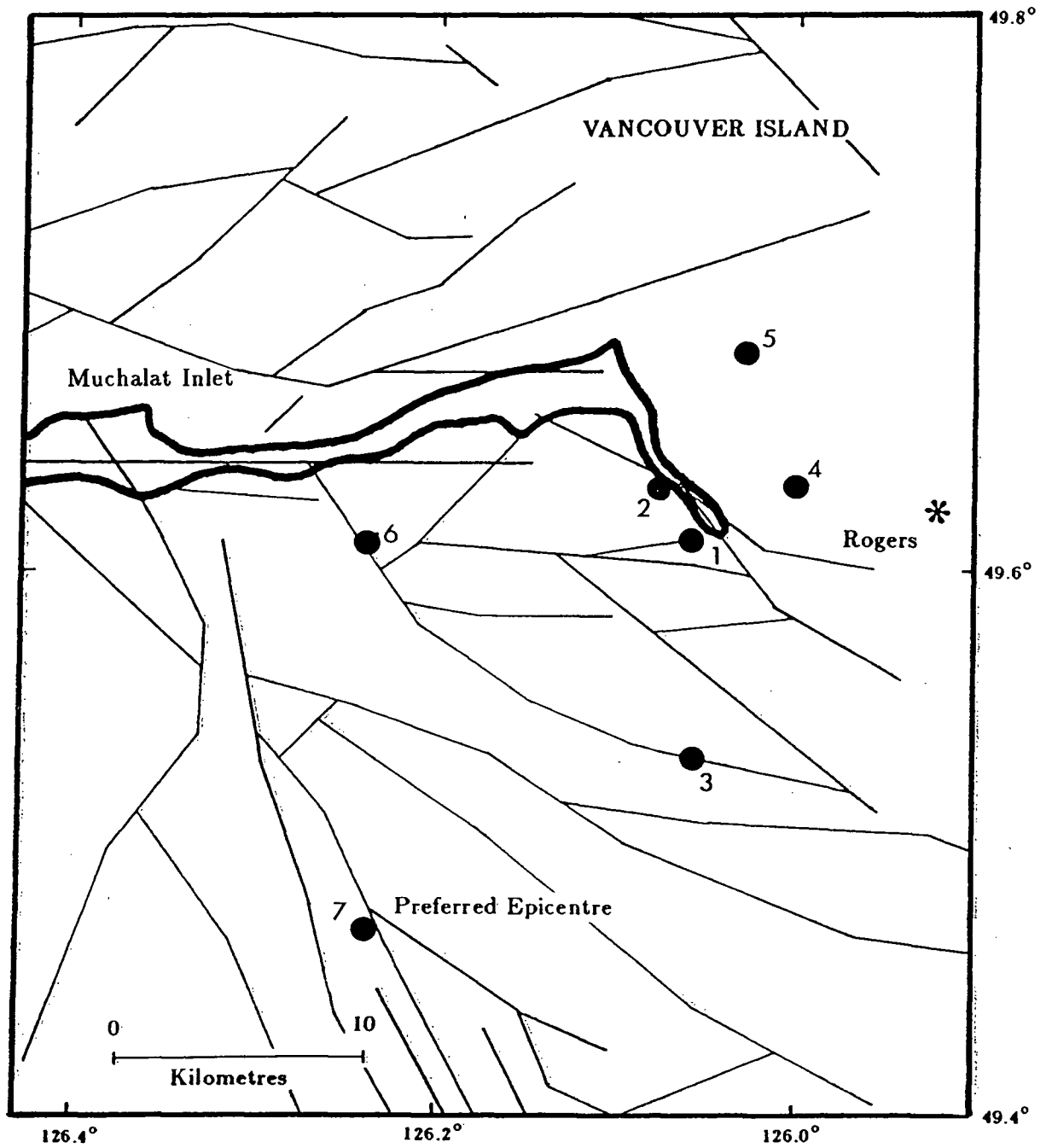


**Figure 24.** Epicentre estimates (at 0 km fixed depth), the preferred solution from this study, and the previous estimate of Rogers (1983). Numbers correspond to the various tests described in text (section 4.2). Thin lines represent surface faults (from Muller *et al.*, 1980).

travel-time residual greater than +2.0 seconds (4 from the United States and 1 from Europe). The result of  $49.63^{\circ}\text{N}$ ,  $126.00^{\circ}\text{W}$  is only slightly east of previous estimates (Figure 24).

Another test included only North American data for the epicentre determination (Test 5). Although this may introduce a bias because of the azimuthal distribution of stations about the epicentre (discussed at the end of this section) it is of interest because this event was better recorded in North America and first arrivals may be more accurate. For this study, the Herrin (1968) earth model and Veith (1975) station corrections were applied. The result of this test is  $49.68^{\circ}\text{N}$ ,  $126.03^{\circ}\text{W}$  (Figure 24). A test which should provide for a more accurate epicentre estimate is to consider only those stations having Dziewonski and Anderson (1983) station corrections. Using the Dziewonski and Anderson earth model, the epicentre obtained from this study (Test 6) is  $49.61^{\circ}\text{N}$ ,  $126.24^{\circ}\text{W}$  (see Table VI, Figure 24). This solution is significantly west of previous estimates (but also has a smaller RMS error). In order to reduce the effect of upper mantle structure (as described in the previous chapter) Test 7 involved only stations at epicentral distances greater than  $20^{\circ}$ , and having Dziewonski and Anderson station corrections. For both the 1972 and 1957 earthquakes, this data set resulted in an epicentre closest to that obtained from "local" methods. The epicentre estimated using this data set (Test 7) is  $49.47^{\circ}\text{N}$ ,  $126.24^{\circ}\text{W}$  (Figure 24, Table VI). This epicentre is southwest of most other estimates and in agreement with other studies – see Chapter III. It should be noted however, that only nine stations are included in the solution. By relaxing the constraints slightly, there are two ways to increase the size of the data set:

- 1) use all stations at epicentral distances greater than  $20^{\circ}$  (not just those having Dziewonski and Anderson station corrections)

- 2) use the 1957 and 1972 earthquakes to generate travel-time corrections for those stations at epicentral distances less than  $20^\circ$ , in order that they may be included in the study.

The first method resulted in an epicentre only  $0.05^\circ$  north of that obtained in Test 7. The second method resulted in an epicentre  $0.12^\circ$  east of that of Test 7. These studies serve to illustrate that the small data set of Test 7 does not produce an unreasonable epicentre. It should also be noted that using only stations at epicentral distances greater than  $20^\circ$  and having Dziewonski and Anderson station corrections (Test 7) shifted the epicentre southwest  $0.2^\circ$  relative to other estimates. This is comparable to the shift introduced using this restricted data set for the 1957 earthquake ( $0.22^\circ$ ), and the 1972 earthquake ( $0.15^\circ$ ).

A final consideration in this study is the azimuthal distribution of stations. Only two stations in the azimuth range  $165^\circ - 325^\circ$  recorded this earthquake, compared to 13 from the quadrant  $0^\circ - 90^\circ$ . An estimate of the effect of this distribution was made by again considering the 1972 earthquake (located just offshore). This event was first located using all data (220 stations, including 27 from azimuths of  $165^\circ - 325^\circ$ ). It was then located using a distribution of stations which matched the 1918 distribution as closely as possible (within  $10^\circ$  azimuth and  $5^\circ$  distance). The results indicate only a slight ( $0.08^\circ\text{N}$ ,  $0.02^\circ\text{E}$ ) shift in epicentre due to the limited data set. An estimate of the effect of using only North American data to locate an earthquake (see previous chapter) is to move an epicentre  $0.11^\circ\text{N}$ ,  $0.07^\circ\text{E}$ . The lack of earthquakes in this region large enough to be recorded worldwide does not permit a more thorough study of the effect of station distribution on epicentre estimates. This study however, indicates that

the limited azimuthal distribution of stations for the 1918 earthquake should not affect the epicentre estimate by more than 15 km.

The preferred epicentre for this earthquake is chosen to be that obtained using only stations at epicentral distances greater than  $20^\circ$  and having Dziewonski and Anderson station corrections (Test 7). This solution, ( $49.47^\circ\text{N}$ ,  $126.24^\circ\text{W}$ ) is preferred because it has the smallest RMS error of all tests (except Test 4 – which did not include stations having large positive residuals). In addition based on studies of the 1972 and 1957 earthquakes, this data set (reducing upper mantle effects) produces the most reliable epicentre estimates. Given the small data set (10–20 stations included in the solutions), the poor quality of many of the seismograms, and the limited azimuthal distribution of the stations, an uncertainty of  $\pm 30$  km must be considered possible for this earthquake. Surface faults of this region are shown in Figure 24. It is interesting to note that there are several mapped faults in the region of the preferred epicentre, including some of length 20 km or more (an earthquake of  $M_s = 7$  may have a rupture length of up to 35 km (Acharya, 1979)). It should be noted however, that many of these are inferred faults which are based on drainage patterns (inlets, stream beds, etc.) (see Muller *et al.*, 1980).

### 4.3 Focal Depth

Due to the poor quality of the body wave data, the phase pP could not be identified on any seismograms. In addition, for the preferred epicentre, travel-time residuals are insensitive to focal depth over the range 0–60 km, and therefore provide no information on the depth of this earthquake.

The focal depth was estimated by comparing the observed radiation pattern of surface waves with theoretical patterns generated at various depths. The surface wave correlation factor (as described in section 3.3) was calculated for the best fit mechanism (see section 4.5) at depths of 5 km to 50 km. Figure 25 shows the good fit at depths of 5 to 20 km, and the maximum correlation at a depth of 15 km. Based on these data (Figure 25), the preferred focal depth is 15 km, with bounds of 5 – 20 km estimated. However, these bounds must be considered a lower limit on the uncertainty, as the surface wave data set is small, and subject to intrinsic errors (see section 4.5).

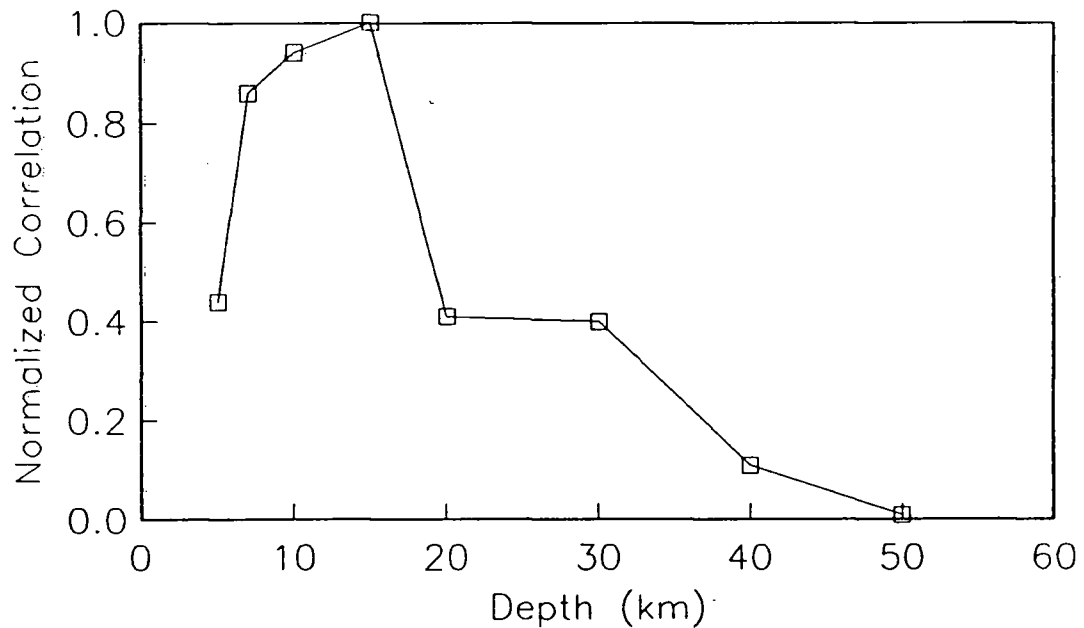


**Figure 25.** Plot of normalized surface wave correlation factor as a function of focal depth for the preferred mechanism.

A study by Page (1968) determined that well developed aftershock sequences only occur for shallow (<20 km depth) earthquakes. The large number of aftershocks (13 – 14) recorded for this event therefore support a shallow focal depth estimate. For a

magnitude 7 earthquake at a depth of 15 km, surface rupture is a distinct possibility (see Figure 24 for observed surface faults).

#### 4.4 Magnitude

Broad-band body wave (Gutenberg and Richter, 1956), surface wave (Vanek *et al.*, 1962; Gutenberg, 1945) and felt area (Topozada, 1975) magnitudes were determined for this earthquake. Although the Gutenberg surface wave magnitude is not in common use today, it was calculated in order to make a comparison with the magnitude determined for this earthquake by Gutenberg and Richter (1954). Seismograph calibration information for all stations considered in this study is given in Appendix C. Magnitudes were determined as described in section 3.4.

Results of all magnitude estimates are summarized in Appendix C. Using all data (if more than one magnitude estimate per station exists an average is taken, and magnitude estimates from seismograms are chosen over bulletin estimates) the following magnitudes are obtained:

$$M_s = 6.89 \pm 0.28 \quad (20 \text{ stations})$$

$$M_s^G = 6.75 \pm 0.25 \quad (17 \text{ stations})$$

$$m_b = 7.19 \pm 0.42 \quad (18 \text{ stations})$$

If only the "best" data are used (no station bulletin readings and only those stations for which two components were available and calibration data was sent with the records) the results are:

$$M_s = 7.00 \pm 0.19 \quad (3 \text{ stations})$$

$$M_s^G = 6.77 \pm 0.06 \quad (3 \text{ stations})$$

$$m_b = 6.95 \pm 0.49 \quad (2 \text{ stations})$$

In this case the larger data set probably results in the best estimate. The magnitude is therefore,  $M_s = 6.9 \pm 0.3$ ,  $M_s^G = 6.8 \pm 0.3$  and  $m_b = 7.2 \pm 0.4$ . Applying the equation of Gutenberg and Richter (1956) (see section 3.4) relating  $M_s$  and  $m_b$  results in an  $m_b = 6.8$  for a surface wave magnitude of 6.9.

If the Kelowna reports (section 4.1) can be attributed to this earthquake, then the total felt area (assuming a circular total felt area and extrapolating over oceanic regions) is 690,000 km<sup>2</sup>. Applying Topozada's (1975) equation for total felt area results in  $M_I = 7.0$ . A lower limit for the total felt area (assuming Seattle is the most distant felt report) is 430,000 km<sup>2</sup>. This results in a magnitude of  $M_I = 6.7$ . These values agree (within the estimated  $\pm 0.25$  uncertainty) with other magnitude estimates.

#### 4.5 Source Mechanism

Due to the poor quality of the body wave data a P-nodal study would not be useful for this earthquake. The first motions were in general very small, for most stations the polarity of the instruments were not known, and for several stations even the seismograph component was not indicated. Of the 15 first motions listed in Appendix C, only one (WAS) had both a clear arrival and the component and polarity indicated on the seismograms.

## Surface Wave Analysis

Surface waves generated by this earthquake recorded at ten stations with azimuths from  $327^\circ$  to  $164^\circ$  were available for analysis. The digitized surface waves are shown in Appendix C. Overall, the data is of poorer quality than that for the 1957 earthquake, the major problem being uncertainty in instrument parameters. In addition, all but one of the stations had seismographs with pendulum periods less than 20 seconds (and therefore are most sensitive to short period waves). For a magnitude 7 earthquake, which may have a rupture length of up to 35 km (Acharya, 1979), the point source approximation (discussed in section 3.5.2) may begin to break down for waves having periods less than 20 - 25 seconds (depending on the rupture velocity and orientation of the stations with respect to the fault (Tsai and Aki, 1970)). Therefore, this approximation must be considered another possible source of error in this analysis.

The program suite of Herrmann (1978) was again applied to the data to determine a total of 232 Love, Rayleigh horizontal and Rayleigh vertical spectral amplitudes (over a period range of 14 to 56 seconds) for the ten stations. Using these data with the earth model of Ben-Menahem and Singh (1981), the world-wide averaged attenuation values of Tsai and Aki (1970) and the program QUESTION, the best fit was determined to be slip =  $67^\circ$ , dip =  $76^\circ$  and strike =  $9^\circ$  (Figure 26) at a depth of 3 km, and with a seismic moment of  $0.9 \times 10^{26}$  dyne-cm.

Theoretical radiation patterns for Love and Rayleigh waves for this mechanism are compared to the observed data in Figure 27. This diagram shows that this "best fit" mechanism provides a good fit to the Love wave data but a poor fit to the Rayleigh wave data. For such a small data set a least squares approach (i.e. the program QUESTION) may not be very useful.

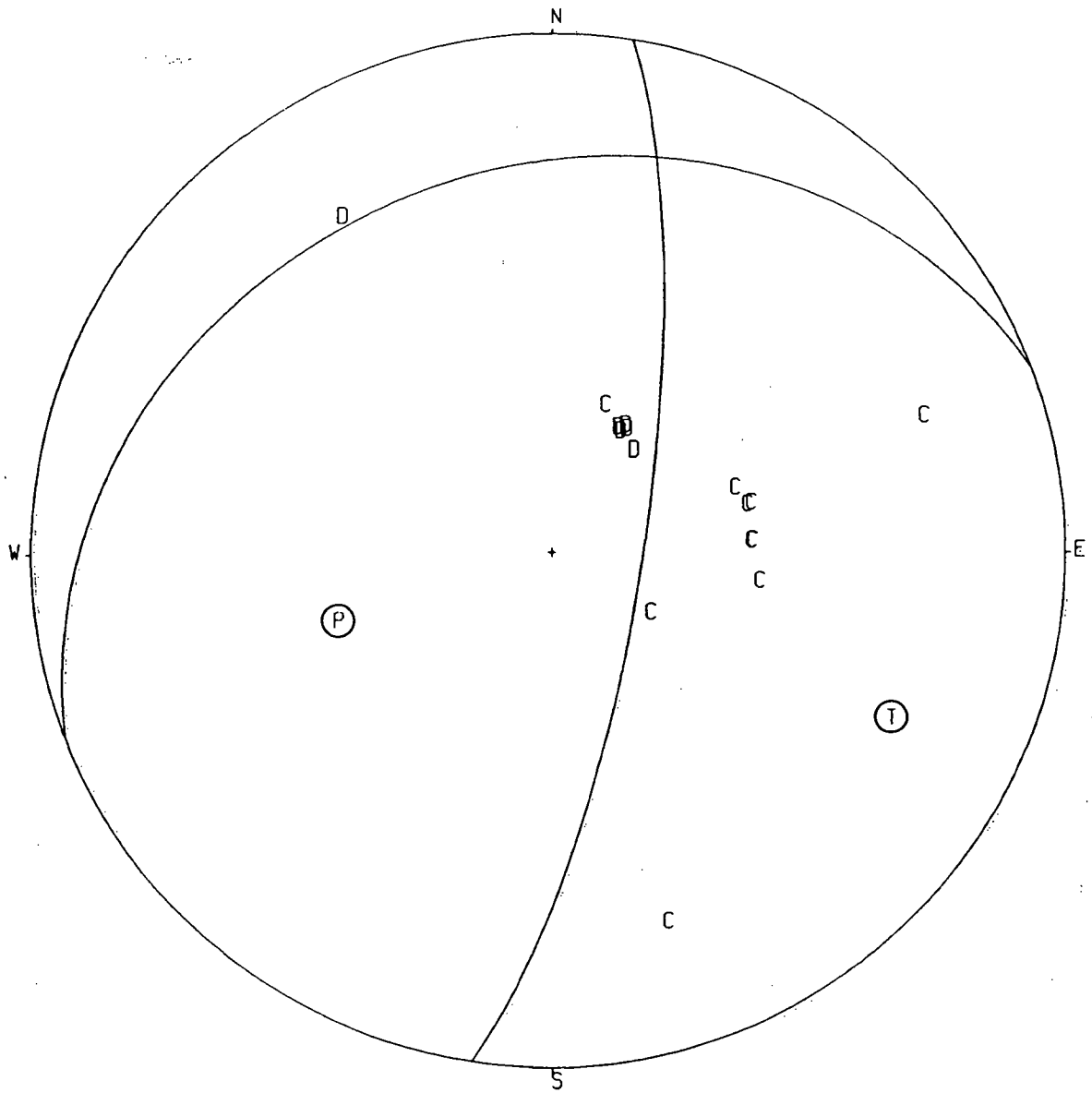


**Figure 26.** Best fit mechanism determined by the program QUESTION. Poorly defined first motion estimates have been superimposed on this plot; C's represent compressional arrivals; D's represent dilational arrivals; P and T represent the pressure and tension axes respectively.

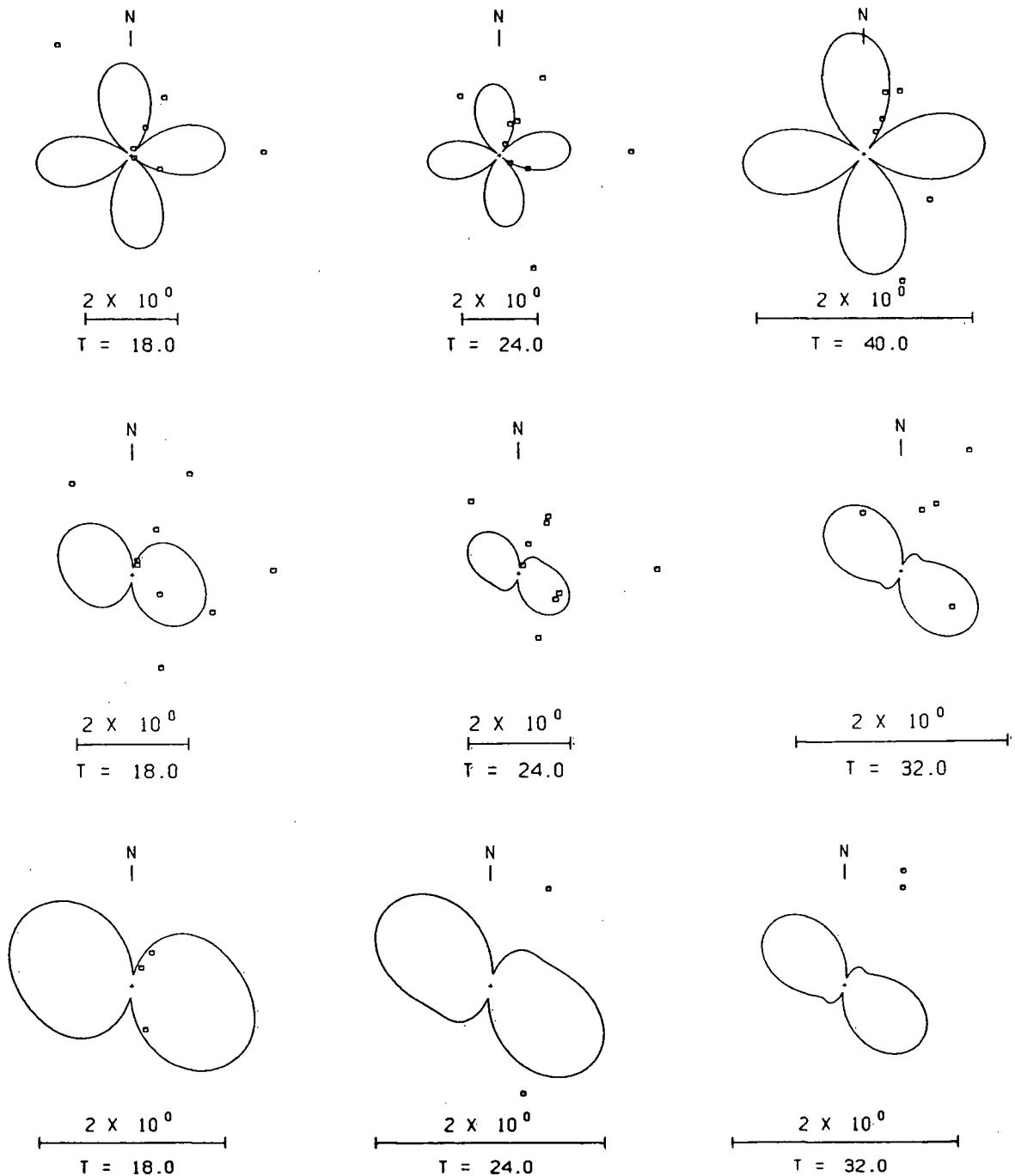


**Figure 27.** Observed (dots) and theoretical (solid lines) Love wave (top), Rayleigh horizontal (middle) and Rayleigh vertical (bottom) radiation patterns for the mechanism shown in Figure 26. Each dot represents the spectral amplitude at a station. The azimuth of the dot represents the station azimuth, and the distance from the centre of the pattern is proportional to the spectral amplitude (normalized to 1000 km). The period, as well as a scale relating the plot size to units of dyne-cm is written below each pattern.

For this case, the radiation pattern for mechanisms of other earthquakes in this region (1946, 1972, 1975 (see Figure 3), and the 1957 event (Figure 15)) were generated and compared to the observed data. In addition, the radiation patterns of thrust and normal mechanisms with a fault strike orientated parallel to the subduction zone (coastline) and dips ranging from  $10^\circ - 30^\circ$  (Figure 28), were generated and compared to the observed data. Due to the symmetry involved in surface wave patterns the thrust and normal mechanisms have the same theoretical radiation pattern. These mechanisms however, provide a poor fit to the observed data (Figure 29), and rule out this type of solution.

The 1975 mechanism (Figure 30), at a focal depth of 15 km and with a seismic moment of  $0.74 \times 10^{26}$  provides the best fit to the data. This solution, together with the few first motions available indicates either left-lateral, predominantly strike-slip motion along a fault striking  $N77^\circ E$  and dipping  $48^\circ NW$ , or predominantly right-lateral strike-slip motion with a large component of thrust along a fault striking  $N19^\circ W$  and dipping  $83^\circ SW$ . The pressure axis is orientated at  $217^\circ$  with a dip of  $23^\circ$ , and the tension axis is  $110^\circ$  with a dip of  $34^\circ$ .

Figures 31 - 33 show the observed and theoretical radiation patterns for this mechanism. The Love wave pattern provides a good fit to the data, and the Rayleigh wave pattern fits the nearly E-W lobe observed in the data (especially for periods near 18 - 24 seconds where the surface wave energy was best recorded). The stations which deviate the most from these patterns are again those stations (MHC, SIT) for which surface waves have propagated along the continental/oceanic boundary.

The fits provided by the other mechanisms (1946, 1957 and 1972) are given in Appendix C. The 1957 mechanism provides only a slightly poorer fit than the 1975

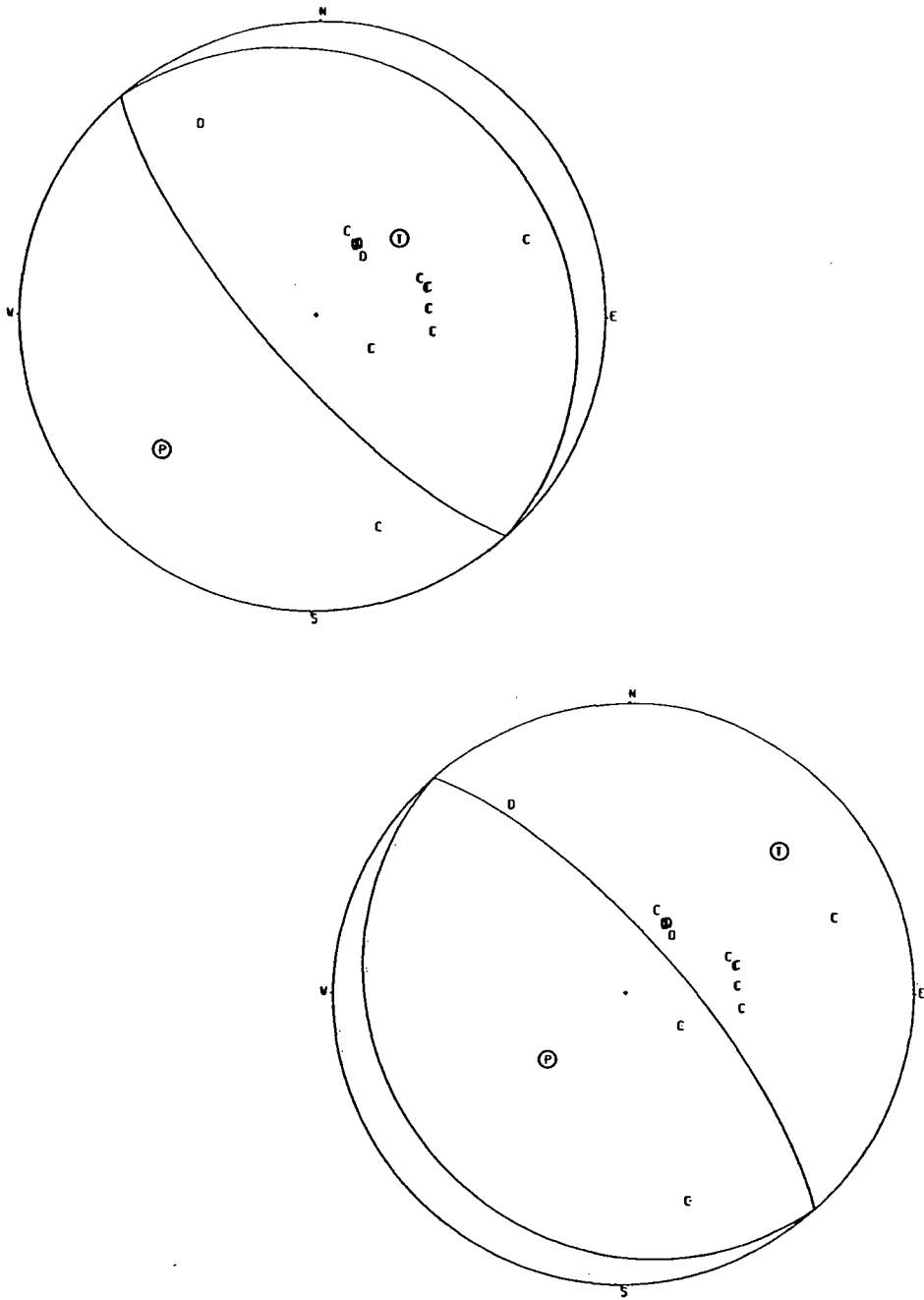


**Figure 28.** Examples of the thrust (top) and normal (bottom) mechanisms considered in the surface wave analysis. Circles represent the lower hemisphere projection of the focal sphere. Poorly defined first motion estimates have been superimposed on this plot; C's represent compressional arrivals; D's represent dilational arrivals; P and T represent the pressure and tension axes respectively.

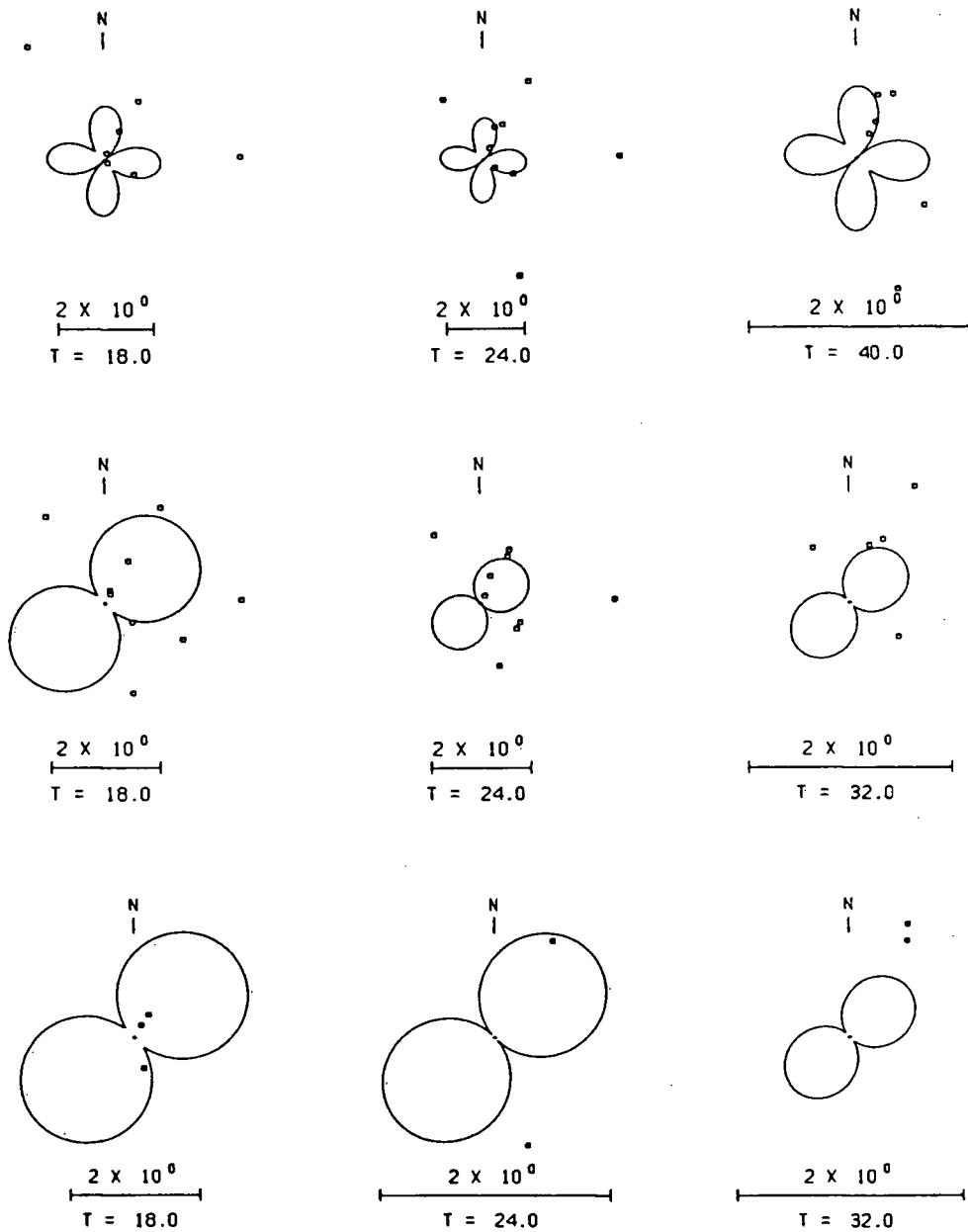


**Figure 29.** Observed (dots) and theoretical (solid line) Love wave (top), horizontal Rayleigh wave (middle), and vertical Rayleigh wave (bottom) radiation patterns for the thrust and normal mechanisms shown in Figure 29. Each dot represents the spectral amplitude at a station. The azimuth of the dot represents the station azimuth, and the distance from the centre of the pattern is proportional to the spectral amplitude (normalized to 1000 km). The period, as well as a scale relating the plot size to units of dyne-cm is written below each plot.

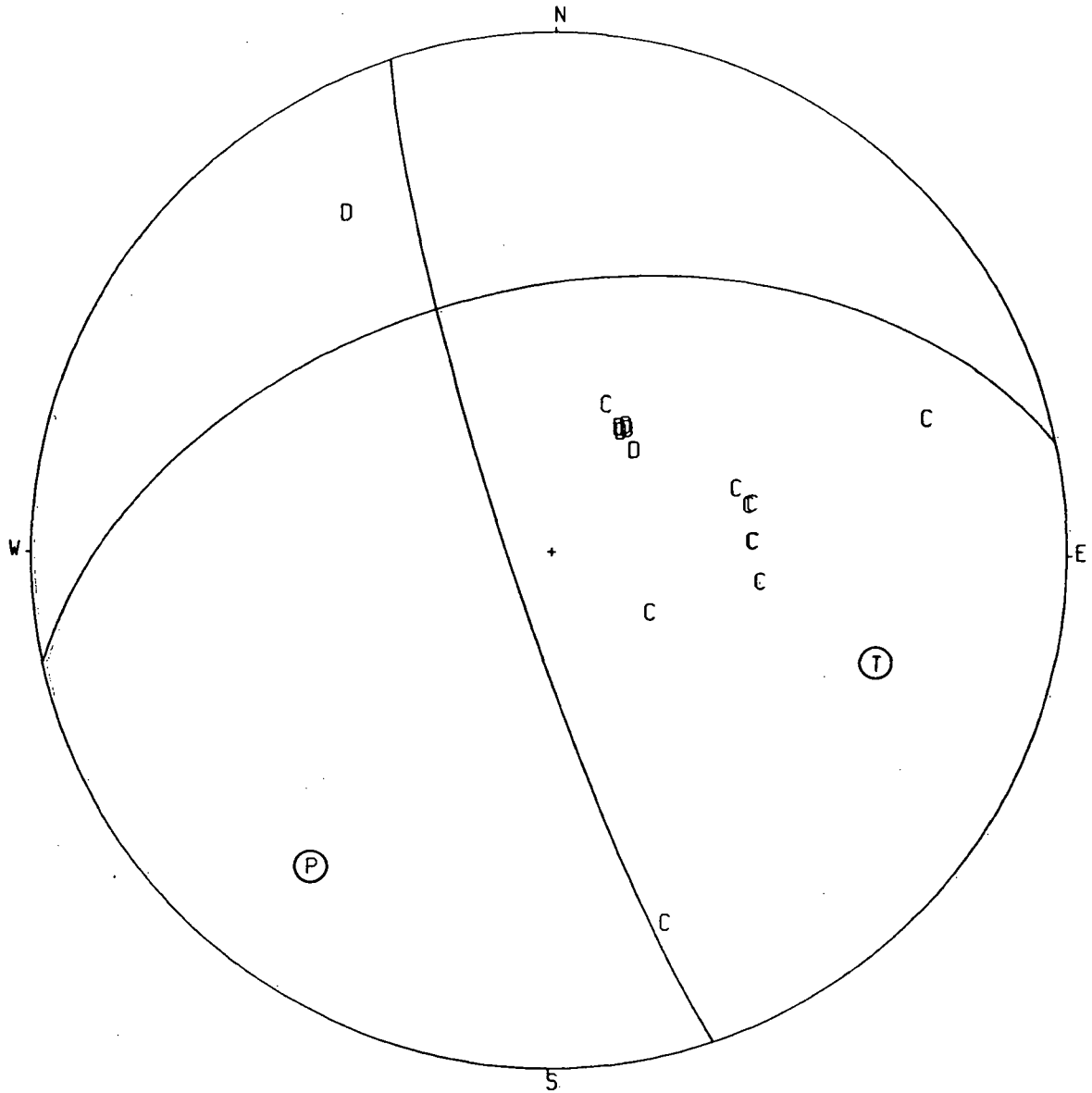


**Figure 30.** P-nodal mechanism of the 1975 earthquake (Figure 3) which provides a good fit to the observed surface wave data for the 1918 event. Poorly defined first motion estimates have been superimposed on this plot; C's represent compressional arrivals; D's represent dilational arrivals; P and T represent the pressure and tension axes respectively.

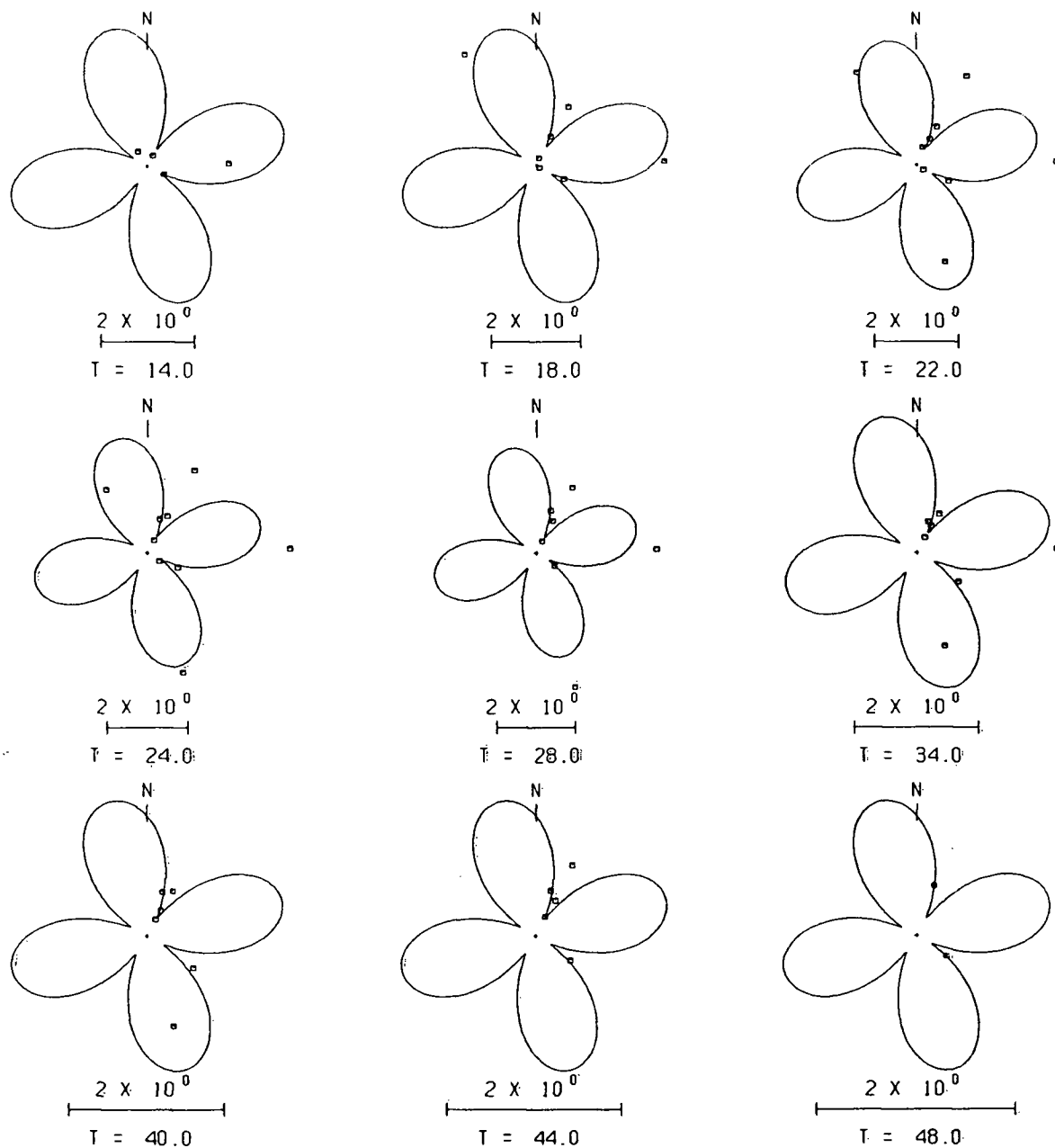


**Figure 31.** Observed (dots) and theoretical (solid lines) Love wave radiation patterns for the 1918 earthquake (assuming 1975 mechanism). Each dot represents the spectral amplitude at a station. The azimuth of the dot represents the station azimuth, and the distance from the centre of the pattern is proportional to the spectral amplitude (normalized to 1000 km). The period, as well as a scale relating the plot size to units of dyne-cm is written below each pattern.

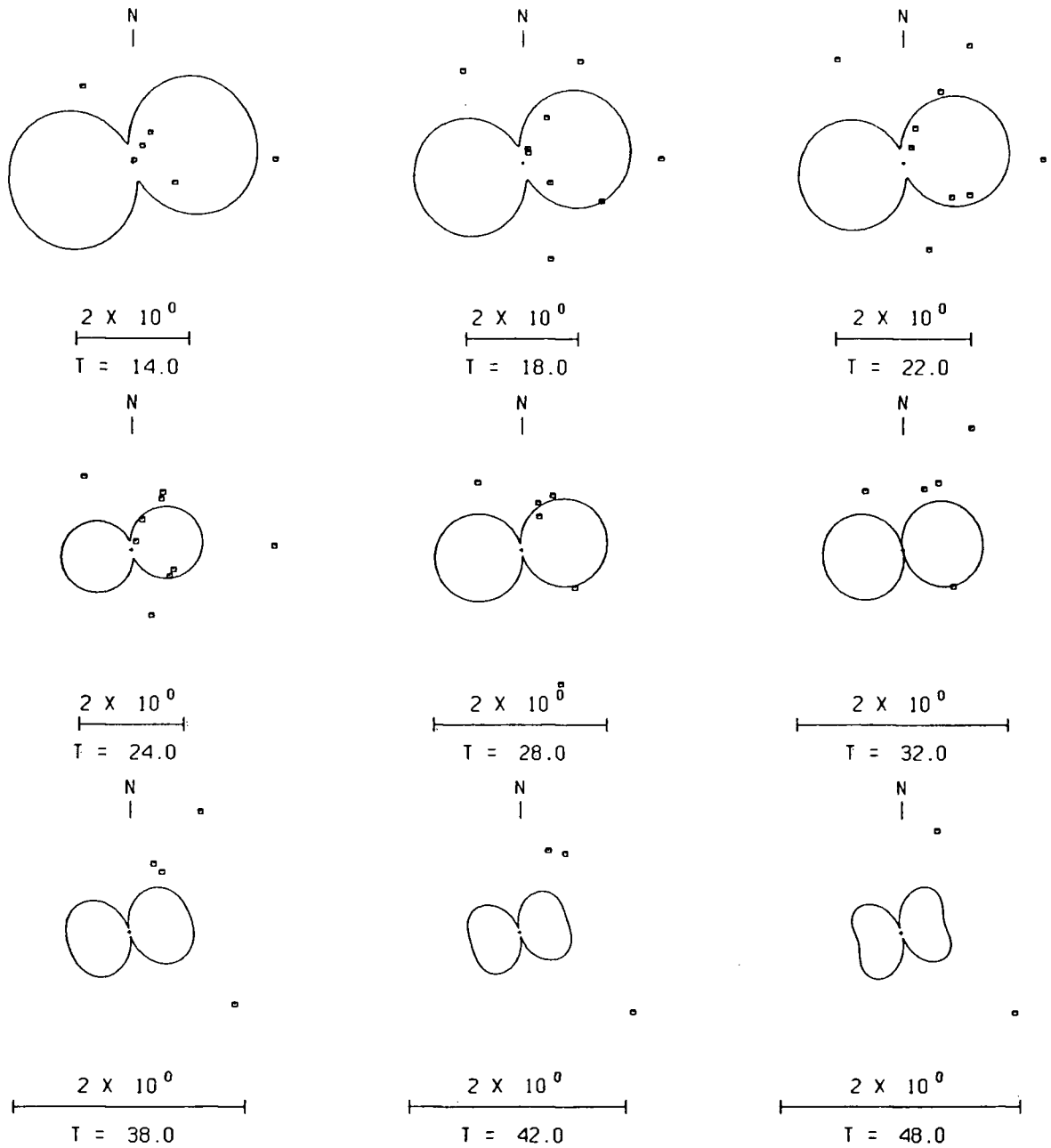


**Figure 32.** Observed (dots) and theoretical (solid lines) Rayleigh horizontal radiation patterns for the 1918 earthquake (assuming 1975 mechanism). Each dot represents the spectral amplitude at a station. The azimuth of the dot represents the station azimuth, and the distance from the centre of the pattern is proportional to the spectral amplitude (normalized to 1000 km). The period, as well as a scale relating the plot size to units of dyne-cm is written below each pattern.

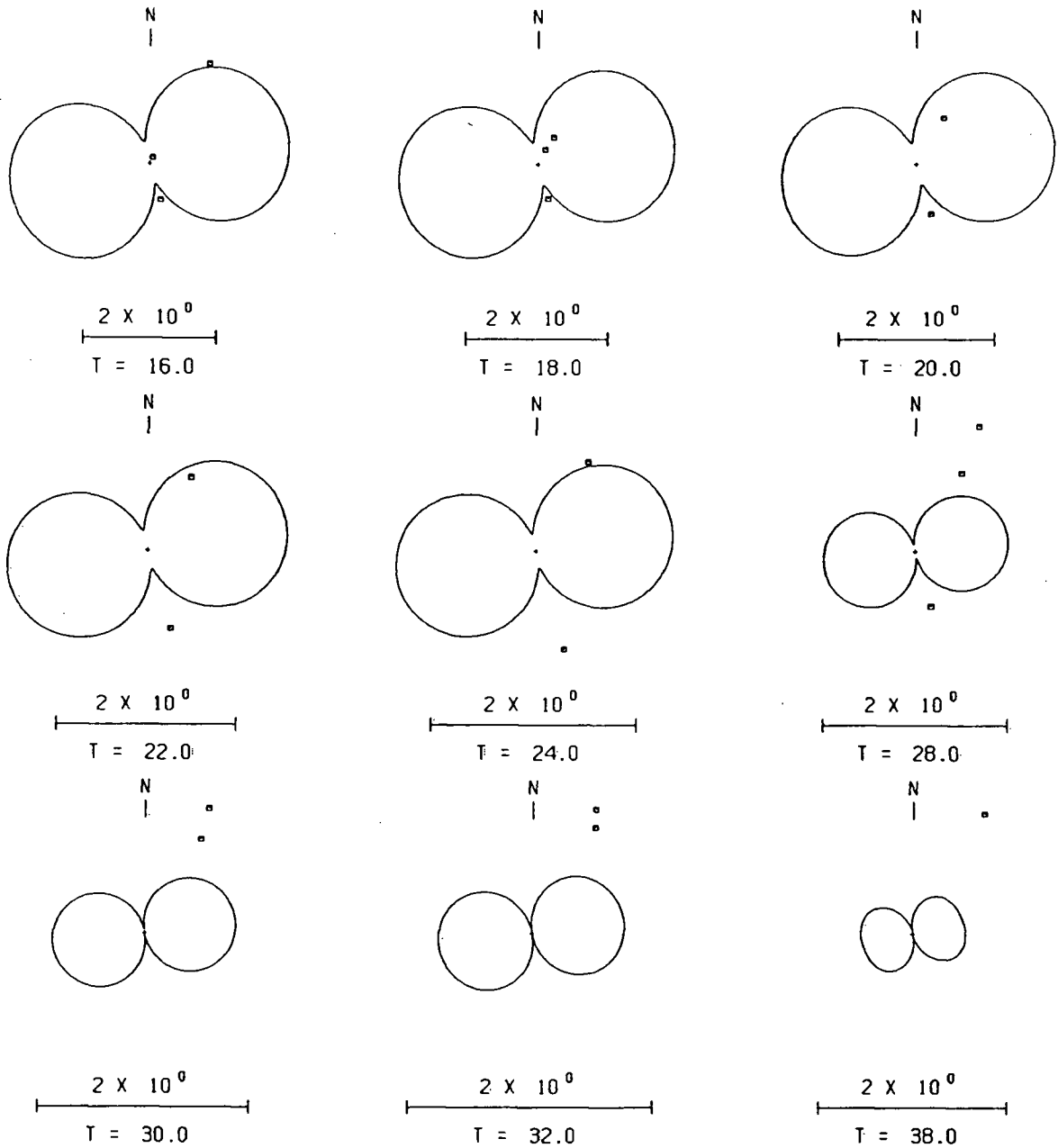


**Figure 33.** Observed (dots) and theoretical (solid lines) Rayleigh vertical radiation patterns for the 1918 earthquake (assuming 1975 mechanism). Each dot represents the spectral amplitude at a station. The azimuth of the dot represents the station azimuth, and the distance from the centre of the pattern is proportional to the spectral amplitude (normalized to 1000 km). The period, as well as a scale relating the plot size to units of dyne-cm is written below each pattern.

mechanism and serves to illustrate that the solution for the 1918 earthquake is poorly constrained due to the small data set, uncertainties involved in instrument response and mixed travel paths.

#### 4.6 Seismic Moment, Stress Drop and Aftershocks

The seismic moment for this earthquake, estimated from surface wave amplitudes using the program QUESTION and assuming the 1975 mechanism with a focal depth of 15 km, is  $0.74 \times 10^{26}$  dyne-cm. Applying the Kanamori and Anderson (1975) relation between seismic moment and surface wave magnitude results in a stress drop of 122 bars, which is within the range observed for intraplate earthquakes ( $> 100$  bars) (Kanamori and Anderson, 1975). The seismic moment is however, subject to large uncertainties; doubling the moment estimate (which is not unreasonable in this case) reduces the stress drop to only 65 bars.

Applying the seismic energy - magnitude relation of Gutenberg and Richter (1956) (see section 3.6) results in an energy estimate of  $1.4 \times 10^{22}$  erg.

This earthquake had 13 (possibly 14) felt aftershocks. The largest occurred approximately four hours after the main shock and was felt throughout central Vancouver Island (Port Alberni, Estevan Point and Cape Lazo). Ten smaller aftershocks occurred the following day and were felt at Estevan Point. On December 11 at 01:00 local time, two additional aftershocks were reported at Estevan Point (Denison, unpublished journal). A possible aftershock was felt in Alberni on December 16 at 04:00 local time (Milne, 1956), although there are no reports of this being felt at Estevan Point, or indications of it being recorded at VIC (Denison, unpublished journal).

Prior to this study, the magnitude of the largest aftershock was believed to be about 4.5, based on felt reports (Rogers, 1983). A record of this aftershock obtained from the European station DBN, permitted a surface wave magnitude determination. The estimate of  $M_s = 5.9$  may be slightly large, as the magnitude estimate of the main shock at this station is 0.3 units higher than the mean. The actual magnitude of this aftershock is likely close to 5.6. A felt area magnitude can be determined based on Topozada's equation. Assuming a circular felt area about the preferred main shock epicentre, limited in radius by Port Alberni, results in a total felt area of 38,700 km<sup>2</sup>. For an earthquake occurring at night, people would not be awakened unless the Mercalli intensity was IV or higher (during the day intensity III would generally be felt). Therefore applying Topozada's total felt area - magnitude equation will yield a lower limit for the magnitude. A felt area of 38,700 km<sup>2</sup> results in  $M_I = 5.1$ . By assuming that, in the regions where it was felt, the earthquake was intensity V (i.e. "many awakened"), we are able to apply another of Topozada's (1975) equations to estimate magnitude. The equation Topozada (1975) derived between the felt area of intensity V ( $A_V$ ) and magnitude:

$$M_I = 0.86 + 1.09A_V$$

yields an estimate of  $M_I=5.9$ . This must be considered an upper limit however, as newspaper reports do not state that "many people were awakened". Therefore, in regions where it was felt it may have only been an intensity IV. This range of felt magnitudes (5.1-5.9) is in agreement with the preferred magnitude of 5.6. This aftershock could not be located due to very few, and small first arrivals. The large number of aftershocks support (Page, 1968) the shallow focal depth of 15 km, estimated for the main earthquake based on surface waves.

## CHAPTER V

## SUMMARY AND CONCLUSIONS

The results for the 1957 earthquake are summarized below:

|               |   |
|---------------|---|
| Origin Time : | 17 27 51.0  |
| Epicentre :   | 49.65°N, 127.02°W (± 20 km)   |
| Depth :       | 30 km, estimated bounds (25–40 km)  |
| Magnitude :   | $M_s = 5.9 \pm 0.2$ , $m_b = 6.3 \pm 0.3$ , $M_I = 5.7$   |
| Mechanism :   | predominantly strike-slip along either:<br>Strike N65°E      Dip 62°NNW    (left-lateral)<br>Strike N26°W      Dip 88°SW    (right-lateral)<br>P axis 203°, dipping 18°<br>T axis 106°, dipping 21° |
| $M_0$ :       | $8.14 \times 10^{24}$ dyne-cm   |
| $E_S$ :       | $5.3 \times 10^{20}$ erg  |
| Stress Drop : | 36 bars   |
| Aftershocks : | only one, $M_L = 2.8$ .   |

This study indicates that the epicentre is  $\approx 40$  km southwest of previous estimates by the ISS and Tobin and Sykes (1968). The preferred epicentre, determined using the teleseismic technique, is supported by both local data and felt information. The depth estimate of 30 km obtained from surface wave studies suggests that this earthquake occurred in the upper portion of the subducting oceanic plate (see Figure 34). However, given the uncertainty in the depth (see error bars – Figure 34) and recalling that the

“true” uncertainty is likely larger than the estimated bounds, the possibility of this earthquake having occurred in the lower region of the continental crust cannot be ruled out. The focal mechanism of this earthquake determined by P-nodal and surface wave analyses are similar. They suggest a predominantly strike-slip earthquake occurring along a fault striking approximately NE or NW. The preferred surface wave solution (Figure 15) has a pressure axis near  $200^\circ$ , similar to those of other large events in this region (Figure 4).

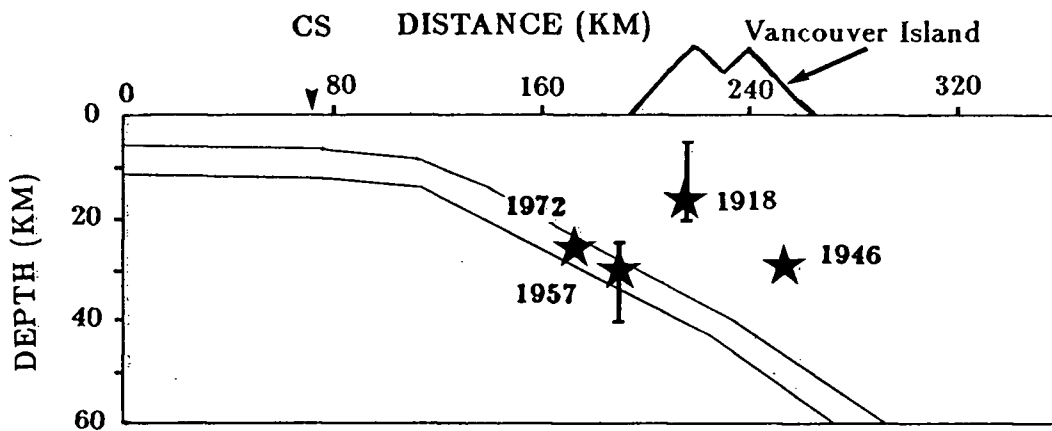


**Figure 34.** Cross-section of the subduction zone near Vancouver Island. This diagram shows the depth of the largest central Vancouver Island earthquakes in relation to the subducting oceanic plate. Error bars for the 1918 and 1957 earthquakes are based on the surface wave correlation factor (sections 3.3, 4.3), and must be considered a minimum estimate of the uncertainty – see discussion in text. CS indicates the location of the outer edge of the continental shelf. Note vertical exaggeration of 2:1. This diagram is based upon the work of Spence (1984) and J.Drew (personal communication).

The similarity of this event to the 1972 earthquake, which occurred about 22 km to the southwest, should not go unnoticed. The depth, focal mechanism (see Figure 3, 15) and aftershock patterns of these earthquakes are nearly identical. Within uncertainties,

these earthquakes may have occurred in the same location. The northwest striking plane is the same for each earthquake, and the northeast plane differs by only  $1^\circ$  in strike and  $10^\circ$  in dip, differences which are not significant given the resolution and uncertainty in the surface wave analysis. The focal mechanism (left-lateral strike-slip, possibly along a fault striking approximately NE), depth (in the upper portion of the subducting plate) and low stress drop (indicative of an interplate earthquake) of the 1957 event are consistent with left-lateral slip between the Juan de Fuca and Explorer plates along the subducting Nootka fault zone. The occurrence of two earthquakes of such similar character along the approximately NE-SW projection of the Nootka fault zone supports this interpretation. In addition the aftershock of the 1972 event may lie along this projection - 15 km to the southwest (Rogers, 1976). The 1957 and 1972 earthquakes may therefore define the position of this fault zone as it subducts beneath Vancouver Island. Moment rate calculations were made assuming a differential slip rate of 20 mm/yr along the Nootka fault, a rigidity value ( $\mu$ ) of  $3 \times 10^{10}$  N/m<sup>2</sup>, and a fault area of approximately 16 km<sup>2</sup> for the 1972 earthquake ( $m_b = 5.7$ ). The results indicate that over the 15 year period 1957 to 1972, strain accumulation along this fault zone due to differential motion between the Juan de Fuca and Explorer plates is consistent with the occurrence of a magnitude 5.7 earthquake in 1972. However, the possibility that both of these earthquakes occurred along approximately NW striking faults cannot be ruled out. This interpretation was favoured for the 1972 earthquake (Rogers, 1976) based on observed faults on the ocean floor and on Vancouver Island, and a NW-SE gravity low in the epicentral region. A movement of only 5 km in the depths of these earthquakes could place them in the lower continental crust. In this case, these earthquakes would not result directly from the Juan de Fuca-Explorer-America plate

interaction, but rather from the stress regime generated by the complicated interaction and coupling of these plates.

The results for the 1918 earthquake can be summarized as follows:

Origin Time : 08 41 06.2

Epicentre : 49.47°N, 126.24°W ( $\pm 30$  km)

Depth : 15 km, estimated bounds 5–20 km

Magnitude :  $M_s = 6.9 \pm 0.3$ ,  $m_b = 7.2 \pm 0.4$ ,  $M_I = 7.0$

Mechanism : predominantly strike-slip along either:  
                   Strike N77°E      Dip 48°NW      (left-lateral)  
                   Strike N19°W      Dip 83°SW      (right-lateral)  
                   P axis 217°, dipping 23°  
                   T axis 110°, dipping 34°

$M_0$  :  $7.40 \times 10^{25}$  dyne-cm

$E_S$  :  $1.4 \times 10^{22}$  erg

Stress Drop : 122 bars

Aftershocks : thirteen felt, the largest of magnitude  $\simeq 5.6$ .

The epicentre estimated for this earthquake is about 30 km southwest of the previous estimate of Rogers (1983). The depth of 15 km, estimated from surface waves, is supported by the large number of aftershocks observed for this event. This indicates that the earthquake occurred in the overlying continental lithosphere rather than in

the subducting plate (see Figure 34). It is interesting to note that there are NNW striking faults in the epicentral region (Figure 24), in agreement with a NNW nodal plane for the preferred surface wave solution (Figure 30). Magnitude estimates for this earthquake are in agreement with previous estimates of Gutenberg and Richter (1954), Rogers (1983) and Abe (1981). The poorly constrained mechanism appears to be predominantly strike-slip and similar to the mechanism of the 1975 earthquake, which occurred approximately 30 km southeast (Figure 3). The observed data are not consistent with either a thrust or normal mechanism. The large stress drop of 122 bars suggests that this is an intraplate event (in agreement with the shallow focal depth). The 1918 earthquake is different from the other large events (1946, 1957 and 1972) in that it has a pressure axis orientated in a more NE-SW direction (rather than N-S), and it had a large number of aftershocks, including one that was relatively large ( $M \approx 5.6$ ). It is similar to the others in that it is predominantly strike-slip, and similar to the 1946 earthquake in that it occurred in the continental crust, and further inland than the other events.

In summary this study has provided estimates of the location, depth, focal mechanism and character of the 1918 and 1957 Vancouver Island earthquakes. One of the most significant results is that these earthquakes do not appear to have thrust type mechanisms which are often associated with subduction zones (Isacks *et al.*, 1968). The quality of the data used in this study does not allow for an unambiguous interpretation of these events in terms of seismotectonic models. However, the preferred estimates for the location, depth and stress drop of the 1918 event suggest that this was a crustal, intraplate earthquake. Rather than being directly associated with the subducting Nootka fault zone, this earthquake is likely due to the stress regime in the continental crust

which results from the coupling of the America plate with the Explorer and Juan de Fuca plates (model #1 - section 1.3). This study has shown that the 1957 earthquake is very similar in nature to the 1972 event. The preferred estimates for the epicentre, focal depth, and stress drop for the 1957 earthquake suggest that it occurred along the Nootka fault, and is a result of differential motion between the Juan de Fuca and Explorer plates (model #2, section 1.3). However, given the uncertainty in each of the above parameters, the possibility of this earthquake having occurred in the continental crust, along a NW trending fault cannot be ruled out. In this case the earthquake would result from the complicated stress regime generated by the coupling of the America plate with the subducting oceanic plates (model #1, section 1.3).

In addition to providing information on these two earthquakes, this study is also significant in that it has shown the method of surface wave analysis is a useful technique even for historical earthquakes. In this study, although the technique suffers from several problems - uncertainty in instrument response, relatively short period seismometers which do not record the desirable long period waves, uncertainties due to mixed (continental/oceanic) travel paths, and uncertainty in attenuation values - it is encouraging that it produces results compatible with those obtained from P-nodal studies.

Some future work which may provide better insight into the seismicity and tectonics of this region include:

- 1) Surface wave studies of the other earthquakes in this region (1946, 1972, 1975 and 1986) which could be compared to P-nodal studies. This may provide information on the accuracy and limitations of surface wave analysis. In addition it may be possible to estimate the effect on surface wave amplitudes of traversing the continental/oceanic boundary (e.g. for California and Alaska stations). These corrections

could then be applied to the spectral amplitudes observed for the 1918 and 1957 earthquakes to provide a more accurate focal mechanism estimate. A study of all earthquakes in this region might also provide estimates for surface wave attenuation for various source – receiver paths. These also could be applied to the 1918 and 1957 earthquakes to provide more reliable seismic moment and focal mechanism estimates.

- 2) Body wave travel-time studies of the 1946, 1972, 1975 and 1986 earthquakes could be used to generate travel-time corrections for various source-receiver paths. These could be applied to the 1918 and 1957 earthquakes to give more accurate epicentre and depth estimates. A comprehensive study of the effect of azimuthal distribution of recording stations would also be useful. For the 1918 and 1957 earthquakes it would be desirable to use only North American data , with an azimuthal distribution “correction” applied, to locate the epicentre. To date, the lack of enough events large enough to be recorded world-wide limits such a study.
- 3) Waveform matching of body-waves (see Kanamori and Stewart, 1975) may also be useful in determining source parameters of modern earthquakes. However, this method does not appear to be practical for the 1918 or 1957 earthquakes due to the poor quality of body waves at teleseismic distances.

## BIBLIOGRAPHY

- Abe, K., 1981. Magnitudes of large shallow earthquakes from 1904 to 1980, *Phys. Earth Planet. Int.*, **27**, 72–92.
- Acharya, H.K., 1979. Regional variations in the rupture-length magnitude relationship and their dynamical significance, *Bull. Seism. Soc. Am.*, **69**, 2063–2084.
- Ben-Menahem, A. and Harkrider, D.G., 1964. Radiation patterns of seismic surface waves from buried dipolar point sources in a flat stratified earth, *J. Geophys. Res.*, **69**, 2605–2620.
- Ben-Menahem, A. and Singh, S.J., 1981. *Seismic Waves and Sources*, Springer-Verlag, New York, 1108 pp.
- Bolduc, P.M., Ellis, R.M. and Russell, R.D., 1972. Determination of the seismograph phase response from the amplitude response, *Bull. Seism. Soc. Am.*, **62**, 1665–1672.
- Bostwick, T.K., 1984. A re-examination of the August 22, 1949 Queen Charlotte earthquake, *M.Sc. Thesis*, University of British Columbia, Vancouver, 115 pp.
- Chapman, J.D. and Turner, D.B., Eds., 1956. British Columbia Atlas of Resources, British Columbia Natural Resources Conference, Vancouver, 92 pp.
- Charlier, C. and Van Gils, J.M., 1953. *Liste des Stations Seismologiques Mondiales*, Service Seismologique, Observatoire Royal de Belgique, Uccle, Belgium.
- Denison, F.N., 1919. The British Columbia earthquake of December 6, 1918, *Bull. Seism. Soc. Am.*, **9**, 20–23.
- Dziewonski, A.M. and Anderson, D.L., 1981. Preliminary Reference Earth Model (PREM), *Phys. Earth Planet. Int.*, **25**, 297–356.
- Dziewonski, A.M. and Anderson, D.L., 1983. Travel times and station corrections for P waves at teleseismic distances, *J. Geophys. Res.*, **88**, 3295–3314.
- Fitch, T.J., 1972. Plate convergence, transcurrent faults, and internal deformation adjacent to southeast Asia and the western Pacific, *J. Geophys. Res.*, **77**, 4432–4460.
- Gibowicz, S.J., 1973. Stress drop and aftershocks, *Bull. Seism. Soc. Am.*, **63**, 1433–1446.
- Gregerson, S. and Alsop, L.E., 1976. Mode conversion of Love waves at a continental margin, *Bull. Seism. Soc. Am.*, **66**, 1855–1872.
- Gutenberg, B., 1945. Amplitudes of surface waves and magnitudes of shallow earthquakes, *Bull. Seism. Soc. Am.*, **35**, 3–12.
- Gutenberg, B. and Richter, C.F., 1954. *Seismicity of the Earth and Associated Phenomena*, Princeton University Press, Princeton, N.J., 2nd Edition, 310 pp.

- Gutenberg, B. and Richter, C.F., 1956. Magnitude and energy of earthquakes, *Ann. Geofis. (Rome)*, **9**, 1–15.
- Hagiwara, T., 1958. A note on the theory of the electromagnetic seismograph, *Bull. Earthq. Res. Inst. Tokyo Univ.*, **36**, 139–164.
- Heaton, T.H. and Kanamori, H., 1984. Seismic potential associated with subduction in the northwestern United States, *Bull. Seism. Soc. Am.*, **74**, 933–941.
- Herrin, E., 1968. Seismological table for P phases, *Bull. Seism. Soc. Am.*, **58**, 1193–1241.
- Herrmann, R.B., ed., 1978. *Computer Programs in Earthquake Seismology*, 2 Volumes, Department of Earth and Atmospheric Sciences, St. Louis University.
- Herrmann, R.B., 1979. FASTHYPO – A hypocentre location program, *Earthquake Notes*, Vol. 50, No. 2, 25–37.
- Hodgson, J.H. and Allen, J.F.J., 1954a. Tables of extended distances for PKP and PcP, *Publ. Dominion Obs.*, **26**, No. 10, 329–348.
- Hodgson, J.H. and Allen, J.F.J., 1954b. Tables of extended distances for PP and pP, *Publ. Dominion Obs.*, **26**, No. 11, 351–362.
- Hodgson, J.H. and Storey, R.S., 1953. Tables extending Byerly's fault-plane technique to earthquakes of any focal depth, *Bull. Seism. Soc. Am.*, **43**, 49–61.
- Hyndman, R.D., Riddihough, R.P. and Herzer, R., 1979. The Nootka fault zone – a new plate boundary off western Canada, *Geophys. J. R. Astr. Soc.*, **58**, 667–683.
- Isacks, B., Oliver, J. and Sykes, L.R., 1968. Seismology and the new global tectonics, *J. Geophys. Res.*, **73**, 5855–5899.
- Jeffreys, H. and Bullen, K.E., 1940, 1958. *Seismological Tables*, Brit. Assn., Gray-Milne Trust.
- Kanamori, H. and Anderson, D.L., 1975. Theoretical basis of some empirical relations in seismology, *Bull. Seism. Soc. Am.*, **65**, 1073–1095.
- Kanamori, H. and Stewart, G.S., 1975. Mode of the strain release along the Gibbs fracture zone, mid-Atlantic ridge, *Phys. Earth Planet. Int.*, **11**, 312–332.
- Keen, C.E. and Hyndman, R.D., 1979. Geophysical review of the continental margins of eastern and western Canada, *Can. J. Earth Sci.*, **16**, 712–747.
- Lahr, J.C., 1984. HYPOELLIPSE/VAX: A computer program for determining local earthquake hypocentral parameters, magnitude, and first motion pattern, *Open-File Report*, U.S. Geological Survey, Menlo Park, Ca., 67pp.
- McMechan, G.A. and Spence, G.D., 1983. P-wave velocity structure of the Earth's crust beneath Vancouver Island, *Can. J. Earth Sci.*, **20**, 742–752.

- Meteorological Service of Canada, 1919. Records at Toronto and Victoria, B.C. of the earthquake off Vancouver Island, December 6<sup>th</sup>, 1918. *J. R. Astr. Soc. Canada*, **13**, 69–70.
- Milne, W.G., 1956. Seismic activity in Canada west of the 113° meridian, 1841–1951, *Publ. Dominion Obs.*, **18**, 119–145.
- Milne, W.G. and Lucas, K.A., 1961. Seismic activity in western Canada, 1955 to 1959 inclusive, *Publ. Dominion Obs.*, **26**, 3–23.
- Muller, J.E., Cameron, B.E.B. and Northcote, K.E., 1980. Geology and mineral deposits of Nootka sound map–area Vancouver Island, British Columbia, *Geol. Surv. Canada*, paper 80–16, Ottawa, 53 pp.
- Page, R., 1968. Focal depths of aftershocks, *J. Geophys. Res.*, **73**, 3897–3903.
- Poppe, B.B., 1980. *Directory of World Seismograph Stations Volume I – The Americas*, Report SE-25, World Data Center A, U.S. Department of Commerce, Boulder, Colorado, 465 pp.
- Richter, C.F., 1958. *Elementary Seismology*, W.H. Freeman Co., San Francisco, 768 pp.
- Riddihough, R.P., 1977. A model for recent plate interactions off Canada's west coast, *Can. J. Earth Sci.*, **14**, 384–396.
- Riddihough, R.P., 1984. Recent movements of the Juan de Fuca plate system, *J. Geophys. Res.*, **89**, 6980–6994.
- Rogers, G.C., 1976. The Vancouver Island earthquake of 5 July, 1972, *Can. J. Earth Sci.*, **13**, 92–101.
- Rogers, G.C., 1979. Earthquake fault plane solutions near Vancouver Island, *Can. J. Earth Sci.*, **16**, 523–531.
- Rogers, G.C., 1983. Seismotectonics of British Columbia, *Ph.D. Thesis*, University of British Columbia, Vancouver, 247 pp.
- Rogers, G.C. and Hasegawa, H.S., 1978. A second look at the British Columbia earthquake of 23 June, 1946, *Bull. Seism. Soc. Am.*, **68**, 653–675.
- Seismological Service of Canada, 1958. *Seismological Bulletin*, January–March, 1958, Dominion Observatory, Ottawa.
- Slawson, W.F. and Savage, J.C., 1979. Geodetic deformation associated with the 1946 Vancouver Island, Canada, earthquake, *Bull. Seism. Soc. Am.*, **69**, 1487–1496.
- Spence, G.D., 1984. Seismic structure across the active subduction zone of western Canada, *Ph.D. Thesis*, University of British Columbia, Vancouver, 191 pp.
- Spence, G.D., Clowes, R.M. and Ellis, R.M., 1985. Seismic structure across the active subduction zone off western Canada, *J. Geophys. Res.*, **90**, 6754–6772.

- Stevens, A.E., Milne, W.G., Wetmiller, R.J. and Horner, R.B., 1972. Canadian earthquakes - 1966, Seismological Series of the Earth Physics Branch, No. 62, 55 pp.
- Tobin, P.G. and Sykes, L.R., 1968. Seismicity and tectonics of the north-east Pacific Ocean, *J. Geophys. Res.*, **73**, 3821-3846.
- Topozada, T.R., 1975. Earthquake magnitude as a function of intensity data in California and western Nevada, *Bull. Seism. Soc. Am.*, **61**, 1223-1238.
- Tsai, Y.-B. and Aki, K., 1970. Precise focal depth determination from amplitude spectra of surface waves, *J. Geophys. Res.*, **75**, 5729-5743.
- United States Coast and Geodetic Survey, 1958. Seismological Bulletin, MSI-205, January, 1958, U.S. Department of Commerce, Washington.
- Vaněk, J., Zátopek, A., Kárník, V., Kondorskaya, N.V., Riznichenko, Y.V., Savarensky, E.F., Solov'ev, S.L. and Shebalin, N.V., 1962. Standardization of magnitude scales, *Bull. Acad. Sci. USSR, Geophys. Ser.* 108-111 (English translation).
- Veith, K.F., 1975. Refined hypocentres and accurate reliability estimates, *Bull. Seism. Soc. Am.*, **65**, 1199-1222.
- Washington Public Power Supply System, 1983. Final safety analysis report, Supply System Nuclear Project No. 3, vol 4.
- Weichert, D.H. and Newton, J.C., 1970. Epicentre determination from first arrival times at Canadian stations, Seismological Series of the Earth Physics Branch, No. 59, Ottawa, 16 pp.
- Wickens, A.J. and Hodgson, J.H., 1967. Computer re-evaluation of earthquake mechanism solutions 1922-1962, *Publ. Dominion Obs.*, **33**, 1-560.
- Wood, H.O., 1921. A list of seismological stations of the world, Bulletin of the National Research Council, **15**, 397-538.

## APPENDIX A

Regional earth models used in epicentre studies

$V_p$  = compressional wave velocity,  $Z$  = depth to layer

Canadian Standard Model (Stevens *et al.*, 1972)

| $V_p$ (km/s) | $Z$ (km) |
|--------------|----------|
| 6.2          | 0.0      |
| 8.2          | 36.0     |

Vancouver Island–Puget Sound Model (Rogers, 1983)

| $V_p$ (km/s) | $Z$ (km) |
|--------------|----------|
| 5.0          | 0.0      |
| 6.0          | 1.0      |
| 6.7          | 6.0      |
| 7.1          | 30.0     |
| 7.75         | 45.0     |

McMechan and Spence (1983), no low velocity zone

| $V_p$ (km/s) | $Z$ (km) |
|--------------|----------|
| 5.7          | 0.0      |
| 6.5          | 2.0      |
| 6.7          | 10.0     |
| 7.1          | 16.0     |
| 8.1          | 53.0     |

**APPENDIX B -- 1957 EARTHQUAKE DATA****1. Arrival Times and First Motion Polarity**

For each station considered in the epicentre and P-nodal studies, the following table provides; the P-wave arrival time; the azimuth of the station (with respect to the epicentre); the epicentral distance; the first motion polarity; the weight given the reading (see section 3.5.1); and the source of the arrival time information. ISS represents the 1957 ISS bulletin; BCIS represents the 1957 BCIS bulletin; Bull. indicates that the arrival time was obtained from that stations' bulletin; Seis. indicates that the arrival time was read directly from a seismogram; and Milne indicates that the time was obtained from Milne's original, unpublished worksheets for this earthquake.

| STATION<br>CODE | AZ.<br>(DEG) | DELTA<br>(DEG) | ARRIVAL<br>TIME |    |      | FIRST<br>MOTION | WEIGHT | SOURCE |
|-----------------|--------------|----------------|-----------------|----|------|-----------------|--------|--------|
|                 |              |                | h               | m  | s    |                 |        |        |
| ALB             | 110.7        | 1.4            | 17              | 28 | 15.0 | C               | 50     | Milne  |
| HBC             | 98.7         | 2.4            | 17              | 28 | 29.1 | C               | 50     | Milne  |
| VIC             | 118.0        | 2.6            | 17              | 28 | 30.2 | C               | 100    | Seis.  |
| LLL             | 72.2         | 3.3            | 17              | 28 | 31.8 | C               | 50     | Milne  |
| SEA             | 123.7        | 3.7            | 17              | 28 | 48.0 | C               | 50     | Seis.  |
| COR             | 153.8        | 5.7            | 17              | 29 | 15   | C               | 50     | ISS    |
| HHM             | 94.8         | 8.5            | 17              | 29 | 55   | -               | -      | ISS    |
| SIT             | 328.5        | 8.9            | 17              | 29 | 56.0 | D               | 50     | Seis.  |
| ARC             | 166.6        | 9.1            | 17              | 30 | 03   | -               | -      | ISS    |
| SHS             | 159.3        | 9.6            | 17              | 30 | 10.7 | C               | 50     | BCIS   |
| MIN             | 156.6        | 10.1           | 17              | 30 | 18   | C               | 50     | ISS    |
| BUT             | 106.0        | 10.3           | 17              | 30 | 17.5 | -               | -      | Seis.  |
| UKI             | 165.0        | 11.0           | 17              | 30 | 28.5 | -               | -      | Seis.  |
| BZM             | 105.2        | 11.4           | 17              | 30 | 33.2 | C               | 100    | Seis.  |
| REN             | 151.4        | 11.4           | 17              | 30 | 34   | C               | 50     | ISS    |
| BRK             | 162.8        | 12.4           | 17              | 30 | 47.2 | C               | 100    | Seis.  |
| EUR             | 139.0        | 12.9           | 17              | 30 | 54.7 | -               | -      | Seis.  |
| SCL             | 162.3        | 12.9           | 17              | 31 | 10   | C               | 50     | Bull.  |
| SAS             | 71.8         | 13.0           | 17              | 30 | 49   | -               | -      | ISS    |
| MHC             | 161.2        | 13.0           | 17              | 30 | 55.6 | C               | 50     | BCIS   |
| SLC             | 124.9        | 13.9           | 17              | 31 | 08.8 | C               | 100    | Seis.  |
| FRE             | 155.9        | 14.0           | 17              | 31 | 10   | -               | -      | ISS    |
| FTC             | 155.6        | 16.0           | 17              | 31 | 20.5 | -               | -      | Seis.  |
| BCN             | 143.1        | 16.3           | 17              | 31 | 39   | -               | -      | ISS    |
| PAS             | 154.5        | 16.9           | 17              | 31 | 49.4 | C               | 100    | Seis.  |
| DLT             | 153.5        | 17.0           | 17              | 30 | 39.3 | C               | 50     | Seis.  |
| RCD             | 100.5        | 17.1           | 17              | 31 | 48.5 | -               | -      | Seis.  |
| HAY             | 148.5        | 18.1           | 17              | 32 | 01.7 | C               | 50     | Seis.  |
| BOU             | 114.5        | 18.1           | 17              | 32 | 02   | -               | -      | Bull.  |
| COL             | 331.7        | 18.7           | 17              | 32 | 08   | D               | 100    | Seis.  |
| TUO             | 139.7        | 21.2           | 17              | 32 | 36.5 | C               | 100    | Seis.  |
| LUB             | 121.9        | 24.5           | 17              | 33 | 09   | -               | -      | ISS    |
| LAW             | 103.7        | 24.9           | 17              | 33 | 12.4 | C               | 100    | Seis.  |
| CHH             | 135.5        | 26.4           | 17              | 33 | 30   | -               | -      | ISS    |
| FAY             | 107.7        | 27.3           | 17              | 33 | 34.4 | C               | 50     | Seis.  |
| FLO             | 99.0         | 28.1           | 17              | 33 | 38.8 | C               | 100    | Seis.  |
| SLM             | 99.2         | 28.2           | 17              | 33 | 43.5 | C               | 50     | Seis.  |
| CHK             | 91.3         | 28.2           | 17              | 33 | 47   | -               | -      | ISS    |
| RES             | 17.2         | 28.3           | 17              | 33 | 45.0 | D               | 100    | Seis.  |
| THI             | 95.3         | 29.7           | 17              | 35 | 20   | -               | -      | Bull.  |
| AAM             | 87.4         | 30.6           | 17              | 35 | 04.0 | -               | -      | Seis.  |
| CLE             | 87.3         | 32.3           | 17              | 34 | 20.0 | C               | 100    | Seis.  |
| PIT             | 87.8         | 33.9           | 17              | 34 | 32   | D               | 50     | Bull.  |
| WAY             | 88.8         | 34.0           | -               | -  | -    | C               | 100    | Seis.  |
| OTT             | 77.3         | 34.2           | 17              | 34 | 37.0 | C               | 100    | Seis.  |
| MRG             | 89.0         | 34.3           | 17              | 34 | 36.5 | C               | 50     | Bull.  |
| THU             | 20.6         | 34.9           | 17              | 34 | 42.4 | D               | 100    | Seis.  |

| STATION<br>CODE | AZ.<br>(DEG) | DELTA<br>(DEG) | ARRIVAL<br>TIME |    |      | FIRST<br>MOTION | WEIGHT | SOURCE |
|-----------------|--------------|----------------|-----------------|----|------|-----------------|--------|--------|
|                 |              |                | h               | m  | s    |                 |        |        |
| SCP             | 85.8         | 35.1           | 17              | 34 | 42   | -               | -      | Bull.  |
| MNT             | 76.0         | 35.5           | 17              | 34 | 47   | C               | 50     | ISS    |
| SHF             | 73.9         | 35.6           | 17              | 34 | 48.0 | C               | 50     | Seis.  |
| SFA             | 72.1         | 36.5           | 17              | 34 | 53   | C               | 50     | ISS    |
| GEO             | 87.9         | 36.6           | 17              | 34 | 56   | C               | 50     | Bull.  |
| WAS             | 87.9         | 36.6           | 17              | 34 | 57   | -               | -      | ISS    |
| CSC             | 97.7         | 37.0           | 17              | 35 | 00   | -               | -      | ISS    |
| PAL             | 82.8         | 37.5           | 17              | 35 | 05.5 | C               | 100    | Seis.  |
| TAC             | 134.0        | 37.5           | 17              | 35 | 03   | D               | 50     | ISS    |
| WES             | 79.3         | 38.4           | 17              | 35 | 12.5 | C               | 100    | Seis.  |
| VCM             | 130.1        | 39.1           | 17              | 35 | 16   | D               | 50     | ISS    |
| MER             | 120.7        | 41.2           | 17              | 35 | 39   | -               | -      | ISS    |
| HAL             | 71.8         | 42.1           | 17              | 35 | 45.0 | C               | 100    | Seis.  |
| PET             | 304.1        | 44.6           | 17              | 36 | 00   | -               | -      | ISS    |
| TIK             | 335.5        | 47.8           | 17              | 36 | 26   | -               | -      | ISS    |
| BEC             | 86.6         | 48.6           | 17              | 36 | 36   | -               | -      | ISS    |
| SJP             | 100.3        | 57.3           | 17              | 37 | 37.3 | D               | 50     | Seis.  |
| KIR             | 13.7         | 60.2           | 17              | 37 | 37   | -               | -      | Bull.  |
| SOD             | 11.3         | 61.5           | 17              | 38 | 05   | -               | -      | ISS    |
| CHN             | 118.4        | 62.0           | 17              | 38 | 09   | -               | -      | Bull.  |
| SKA             | 19.3         | 62.5           | 17              | 38 | 14   | -               | -      | Bull.  |
| BOCO            | 117.1        | 63.2           | 17              | 37 | 54   | -               | -      | Bull.  |
| SEN             | 298.3        | 63.3           | 17              | 38 | 27.6 | -               | -      | Bull.  |
| MTJ             | 297.1        | 65.2           | 17              | 38 | 36.7 | -               | -      | BCIS   |
| MAT             | 298.6        | 66.0           | 17              | 38 | 39.0 | -               | -      | BCIS   |
| DUR             | 31.1         | 66.2           | 17              | 38 | 45   | D               | 50     | Bull.  |
| UPP             | 18.6         | 67.0           | 17              | 38 | 42.0 | -               | -      | Bull.  |
| HEL             | 14.8         | 68.0           | 17              | 38 | 56   | -               | -      | ISS    |
| KYO             | 299.0        | 68.5           | 17              | 39 | 01   | D               | 50     | ISS    |
| ABU             | 299.0        | 68.7           | 17              | 39 | 01.3 | -               | -      | Bull.  |
| PUL             | 12.1         | 69.2           | 17              | 39 | 10   | -               | -      | ISS    |
| IRK             | 329.3        | 69.5           | 17              | 39 | 03   | -               | -      | ISS    |
| WIT             | 27.8         | 70.5           | 17              | 39 | 14   | -               | -      | Bull.  |
| DBN             | 29.1         | 70.6           | 17              | 39 | 09.0 | -               | -      | Seis.  |
| HAM             | 25.7         | 70.9           | 17              | 39 | 08   | C               | 50     | Bull.  |
| OBM             | 325.3        | 72.2           | 17              | 39 | 21   | -               | -      | ISS    |
| HLE             | 25.5         | 73.2           | 17              | 39 | 22   | -               | -      | ISS    |
| NGS             | 301.2        | 73.5           | 17              | 39 | 30.6 | -               | -      | BCIS   |
| JEN             | 25.9         | 73.6           | 17              | 39 | 22   | -               | -      | Bull.  |
| CLL             | 24.9         | 73.6           | 17              | 39 | 23   | -               | -      | ISS    |
| PLN             | 25.8         | 74.1           | 17              | 39 | 32   | -               | -      | ISS    |
| STR             | 29.4         | 74.5           | 17              | 39 | 29   | C               | 50     | Bull.  |
| STU             | 28.4         | 74.8           | 17              | 39 | 30.5 | D               | 50     | Seis.  |
| BES             | 31.1         | 75.1           | 17              | 39 | 31.5 | -               | -      | Bull.  |
| PRA             | 24.6         | 75.1           | 17              | 39 | 33   | -               | -      | Bull.  |
| MSS             | 28.8         | 75.2           | 17              | 39 | 33.5 | -               | -      | Bull.  |
| HUA             | 128.0        | 76.3           | 17              | 39 | 39   | C               | 50     | Bull.  |

| STATION<br>CODE | AZ.<br>(DEG) | DELTA<br>(DEG) | ARRIVAL<br>TIME<br>h m s | FIRST<br>MOTION | WEIGHT | SOURCE |
|-----------------|--------------|----------------|--------------------------|-----------------|--------|--------|
| KRA             | 21.3         | 76.5           | 17 39 34                 | -               | -      | ISS    |
| CRT             | 42.7         | 80.0           | 17 40 01                 | D               | 50     | Bull.  |
| MAL             | 43.5         | 78.0           | 17 39 58                 | -               | -      | BCIS   |
| LPZ             | 124.4        | 83.8           | 17 40 18.8               | C               | 100    | Seis.  |
| MES             | 28.8         | 86.3           | 17 40 24                 | -               | -      | ISS    |
| RAB             | 260.4        | 87.4           | 17 40 32                 | -               | -      | Bull.  |
| NAM             | 346.1        | 88.2           | 17 40 47                 | -               | -      | ISS    |
| TIF             | 6.2          | 88.6           | 17 40 44                 | -               | -      | BCIS   |
| KOR             | 281.3        | 90.0           | 17 40 46                 | -               | -      | ISS    |
| TAM             | 43.3         | 96.3           | 17 41 27                 | -               | -      | Bull.  |
| QUE             | 347.9        | 99.4           | 17 45 32                 | -               | -      | BCIS   |
| LWI             | 31.7         | 128.3          | 17 52 45                 | -               | -      | Bull.  |
| BTR             | 30.7         | 129.0          | 17 46 57.6               | -               | -      | Bull.  |
| HLL             | 200.6        | 129.4          | 17 45 05                 | -               | -      | ISS    |
| UVI             | 31.8         | 129.5          | 17 45 52                 | -               | -      | Bull.  |
| BYR             | 178.3        | 129.6          | 17 46 58.7               | -               | -      | Seis.  |
| SPA             | 180.0        | 139.6          | 17 47 09                 | -               | -      | ISS    |
| TAN             | 10.3         | 148.9          | 17 47 40                 | C               | 50     | Bull.  |
| KIM             | 56.3         | 149.9          | 17 47 37                 | -               | -      | Bull.  |
| MIR             | 215.5        | 153.8          | 17 47 45                 | -               | -      | ISS    |

## 2. 1957 Instrumental Constants

The following list provides information on instrument type, and parameters for each station considered in this study. For simple mechanical seismographs the constants are;  $T_0$ , the free period of the seismometer;  $\epsilon$ , the damping ratio; and  $V$ , the static magnification (see Richter, 1958 p. 219). For electromagnetic seismographs the constants are;  $T_0$ , the seismometer period;  $T_1$  the galvanometer period;  $V_{max}$ , the maximum magnification of the instrument;  $h$ , the seismometer damping constant;  $h'$ , the galvanometer damping constant; and  $\sigma^2$ , the coupling coefficient.

Note: if no reference is given, information was sent with the seismograms.

|            |                |   |
|------------|----------------|---|
| <b>SIT</b> | Wiechert       | N: $T_0 = 8.2$ sec, $T_1 = 16.5$ sec, $V = 1000$ , $\epsilon = 20$<br>E: $T_0 = 8.2$ sec, $T_1 = 13.2$ sec, $V = 1000$ , $\epsilon = 5.5$<br>(station bulletin) |
| <b>BZM</b> | McComb-Romberg | N: $T_0 = 11.1$ sec, $V = 270$ , $\epsilon = 11$<br>E: $T_0 = 10.9$ sec, $V = 270$ , $\epsilon = 9$<br>(station bulletin)                                       |
| <b>BRK</b> | Galitzin-Wilip | N, E, Z: $T_0 = T_1 = 12.0$ sec, $V_{max} = 1400$<br>$h = h' = 1$ , $\sigma^2 = 0.0$  |
| <b>SLC</b> | McComb-Romberg | N: $T_0 = 9.9$ sec, $V = 335$ , $\epsilon = 15$<br>E: $T_0 = 10.0$ , $V = 335$ , $\epsilon = 15$<br>(Reference 1 - see end of section)                          |

|            |                              |  |
|------------|------------------------------|--|
| <b>PAS</b> | Press-Ewing                  | N, E, Z: $T_0 = 30 \text{ sec}, T_1 = 90 \text{ sec}$<br>$V_{max} = 2500, h = h' = 1$  |
| <b>HAY</b> | Benioff                      | Z: $T_0 = 1 \text{ sec}, T_1 = 90 \text{ sec}, V_{max} = 3000$   |
| <b>LAW</b> | Sprengnether                 | Z: $T_0 = T_1 = 1.0 \text{ sec}, V_{max} = 26,000$<br>(Poppe, 1980)  |
| <b>FLO</b> | Galitzin-Wilip               | N: $T_0 = T_1 = 12 \text{ sec}, V_{max} = 730$<br>E: $T_0 = T_1 = 12 \text{ sec}, V_{max} = 880$<br>Z: $T_0 = T_1 = 12 \text{ sec}, V_{max} = 740$   |
| <b>SLM</b> | Sprengnether<br>Reef         | N, E: $T_0 = T_1 = 20 \text{ sec}, V_{max} = 2000$<br>Z: $T_0 = T_1 = 1.0 \text{ sec}, V_{max} = 17,600$   |
| <b>RES</b> | Sprengnether<br><br>Benioff  | N: $T_0 = T_1 = 14.1 \text{ sec}, V(1 \text{ sec}) = 450, h = h' = 1$<br>E: $T_0 = T_1 = 16 \text{ sec}, V(1 \text{ sec}) = 450, h = h' = 1$<br>Z: $T_0 = T_1 = 1.4 \text{ sec}, V(1 \text{ sec}) = 9000, h = h' = 1$<br>Z: $T_0 = T_1 = 1.0 \text{ sec}, V(1 \text{ sec}) = 15000$<br>(Seismological Service of Canada, 1958) |
| <b>CLE</b> | Sprengnether<br>Sprengnether | N, E: $T_0 = T_1 = 18 \text{ sec}, V(12 \text{ sec}) = 2200$<br>N, E: $T_0 = T_1 = 1.5 \text{ sec}, V_{max} = 1800$<br>(Poppe, 1980)   |

- OTT** Milne-Shaw                      N, E:  $T_0 = 12 \text{ sec}, V = 300, \epsilon = 20$   
 Benioff                                      Z:  $T_0 = 1 \text{ sec}, T_1 = 0.2 \text{ sec}$   
 $V_{max} = 75000, h = h' = 1$   
 (Seismological Service of Canada, 1958)
- SHF** Willmore                              Z:  $T_0 = 1 \text{ sec}, T_1 = 2 \text{ sec}$   
 $V(1 \text{ sec}) = 28000, h = h' = 1$   
 (Seismological Service of Canada, 1958)
- PAL** Sprengnether                      Z:  $T_0 = 30 \text{ sec}, T_1 = 100 \text{ sec}, V_{max} = 250$
- WES** Benioff                              N, E, Z:  $T_0 = 1 \text{ sec}, T_1 = 60 \text{ sec}, V_{max} = 3000?$
- HAL** Sprengnether                      N, E:  $T_0 = T_1 = 20 \text{ sec}, V(1 \text{ sec}) = 380, h = h' = 1$   
 Willmore                                      Z:  $T_0 = 1 \text{ sec}, T_1 = 1.65 \text{ sec}$   
 $V(1 \text{ sec}) = 16000, h = h' = 1$   
 (Seismological Service of Canada, 1958)
- IVI** Milne-Shaw                              N:  $T_0 = 12 \text{ sec}, V \simeq 325, \epsilon = 22$
- SCO** Galitzin-Wilip                      N, E:  $T_0 = T_1 = 12 \text{ sec}, V_{max} \simeq 1000$

|            |                |   |
|------------|----------------|---|
| <b>SJP</b> | Wenner         | N: $T_0 = 11.0$ sec, $T_1 = 25.5$ sec<br>$V_{max} = 1000$ , $\epsilon = 20$                                   |
|            |                | E: $T_0 = 10.8$ sec, $T_1 = 16.8$ sec<br>$V_{max} = 1000$ , $\epsilon = 20$                                   |
|            | Benioff        | Z: $T_0 = 1.04$ sec, $T_1 = 0.5$ sec<br>$V_{max} = 5000$ , $h = h' = 1$<br>(Reference 1 - see end of section) |
| <b>DUR</b> | Milne-Shaw     | N, E: $T_0 = 12$ sec, $V = 250$ , $\epsilon = 20$   |
| <b>KEW</b> | Galitzin       | N, E: $T_0 = T_1 = 18$ sec, $V_{max} = 490$   |
|            |                | Z: $T_0 = T_1 = 13$ sec, $V_{max} = 250$  |
| <b>DBN</b> | Galitzin-Wilip | N, E: $T_0 = T_1 = 25$ sec, $V_{max} = 310$   |
|            |                | Z: $T_0 = T_1 = 12$ sec, $V_{max} = 740$  |
| <b>UCC</b> | Galitzin       | N: $T_0 = T_1 = 24.5$ sec, $V_{max} = 840$  |
| <b>PAR</b> | Wiechert       | N: $T_0 = 12$ sec, $V = 220$ , $\epsilon = 4$   |
|            |                | E: $T_0 = 12$ sec, $V = 230$ , $\epsilon = 4$<br>(Charlier and Van Gils, 1953)                                |

|            |                |   |
|------------|----------------|---|
| <b>STU</b> | Galitzin-Wilip | N: $T_0 = 12$ sec, $T_1 = 11.9$ sec, $V_{max} = 1330$                                   |
|            |                | E: $T_0 = T_1 = 11.9$ sec, $V_{max} = 1310$   |
|            |                | Z: $T_0 = 11.8$ sec, $T_1 = 11.7$ sec, $V_{max} = 1260$                                 |
|            | Hiller         | Z: $T_0 = 1.45$ sec, $T_1 = 1.0$ sec, $V_{max} = 6700$<br>(Charlier and Van Gils, 1953) |
| <b>LPZ</b> | Galitzin-Wilip | N: $T_0 = T_1 = 12.6$ sec, $V_{max} = 1313$   |
|            |                | Z: $T_0 = 11.7$ sec, $T_1 = 10.0$ sec, $V_{max} = 865$                                  |

Reference 1 : United States Coast and Geodetic Survey, 1958.

## 3. 1957 Magnitude Estimates

## Magnitude Estimates From Seismograms

| STATION<br>CODE | $\Delta$<br>(Deg.) | $M_S$ | $m_b$            | RATING         |
|-----------------|--------------------|-------|------------------|----------------|
| SIT             | 8.8                | 5.4   | 6.5              | B <sup>-</sup> |
| BZM             | 11.4               | —     | 6.2              | B <sup>-</sup> |
| BRK             | 12.3               | 5.7   | 7.1              | A              |
| SLC             | 13.8               | 5.7   | 7.1              | B <sup>-</sup> |
| PAS             | 16.9               | 5.9   | 6.0              | B              |
| HAY             | 18.0               | 5.9   | 6.1              | A <sup>-</sup> |
| LAW             | 24.8               | —     | 6.5 (P), 6.0 (S) | C              |
| FLO             | 27.8               | 6.0   | 6.4 (P), 6.1 (S) | A              |
| SLM             | 28.2               | 5.9   | 6.3              | B <sup>-</sup> |
| RES             | 28.3               | 6.0   | 6.4              | B <sup>-</sup> |
| CLE             | 32.3               | —     | 6.9 (P), 5.9 (S) | B              |
| OTT             | 34.2               | —     | 6.5 (P), 6.0 (S) | A <sup>-</sup> |
| SHF             | 35.5               | —     | 6.1              | A <sup>-</sup> |
| PAL             | 37.5               | 6.1   | 6.0 (P), 5.9 (S) | B              |
| WES             | 38.4               | —     | 6.4              | B <sup>-</sup> |
| HAL             | 42.1               | 5.9   | 6.0 (P), 5.6 (S) | A <sup>-</sup> |
| IVI             | 43.3               | 6.1   | —                | B <sup>+</sup> |
| SCO             | 48.5               | 6.1   | —                | A <sup>-</sup> |
| SJP             | 57.3               | 5.8   | 6.3 (P), 5.6 (S) | B <sup>+</sup> |
| DUR             | 66.0               | 6.0   | —                | A              |
| KEW             | 69.2               | 5.9   | —                | A              |
| DBN             | 70.6               | 6.0   | —                | A              |
| UCC             | 71.3               | 5.7   | —                | B <sup>+</sup> |
| PAR             | 72.5               | 5.9   | —                | B              |
| STU             | 74.8               | 5.9   | 5.8              | B              |
| LPZ             | 83.6               | 5.3   | —                | C              |

Note: if magnitude estimates were available from more than one instrument (i.e. horizontal and vertical) the average value is given in the table. P and S in the  $m_b$  column indicate the type of wave used in this magnitude determination.

The rating scale is described below :

A indicates that calibration data was obtained from the station, both horizontal components were available and amplitudes and periods could be accurately measured.

B indicates that one of the above conditions was not met.

C indicates that two or more of the above conditions were not met.

+ and - serve to indicate the severity of the problem, for example, uncertainties in instrument magnification are generally more serious than uncertainties in measured amplitudes or periods.

#### 1957 Magnitude Estimates From Bulletin Readings

| STATION<br>CODE | $\Delta$<br>(Deg.) | $M_S$ | $m_b$ | RATING |
|-----------------|--------------------|-------|-------|--------|
| SEN             | 63.4               | —     | 6.6   | A      |
| ABE             | 64.1               | 6.2   | —     | B      |
| DUR             | 66.0               | 6.1   | —     | A      |
| ABU             | 68.9               | 5.9   | 6.3   | A      |
| KEW             | 69.2               | 5.9   | —     | A      |
| HUA             | 76.3               | —     | 6.3   | B      |
| CRT             | 79.9               | —     | 6.6   | B      |

Note:

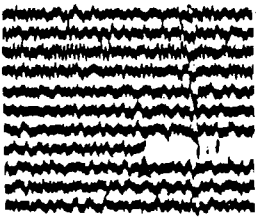
A indicates readings from both horizontal components were available.

B indicates that only one horizontal component was available.

#### 4. 1957 First Motion Data

The following data, 1 – 1 copies of original seismograms, show the quality of the first motion picks. For each seismogram the station code and the component of the ground motion is given. SP refers to short period seismometers ( $< 10$  sec) and LP refers to long period seismometers ( $> 10$  sec). The top of each seismogram corresponds to either ground motion up, North or East (depending on the component). Arrows indicate the location and direction of the first motion pick.

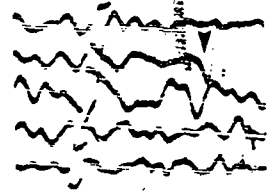
SEA SPZ



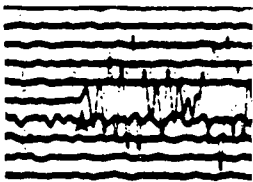
SIT SPZ



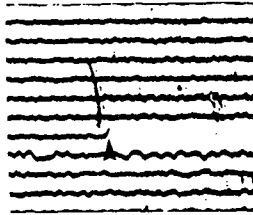
COL SPZ



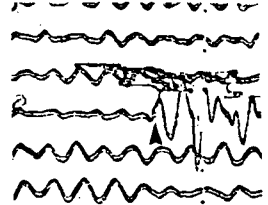
BZM SPZ



SLC SPZ



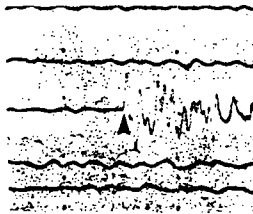
BRK LPZ



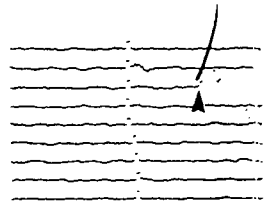
PAS LPZ



HAY LPZ



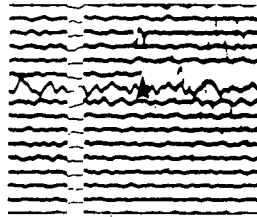
DLT SPZ



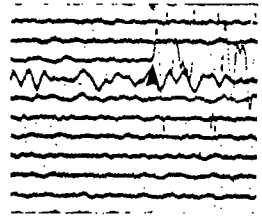
TUO SPZ



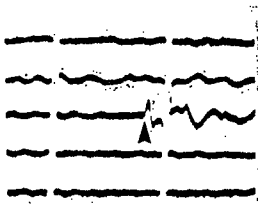
LAW SPZ



FAY SPZ



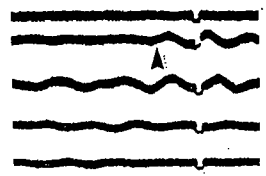
FLO LPZ



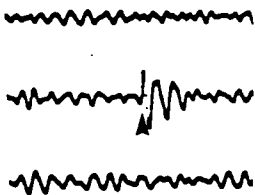
SLM LPN



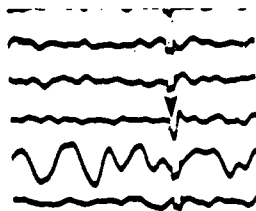
SLM LPE



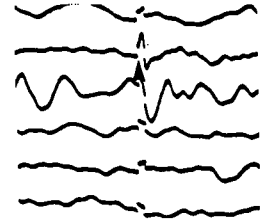
WAY LPZ



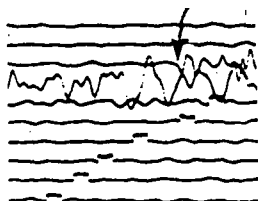
CLE LPN



CLE LPE



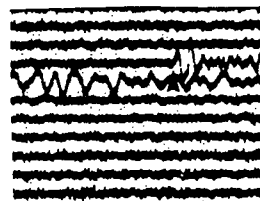
RES SPZ



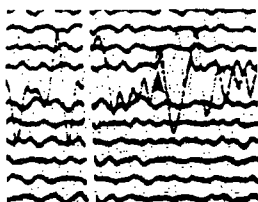
THU SPZ



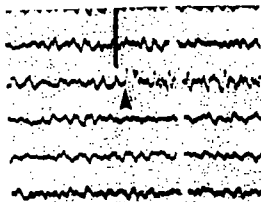
OTT SPZ



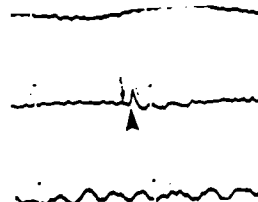
SHF SPZ



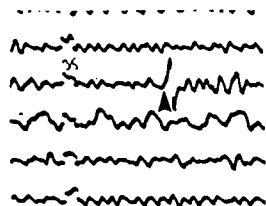
HAL SPZ



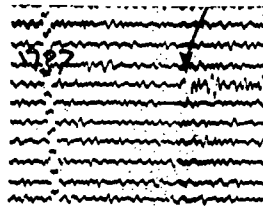
PAL LPZ



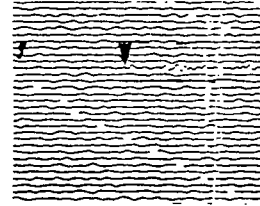
WES SPZ



SJP SPZ



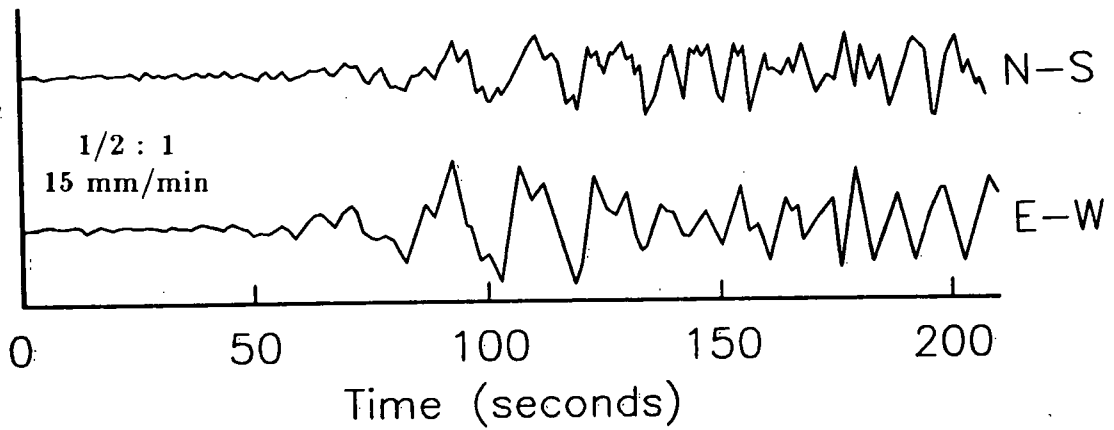
STU SPZ



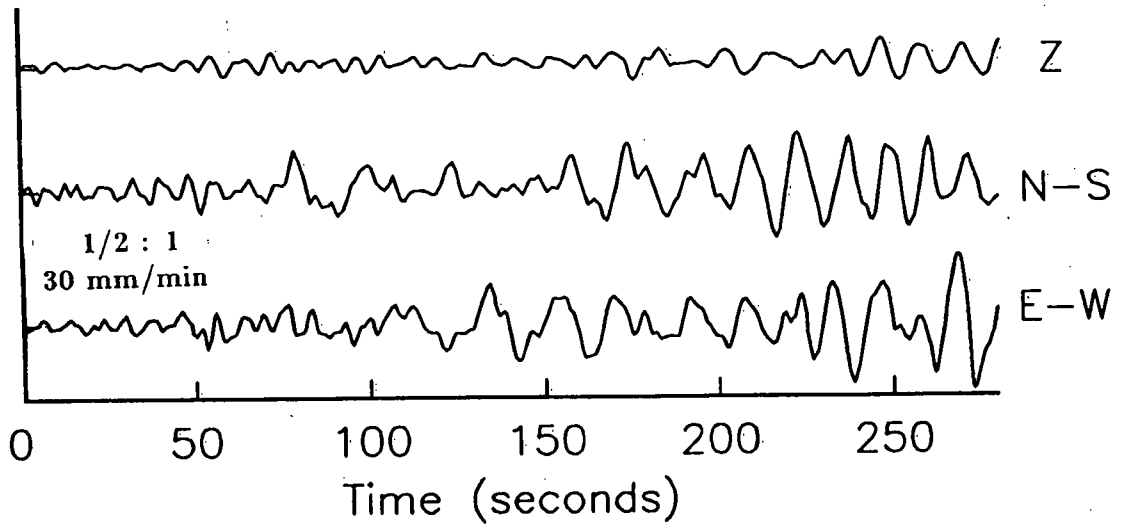
### 5. Digitized Surface Waves of the 1957 Earthquake

The following data are the digitized surface waves of the 1957 earthquake. The component of the ground motion is given to the right of each trace. Also indicated on each diagram are the ratio of the plotted amplitude to the true seismogram amplitude, and the drum speed of the original seismogram. Note that time 0 indicated on each record corresponds to the calculated arrival time, at that station, of surface waves having a group velocity of 5.0 km/sec.

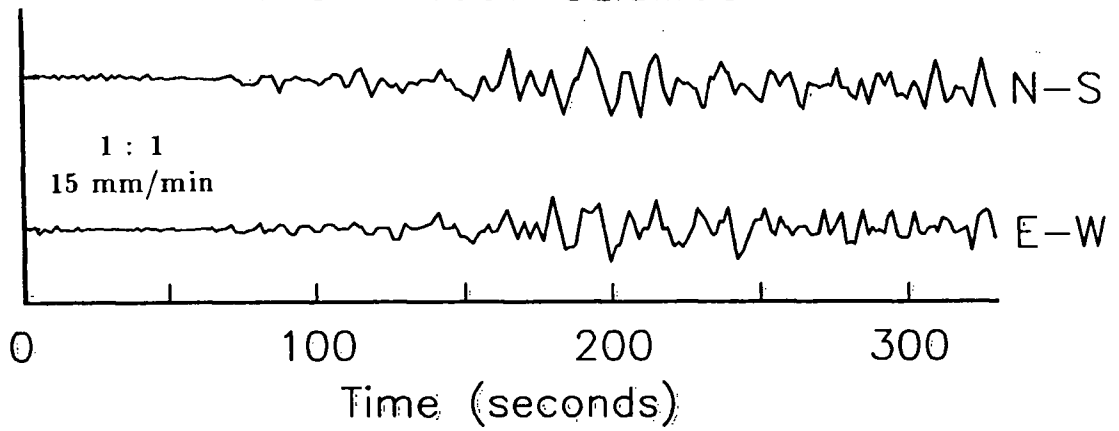
## SIT - 1957 SEISMOGRAMS



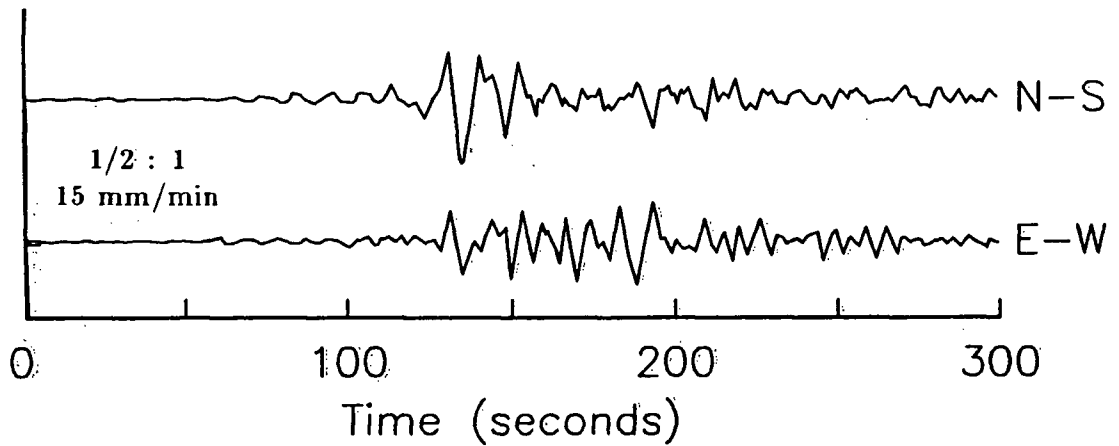
## BRK - 1957 SEISMOGRAMS



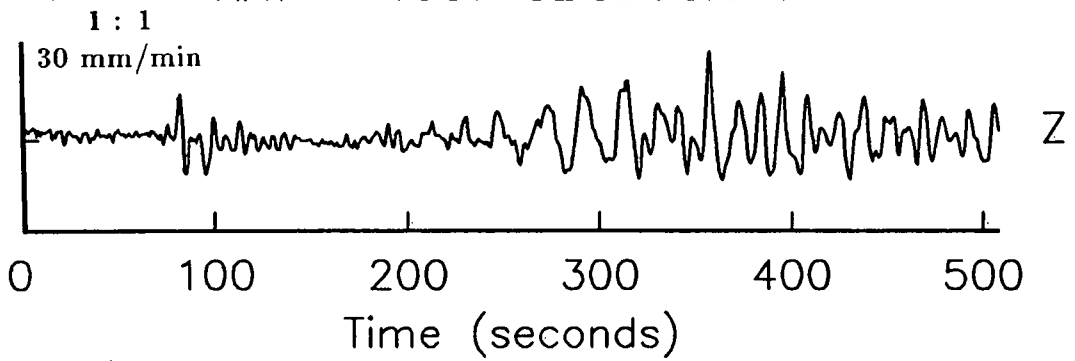
## SLC - 1957 SEISMOGRAMS



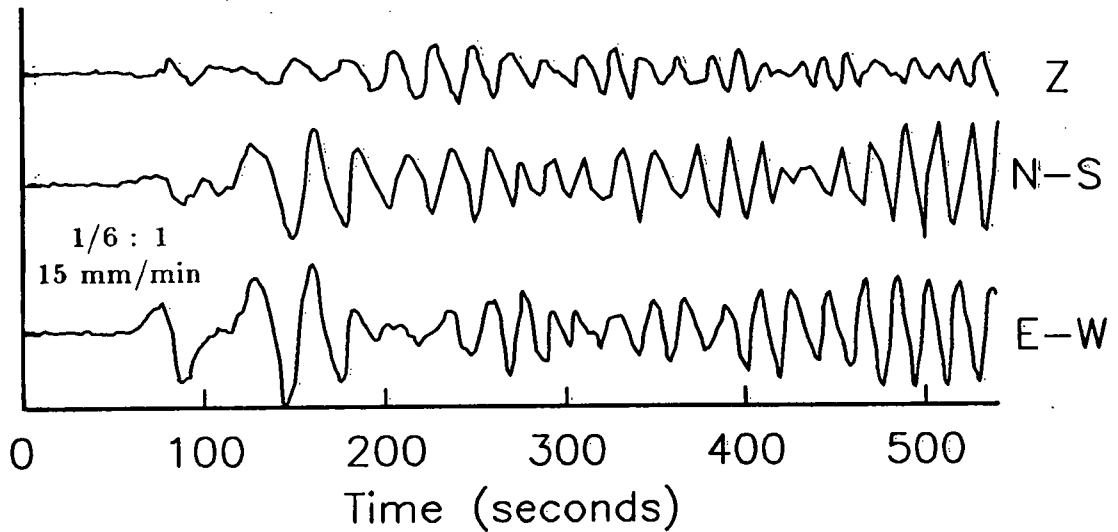
## BZM - 1957 SEISMOGRAMS



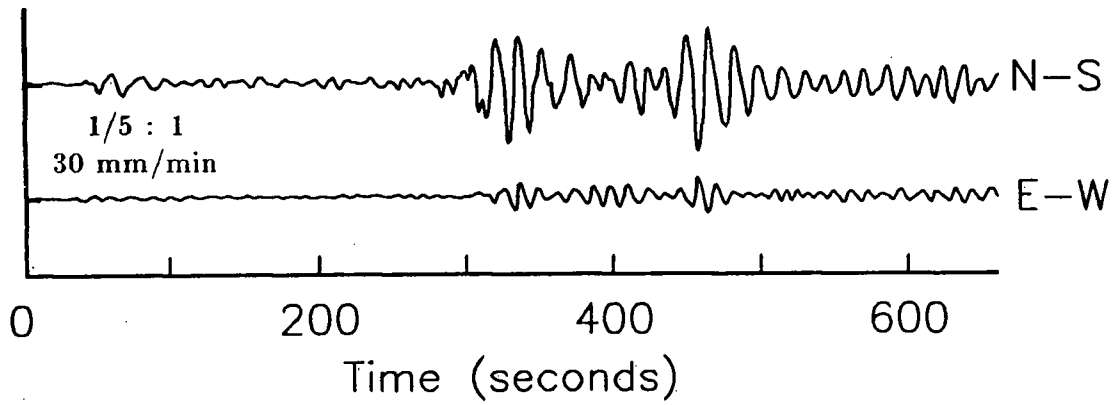
## HAY - 1957 SEISMOGRAM



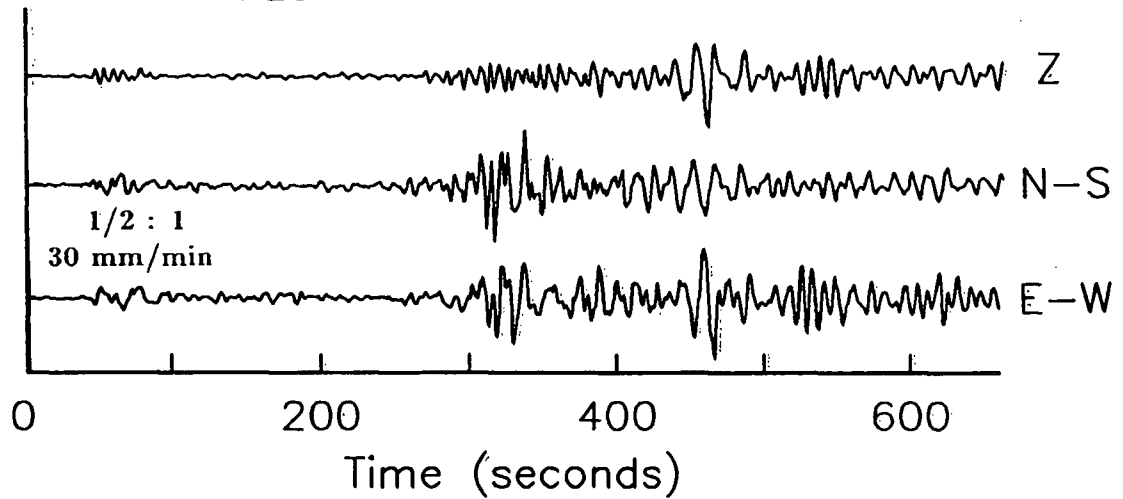
## PAS - 1957 SEISMOGRAMS



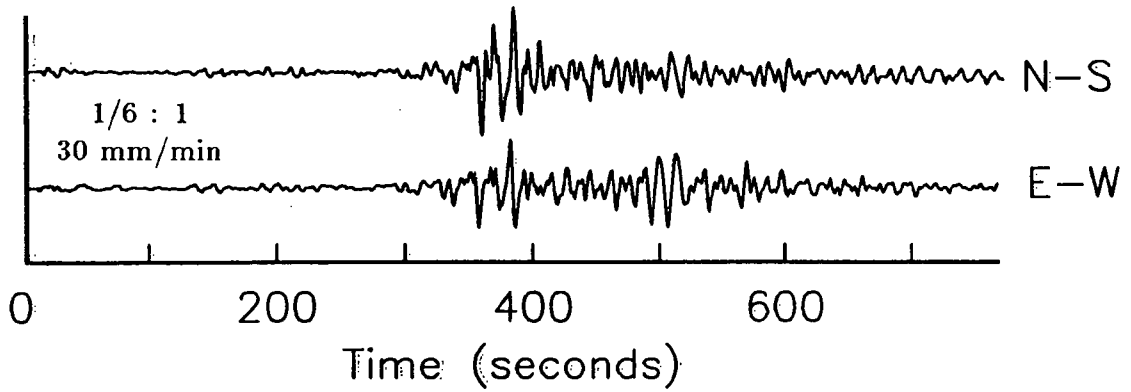
## SLM - 1957 SEISMOGRAMS



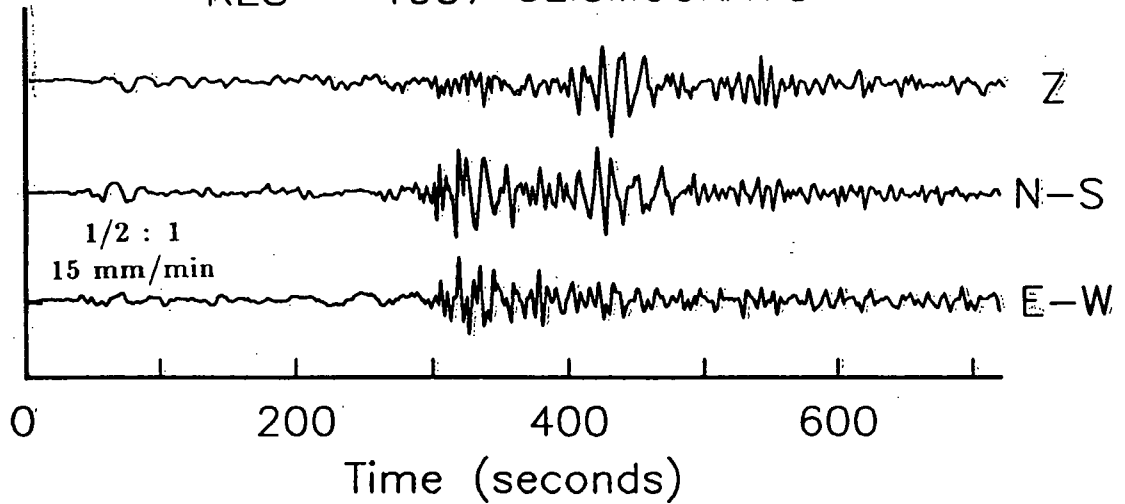
## FLO - 1957 SEISMOGRAMS



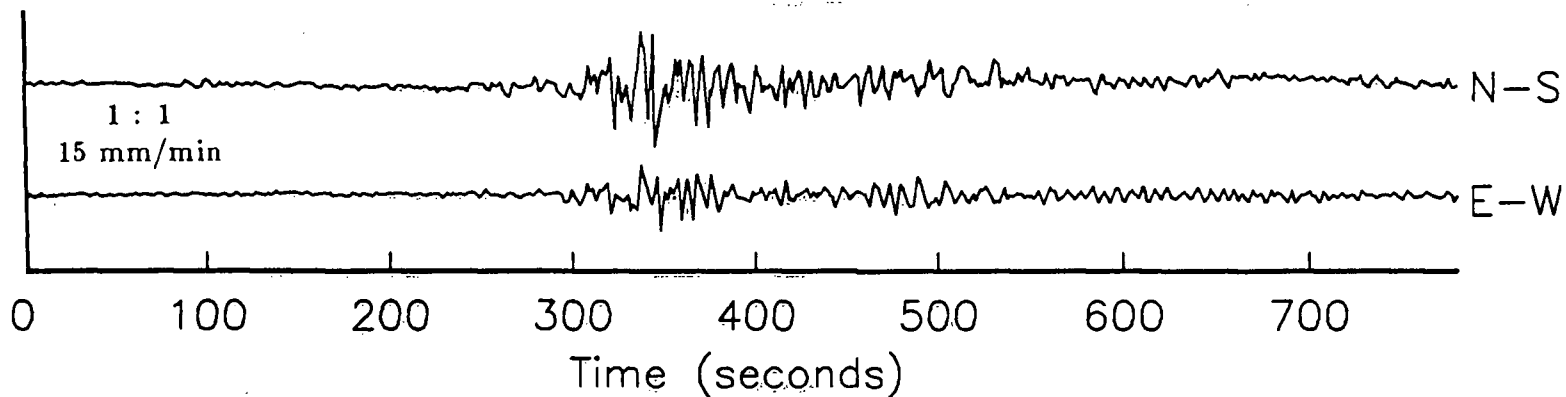
## CLE - 1957 SEISMOGRAMS



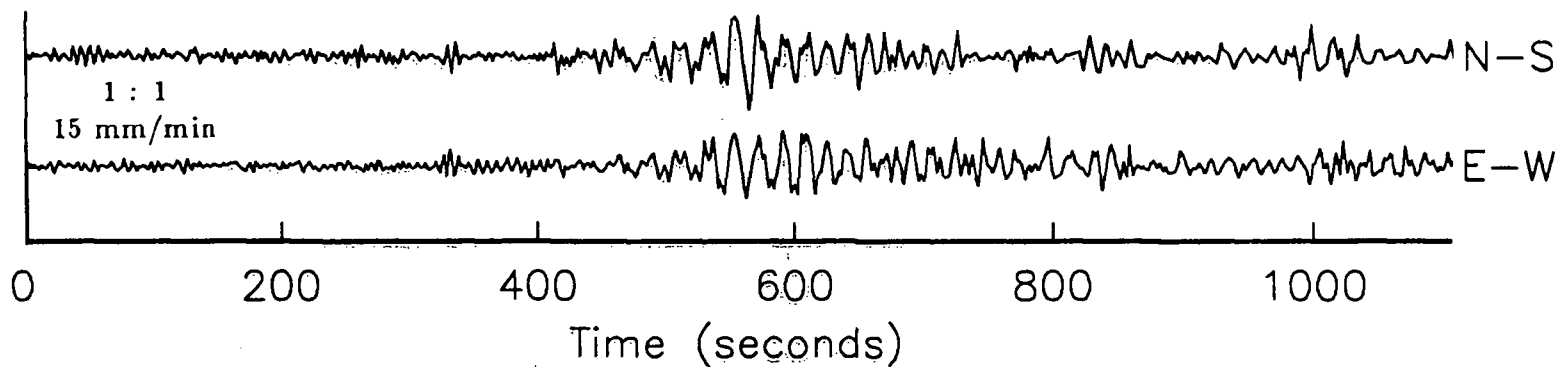
## RES - 1957 SEISMOGRAMS



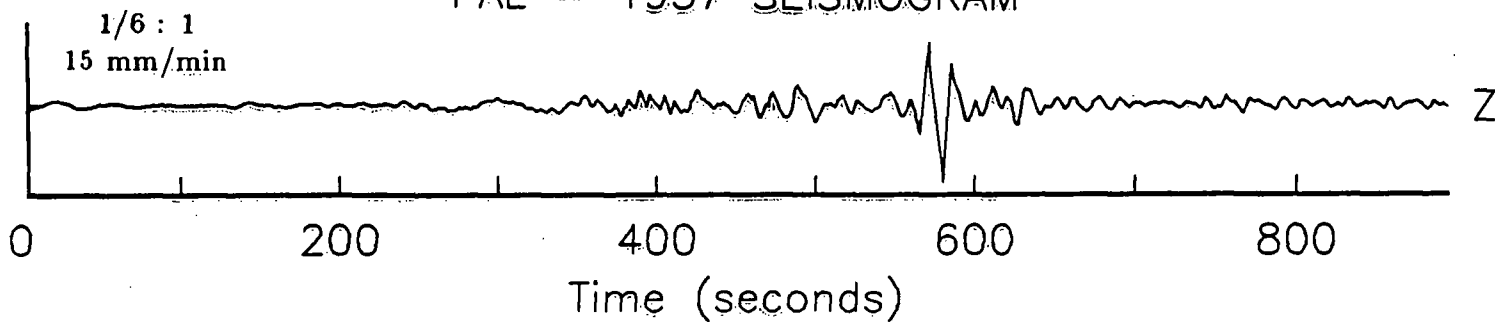
OTT - 1957 SEISMOGRAMS



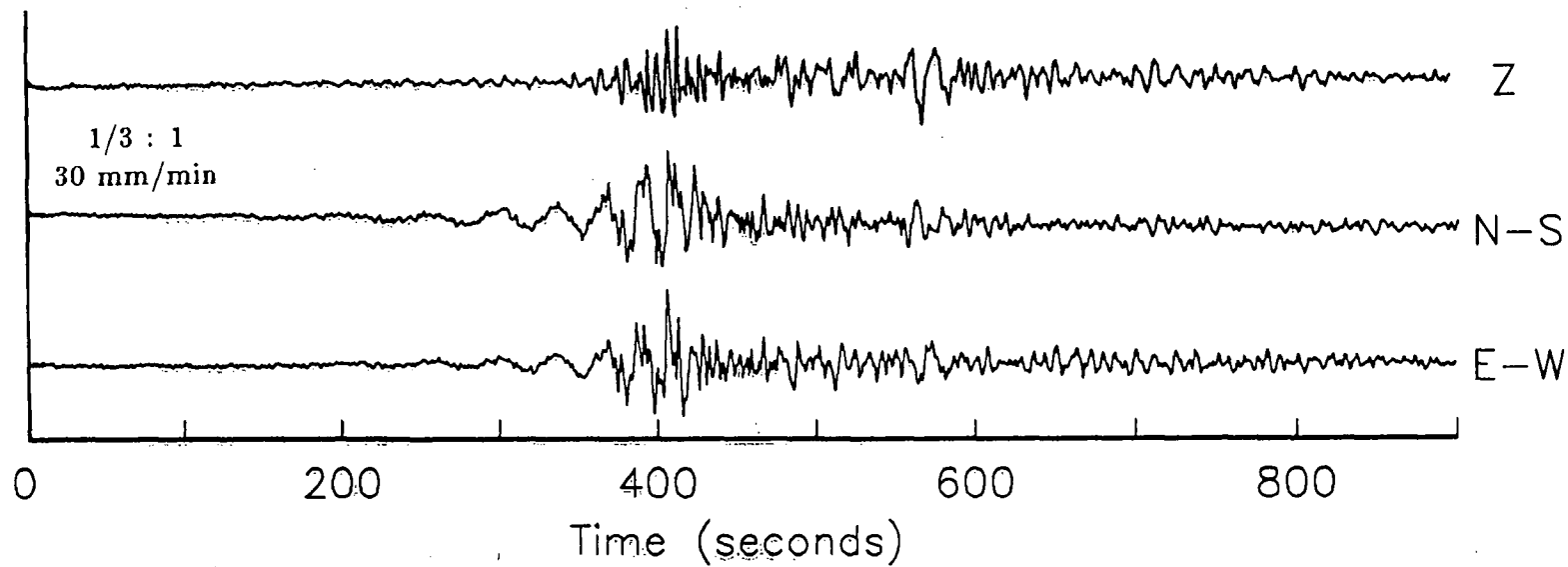
SCO - 1957 SEISMOGRAMS



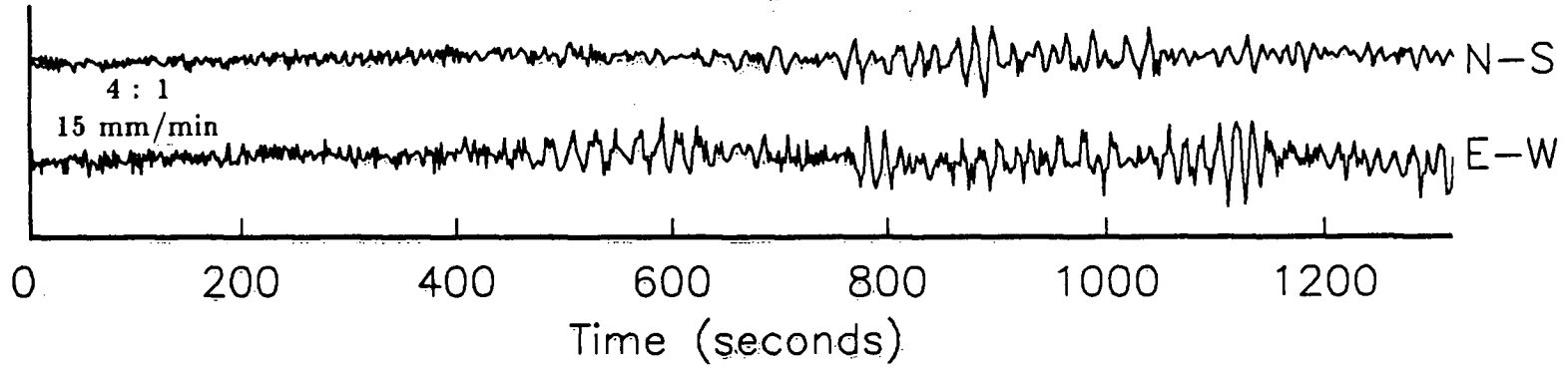
PAL - 1957 SEISMOGRAM



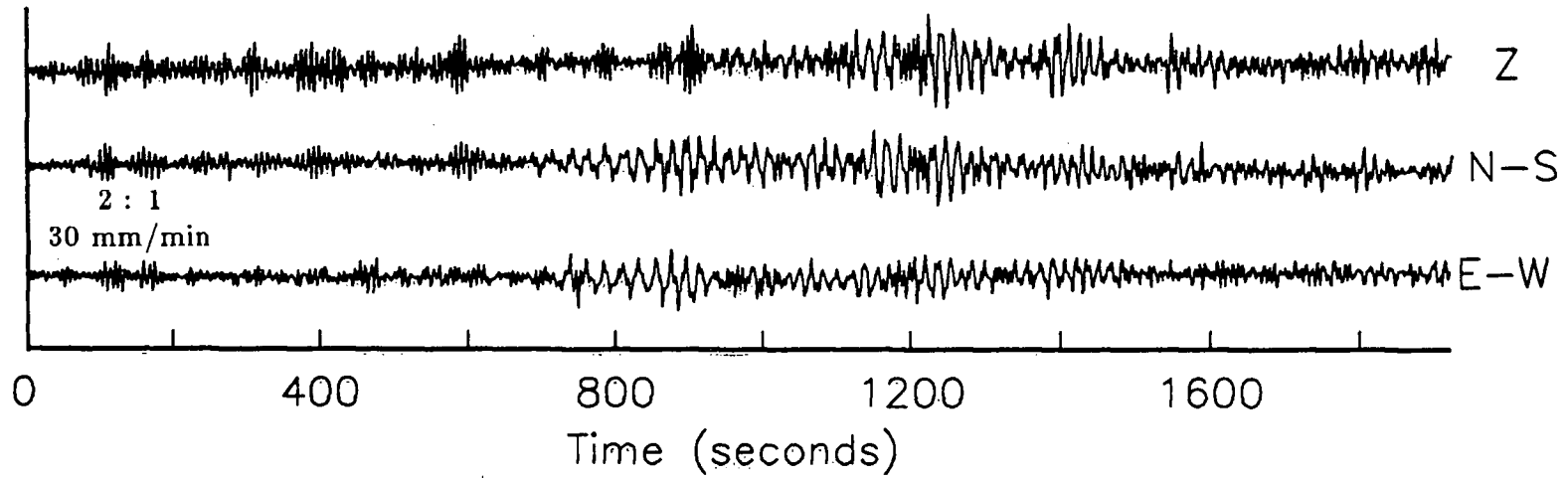
WES - 1957 SEISMOGRAMS



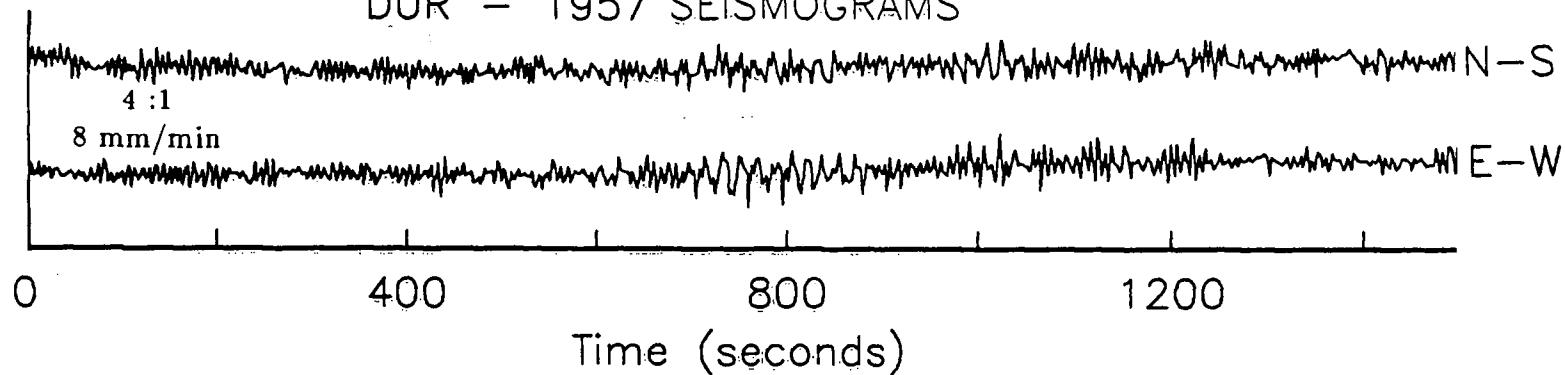
SJP - 1957 SEISMOGRAMS



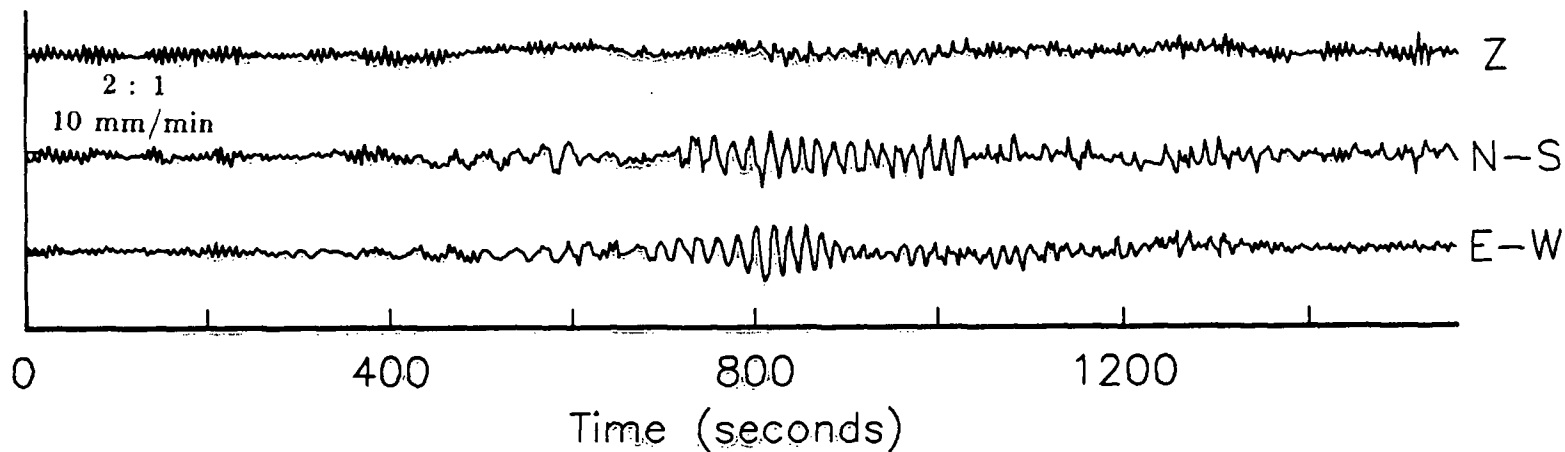
STU - 1957 SEISMOGRAMS

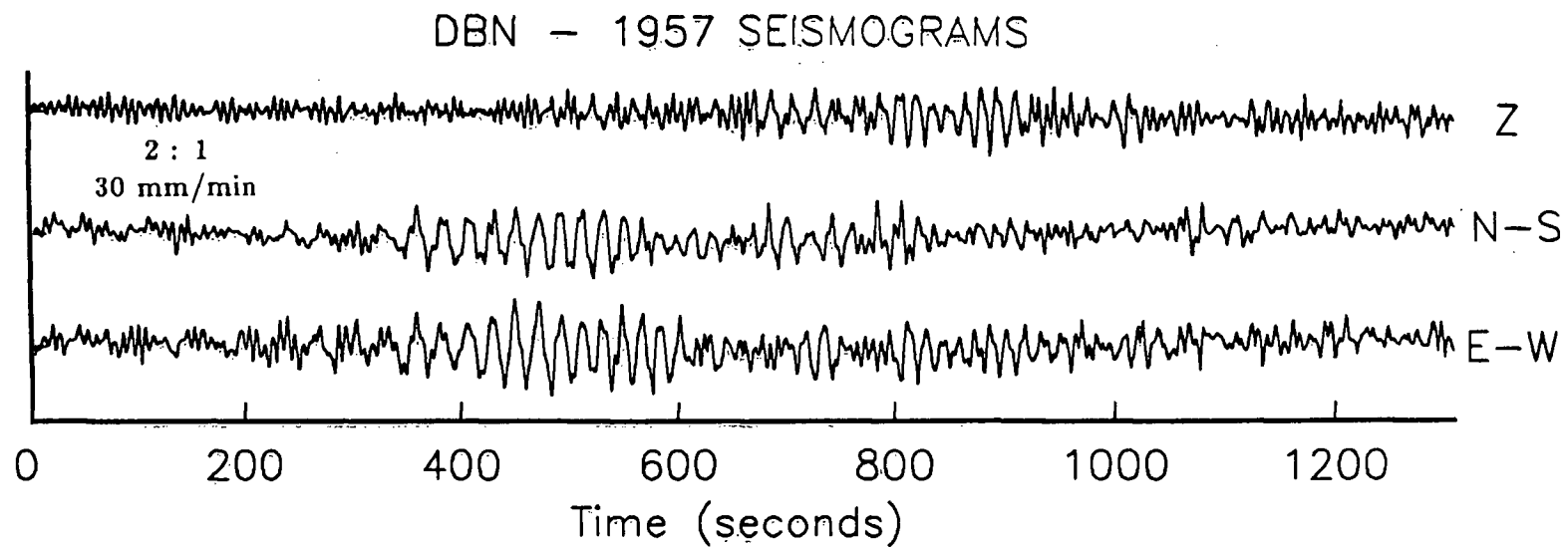
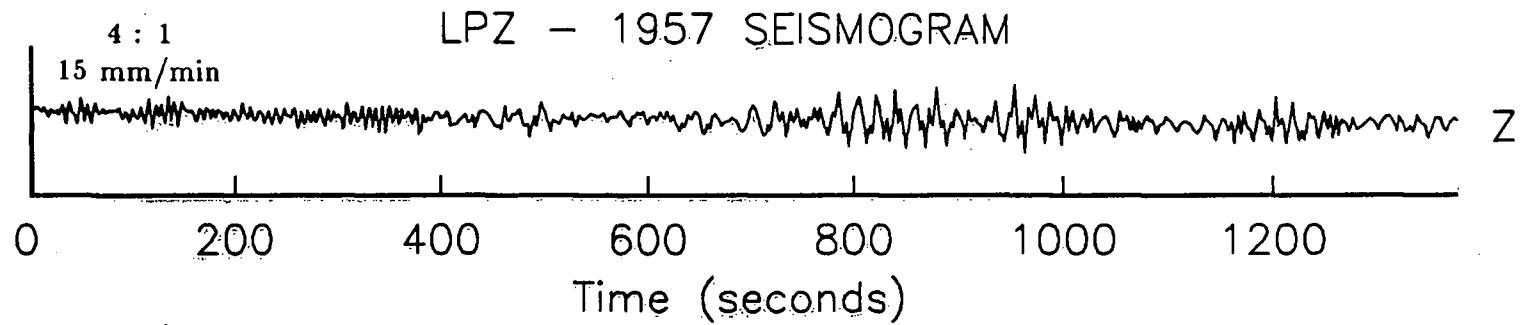


DUR - 1957 SEISMOGRAMS



KEW - 1957 SEISMOGRAMS





**APPENDIX C -- 1918 EARTHQUAKE DATA****1. Arrival Times and First Motion Polarity**

For each station considered in the epicentre study, the following table provides; the P-wave arrival time; the azimuth of the station (with respect to the epicentre); the epicentral distance; the first motion polarity estimate; the weight given the reading (see section 4.5); and the source of the arrival time information. ISS represents the 1918 ISS bulletin; Bull. indicates that the arrival time was obtained from that stations' bulletin; and Seis. indicates that the arrival time was read directly from a seismogram.

| STATION<br>CODE | AZ.<br>(DEG) | DELTA<br>(DEG) | ARRIVAL<br>TIME |    |      | FIRST<br>MOTION | WEIGHT | SOURCE |
|-----------------|--------------|----------------|-----------------|----|------|-----------------|--------|--------|
|                 |              |                | h               | m  | s    |                 |        |        |
| VIC             | 121.4        | 2.1            | 08              | 41 | 44   | -               | -      | ISS    |
| SIT             | 326.9        | 9.3            | 08              | 43 | 23   | D               | 50     | Seis.  |
| BRK             | 165.4        | 12.1           | 08              | 44 | 01.0 | -               | -      | Bull.  |
| SAS             | 71.1         | 12.5           | 08              | 44 | 05.0 | C               | 50     | Seis.  |
| MHC             | 163.7        | 12.7           | 08              | 44 | 11   | C               | 50     | Seis.  |
| DEN             | 115.5        | 17.8           | 08              | 45 | 12.6 | -               | -      | Seis.  |
| TUO             | 141.1        | 20.8           | 08              | 45 | 52   | -               | -      | Seis.  |
| LAW             | 104.2        | 24.4           | 08              | 46 | 24   | -               | -      | ISS    |
| SLM             | 99.7         | 27.7           | 08              | 47 | 00   | C               | 50     | Seis.  |
| AAM             | 87.7         | 30.1           | 08              | 46 | 30   | -               | -      | ISS    |
| TNT             | 82.5         | 32.2           | 08              | 47 | 54   | -               | -      | ISS    |
| OTT             | 77.5         | 33.8           | 08              | 47 | 50   | C               | 50     | Seis.  |
| SHA             | 109.3        | 34.1           | 08              | 47 | 50   | -               | -      | ISS    |
| ITH             | 82.6         | 34.6           | 08              | 48 | 33   | -               | -      | ISS    |
| GEO             | 88.3         | 36.1           | 08              | 48 | 11   | -               | -      | Bull.  |
| WAS             | 88.3         | 36.1           | 08              | 48 | 11.1 | C               | 100    | Seis.  |
| NRT             | 77.7         | 36.2           | 08              | 48 | 13.5 | C               | 50     | Seis.  |
| CLH             | 88.3         | 36.3           | 08              | 48 | 15.0 | C               | 50     | Seis.  |
| TAC             | 134.9        | 37.0           | 08              | 48 | 03   | -               | -      | ISS    |
| HRV             | 79.5         | 37.8           | 08              | 48 | 07   | -               | -      | ISS    |
| HON             | 233.4        | 37.9           | 08              | 48 | 24.0 | -               | -      | Bull.  |
| HAL             | 72.1         | 41.7           | 08              | 48 | 55   | C               | 50     | Seis.  |
| BHP             | 120.1        | 56.0           | 08              | 51 | 00   | -               | -      | ISS    |
| VQS             | 100.5        | 57.4           | 08              | 51 | 32   | -               | -      | ISS    |
| DYC             | 30.2         | 63.9           | 08              | 51 | 48   | -               | -      | ISS    |
| ESK             | 32.0         | 65.1           | 08              | 51 | 58   | -               | -      | Bull.  |
| BID             | 33.2         | 66.7           | 08              | 52 | 42   | -               | -      | Bull.  |
| UPP             | 18.9         | 67.0           | 08              | 52 | 39.4 | -               | -      | Seis.  |
| OSA             | 299.4        | 69.4           | 08              | 52 | 18   | -               | -      | Bull.  |
| DBN             | 29.5         | 70.5           | 08              | 52 | 27   | C               | 50     | Seis.  |
| UCC             | 30.6         | 71.4           | 08              | 52 | 26   | D               | 50     | Seis.  |
| GTT             | 27.0         | 72.5           | 08              | 52 | 35   | D               | 50     | Seis.  |
| HOH             | 28.9         | 74.7           | 08              | 52 | 45   | D               | 50     | Seis.  |
| COI             | 44.6         | 75.1           | 09              | 02 | 25   | -               | -      | ISS    |
| MNC             | 31.6         | 77.5           | 08              | 50 | 28   | -               | -      | ISS    |
| EBR             | 38.5         | 78.4           | 08              | 53 | 10.8 | D               | 50     | Seis.  |
| RDP             | 29.8         | 82.1           | 08              | 53 | 30   | -               | -      | ISS    |
| MCI             | 29.2         | 82.7           | 08              | 53 | 40   | -               | -      | Bull.  |
| ALG             | 38.9         | 82.9           | 08              | 53 | 28   | -               | -      | ISS    |
| LPZ             | 125.0        | 83.3           | 08              | 53 | 36   | C               | 50     | Seis.  |
| PMP             | 29.0         | 83.6           | 08              | 54 | 49   | -               | -      | Bull.  |
| MAN             | 296.7        | 93.0           | 08              | 54 | 00   | -               | -      | Bull.  |
| SMI             | 340.0        | 97.0           | 08              | 51 | 24   | -               | -      | ISS    |
| RIV             | 241.9        | 110.7          | 08              | 56 | 00   | -               | -      | Bull.  |
| KOD             | 333.8        | 116.9          | 09              | 01 | 18   | -               | -      | ISS    |
| COC             | 330.1        | 119.3          | 08              | 44 | 00   | -               | -      | ISS    |
| CTO             | 72.4         | 149.6          | 09              | 46 | 30   | -               | -      | ISS    |
| MRI             | 352.5        | 150.4          | 09              | 58 | 30   | -               | -      | ISS    |

## 2. 1918 Instrumental Constants

The following list provides information on instrument type, and parameters for each station considered in this study. For simple mechanical seismographs the constants are;  $T_0$ , the free period of the seismometer;  $\epsilon$ , the damping ratio; and  $V$ , the static magnification (see Richter, 1958 p. 219). For electromagnetic seismographs the constants are;  $T_0$ , the seismometer period;  $T_1$  the galvanometer period;  $h$ , the seismometer damping constant;  $h'$ , the galvanometer damping constant; and  $\sigma^2$ , the coupling coefficient.

Note: if no reference is given, information was sent with the seismograms.

|            |             |  |
|------------|-------------|--|
| <b>SIT</b> | Bosch-Omori | N: $T_0 = 16$ sec, $V = 10$<br>E: $T_0 = 18$ sec, $V = 10$<br>(Wood, 1921)   |
| <b>SAS</b> | Mainka      | N: $T_0 = 9.1$ sec, $\epsilon = 5$ , $V = 60^1$<br>E: $T_0 = 9.3$ sec, $\epsilon = 5$ , $V = 60^1$<br>(Wood, 1921) |
| <b>MHC</b> | Wiechert    | N, E, Z: $T_0 = 4-8$ sec, $V = 80$ , $\epsilon = 8$<br>(station bulletin)  |
| <b>DEN</b> | Wiechert    | N, E: $T_0 = 6$ sec, $V \simeq 80^2$<br>(Charlier and Van Gils, 1953)  |

|            |                 |  |
|------------|-----------------|--|
| <b>TUO</b> | Bosch-Omori     | N: $T_0 = 18 \text{ sec}, V = 10$<br>E: $T_0 = 14 \text{ sec}, V = 10$<br>(station bulletin)                             |
| <b>SLM</b> | Wiechert        | N, E: $T_0 = 6 \text{ sec}, V = 60-90, \epsilon = 3-5$   |
| <b>OTT</b> | Bosch           | N: $T_0 = 8 \text{ sec}, V = 120, \epsilon = 2^1$<br>E: $T_0 = 7.1 \text{ sec}, V = 120, \epsilon = 8^1$<br>(Wood, 1921) |
| <b>WAS</b> | Marvin Pendulum | N, E: $T_0 = 6.4 \text{ sec}, V = 110$<br>(Wood, 1921)   |
| <b>NRT</b> | Bosch-Omori     | N: $T_0 = 16 \text{ sec}, V = 10$<br>E: $T_0 = 15 \text{ sec}, V = 10$<br>(Wood, 1921)                                   |
| <b>CLH</b> | Bosch-Omori     | N, E: $T_0 = 15 \text{ sec}, V = 10$<br>(Wood, 1921)   |
| <b>HAL</b> | Mainka          | N, E: $T_0 = 10 \text{ sec}, V \simeq 80 ?, \epsilon = 5-7$<br>(Wood, 1921)  |
| <b>EDI</b> | Milne-Shaw      | E: $T_0 = 15.3 \text{ sec}, V = 6, \epsilon = 1.2$   |

|                    |          |   |
|--------------------|----------|---|
| <b>UPP</b>         | Wiechert | N: $T_0 = 9.8 \text{ sec}, V = 189, \epsilon = 3.7$                           |
|                    |          | E: $T_0 = 9.4 \text{ sec}, V = 191, \epsilon = 3.7$                           |
| (Wood, 1921)       |          |   |
| <b>DBN</b>         | Galitzin | N: $T_0 = T_1 = 24.4 \text{ sec}, V_{max} = 311, h = h' = 1$                  |
|                    |          | E: $T_0 = T_1 = 24.9 \text{ sec}, V_{max} = 319, h = h' = 1$                  |
| <b>UCC</b>         | Wiechert | N: $T_0 = 11.2\text{--}11.5 \text{ sec}, V = 150, \epsilon = 3.9\text{--}4.5$ |
|                    |          | E: $T_0 = 10.2\text{--}10.5 \text{ sec}, V = 165, \epsilon = 3.5\text{--}3.7$ |
|                    |          | Z: $T_0 = 4.7\text{--}4.9 \text{ sec}, V = 165, \epsilon = 2.8\text{--}2.9$   |
| <b>GTT</b>         | Wiechert | N: $T_0 = 10.2 \text{ sec}, V = 160$  |
|                    |          | E: $T_0 = 9.5 \text{ sec}, V = 170$   |
|                    |          | Z: $T_0 = 4.0 \text{ sec}, V = 220$   |
| <b>HOH</b>         | Mainka   | N: $T_0 = 9.5 \text{ sec}, V = 150, \epsilon = 5$                             |
| <b>MNH</b>         | Wiechert | N: $T_0 = 11.7 \text{ sec}, V = 208, \epsilon = 5.2$                          |
|                    |          | E: $T_0 = 10.7 \text{ sec}, V = 206, \epsilon = 4.7$                          |
| (station bulletin) |          |   |
| <b>EBR</b>         | Mainka   | N: $T_0 = 15.0 \text{ sec}, V = 200$  |
|                    |          | E: $T_0 = 7.5 \text{ sec}, V = 100$   |

**LPZ** Mainka

N:  $T_0 = 14$  sec,  $V = 180$

E:  $T_0 = 18$  sec,  $V = 80$

(Wood, 1921)

**RIV** Wiechert

N:  $T_0 = 8.4$  sec,  $V = 200$ ,  $\epsilon = 8.2$

E:  $T_0 = 8.5$  sec,  $V = 200$ ,  $\epsilon = 4.0$

<sup>1</sup> parameter estimate from Rogers (personal communication)

<sup>2</sup> V estimate – see Richter, 1958 p.223

## 3. 1918 Magnitude Estimates

## Magnitude Estimates From Seismograms

| STATION<br>CODE | $\Delta$<br>(Deg.) | $M_S^G$ | $M_S$ | $m_b$ | RATING         |
|-----------------|--------------------|---------|-------|-------|----------------|
| SIT             | 9.3                | —       | 6.9   | —     | B <sup>+</sup> |
| SAS             | 12.6               | —       | —     | 8.0   | B <sup>-</sup> |
| MHC             | 12.7               | —       | 6.8   | 8.3   | B              |
| DEN             | 18.0               | 6.7     | 6.9   | 7.2   | B <sup>-</sup> |
| TUO             | 20.8               | 6.8     | 7.0   | 7.3   | B <sup>+</sup> |
| SLM             | 27.8               | —       | —     | 7.1   | B <sup>-</sup> |
| OTT             | 33.8               | —       | —     | 7.1   | B <sup>-</sup> |
| WAS             | 36.2               | —       | —     | 6.9   | B <sup>-</sup> |
| NRT             | 36.3               | 7.3     | 7.5   | 7.1   | B <sup>-</sup> |
| CLH             | 36.4               | 7.3     | 7.5   | 7.5   | C              |
| HAL             | 41.8               | —       | —     | 6.9   | C              |
| EDI             | 64.6               | 6.5     | 6.7   | —     | B <sup>-</sup> |
| UPP             | 66.7               | 6.7     | 6.8   | 7.3   | B <sup>+</sup> |
| DBN             | 70.5               | 6.8     | 7.2   | 7.3   | A              |
| UCC             | 71.4               | 6.5     | 6.7   | 6.8   | B <sup>+</sup> |
| GTT             | 72.5               | 6.7     | 6.9   | 6.6   | A <sup>-</sup> |
| HOH             | 74.8               | 6.6     | 6.8   | 6.8   | B <sup>+</sup> |
| MNH             | 76.0               | 6.8     | 6.9   | —     | A              |
| EBR             | 78.5               | 6.4     | 6.7   | 6.8   | B <sup>-</sup> |
| LPB             | 83.4               | 6.7     | 6.9   | 7.1   | B <sup>+</sup> |
| RIV             | 110.6              | 6.5     | 6.5   | —     | C              |

Note:

if magnitude estimates were available from more than one instrument (i.e. horizontal and vertical) the average value is given in the table.

The rating scale is described below :

A indicates that calibration data was obtained from the station, both horizontal components were available and amplitudes and periods could be accurately measured.

B indicates that one of the above conditions was not met.

C indicates that two or more of the above conditions were not met.

+ and - serve to indicate the severity of the problem, for example, uncertainties in instrument magnification are generally more serious than uncertainties in measured amplitudes or periods.

### 1918 Magnitude Estimates From Bulletin Readings

| STATION<br>CODE | $\Delta$<br>(Deg.) | $M_S^G$ | $M_S$ | $m_b$ | RATING |
|-----------------|--------------------|---------|-------|-------|--------|
| BRK             | 12.1               | —       | 6.3   | —     | C      |
| MHC             | 12.7               | —       | 6.7   | 8.5   | C      |
| ESK             | 65.1               | 6.7     | 6.8   | —     | C      |
| DBN             | 70.5               | 6.8     | 7.1   | —     | A      |
| HOH             | 74.8               | 6.5     | 6.7   | 6.5   | B      |
| FBR             | 78.6               | 6.9     | 7.1   | —     | B      |
| PMP             | 83.6               | 6.8     | 6.9   | 7.3   | B      |
| RIV             | 110.6              | 6.4     | 6.6   | 6.9   | B      |

Note:

A indicates readings from both horizontal components were available.

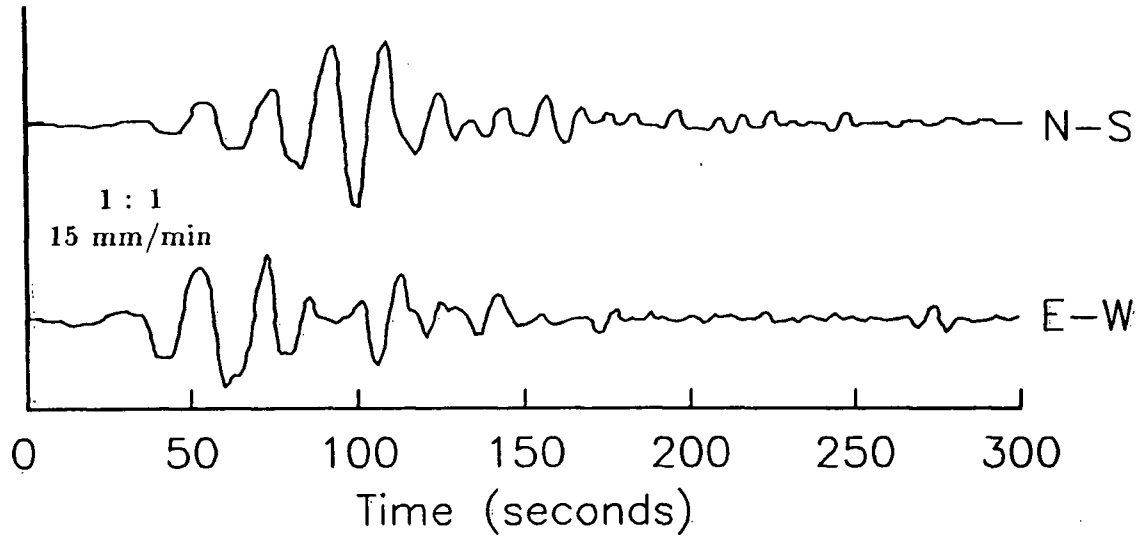
B indicates that only one horizontal component was available.

C indicates that the surface wave periods were slightly (1 - 4 seconds) outside the range for which the magnitude equations are valid.

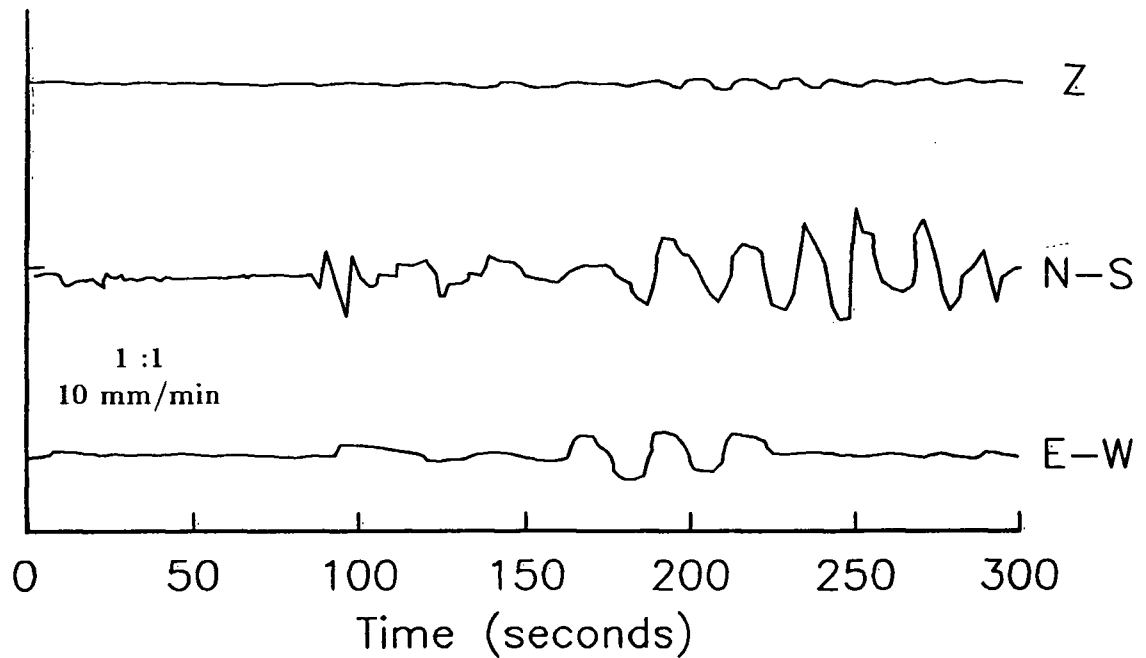
#### 4. Digitized Surface Waves of the 1918 Earthquake

The following data are the digitized surface waves of the 1918 earthquake. The component of the ground motion is given to the right of each trace. Also indicated on each diagram are the ratio of the plotted amplitude to the true seismogram amplitude, and the drum speed of the original seismogram. Note that time 0 indicated on each record corresponds to the calculated arrival time, at that station, of surface waves having a group velocity of 5.0 km/sec.

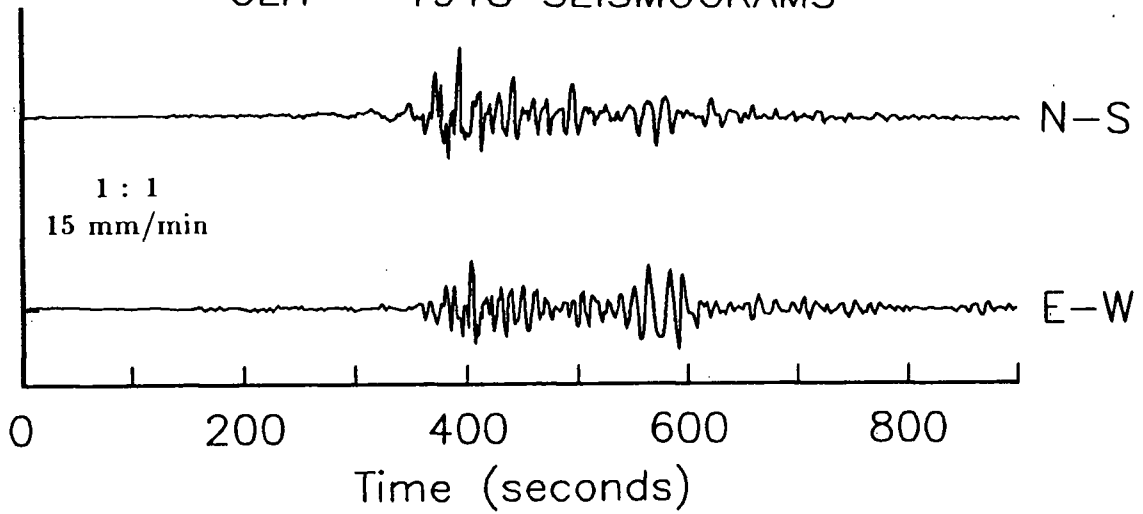
## SIT - 1918 SEISMOGRAMS



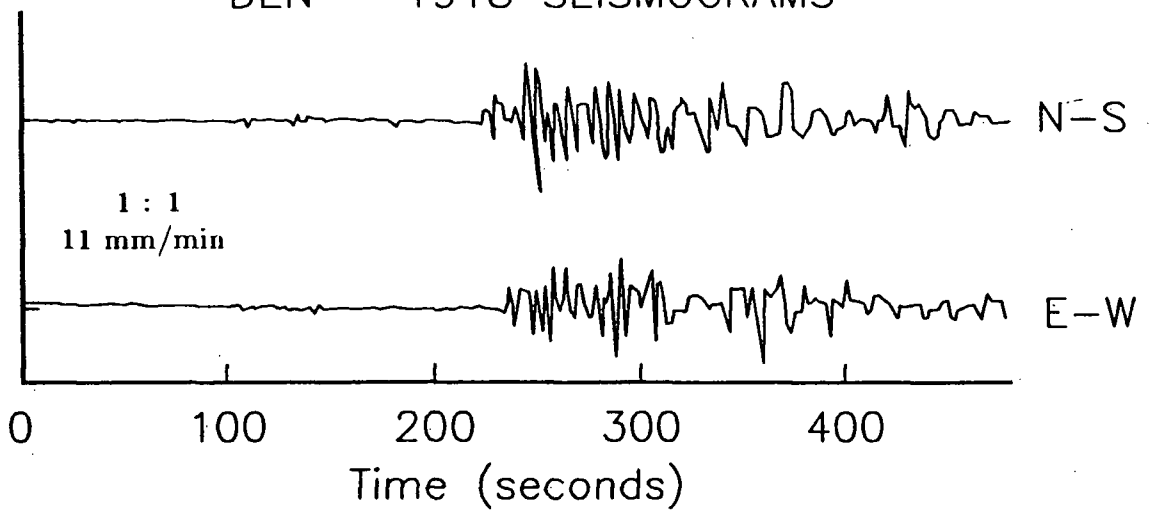
## MHC - 1918 SEISMOGRAMS

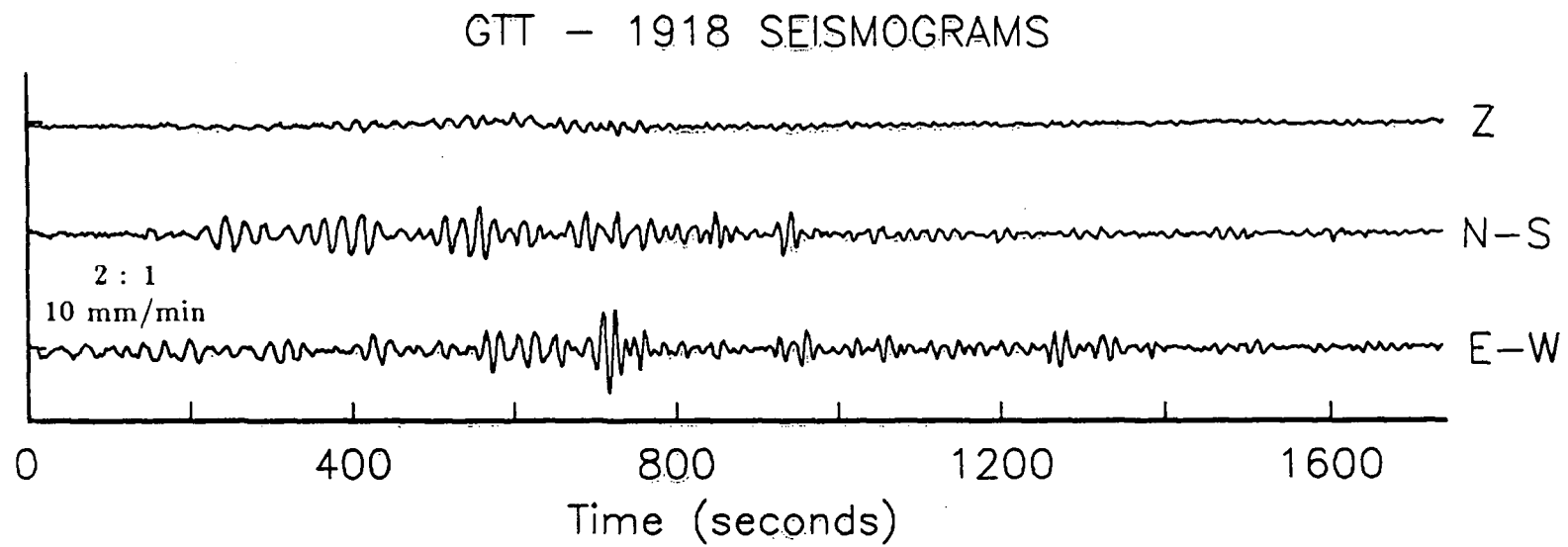
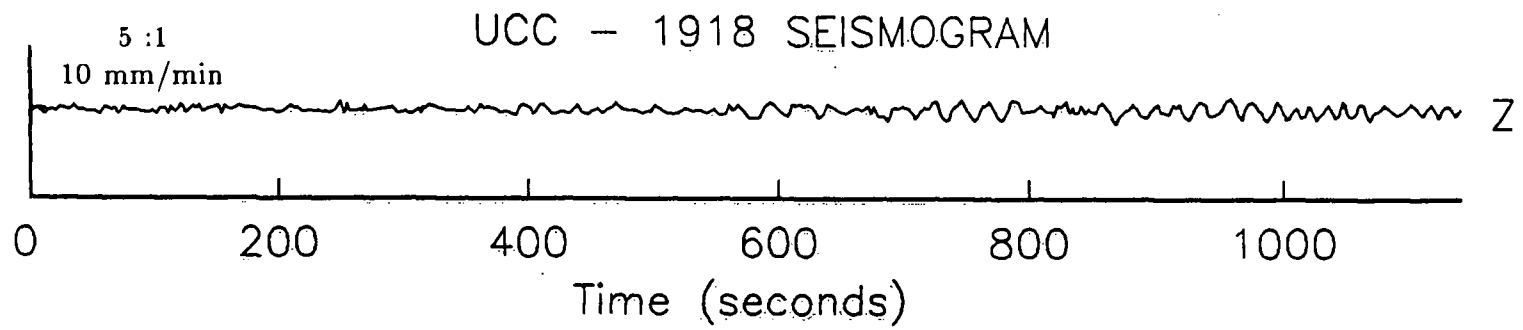


## CLH - 1918 SEISMOGRAMS

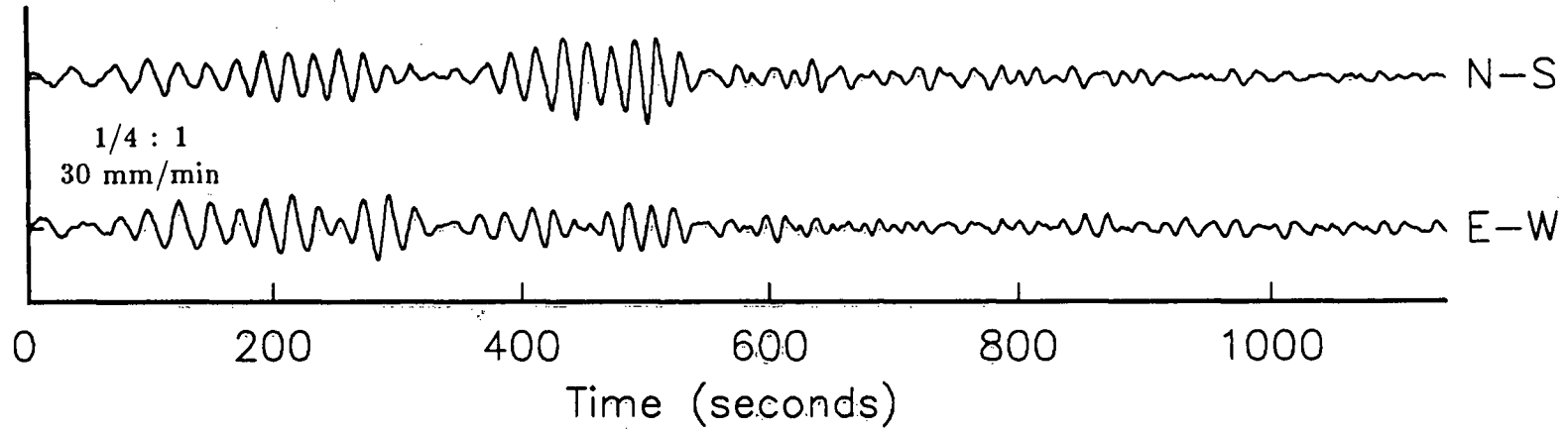


## DEN - 1918 SEISMOGRAMS

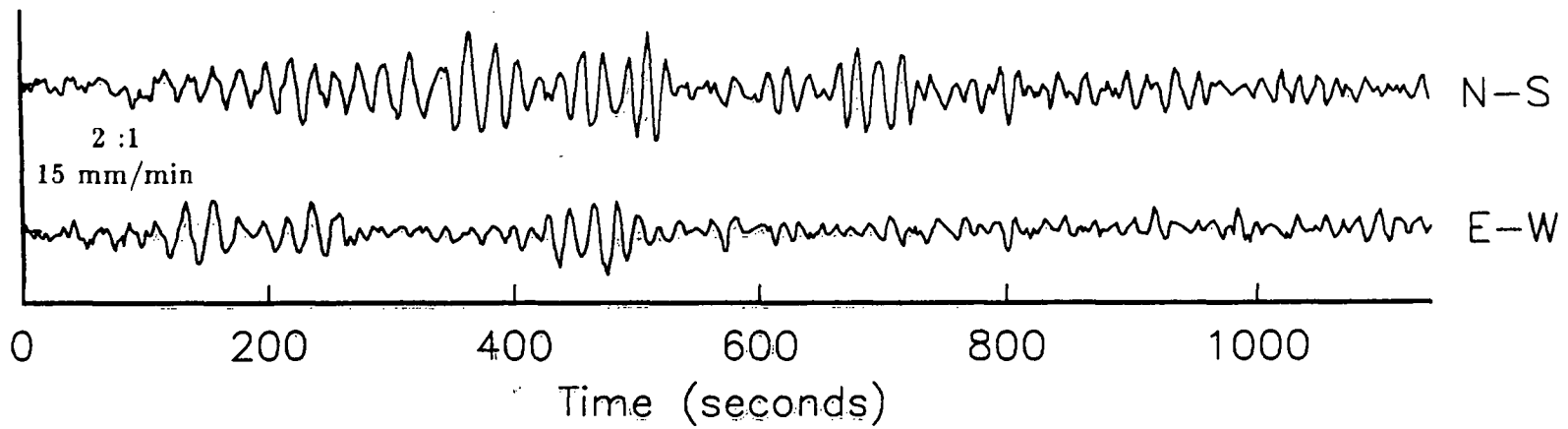




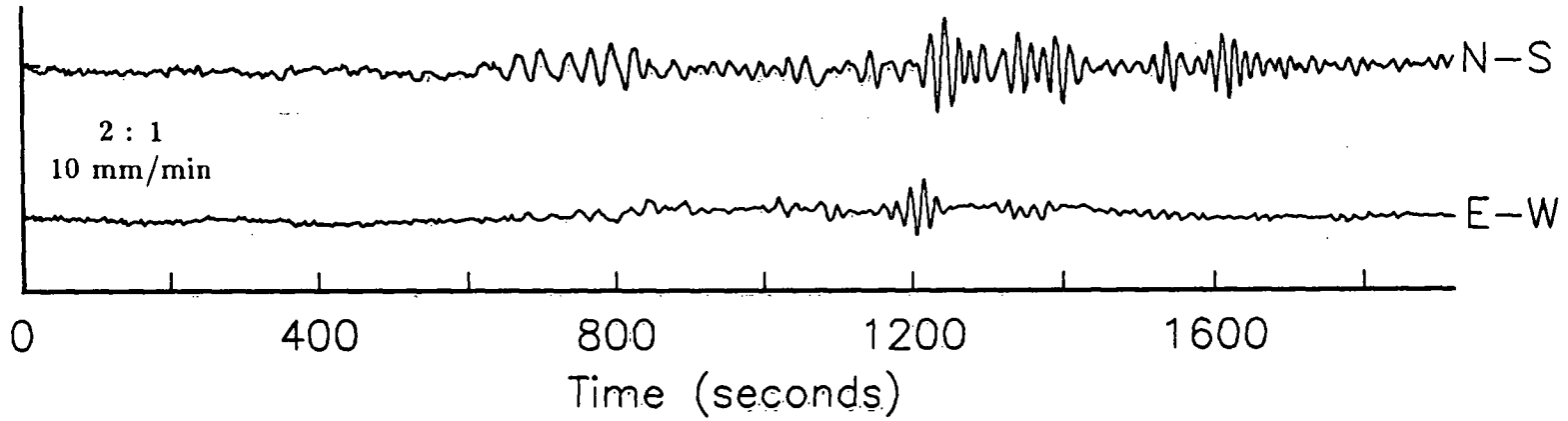
DBN - 1918 SEISMOGRAMS



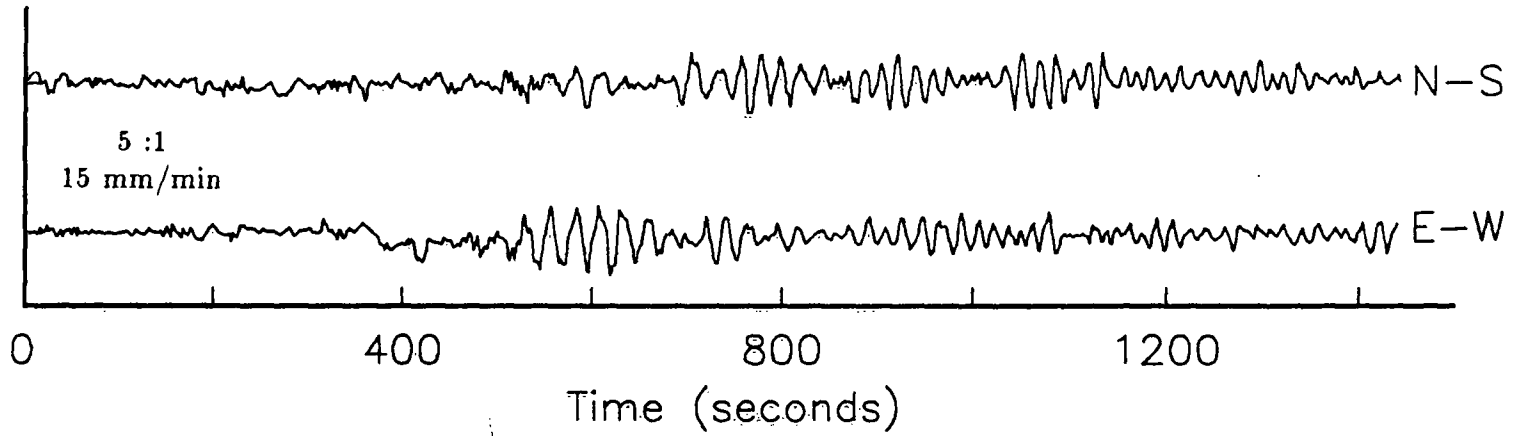
MNH - 1918 SEISMOGRAMS



LPZ - 1918 SEISMOGRAMS



UPP - 1918 SEISMOGRAMS



## 5. 1918 Surface Wave Radiation Patterns

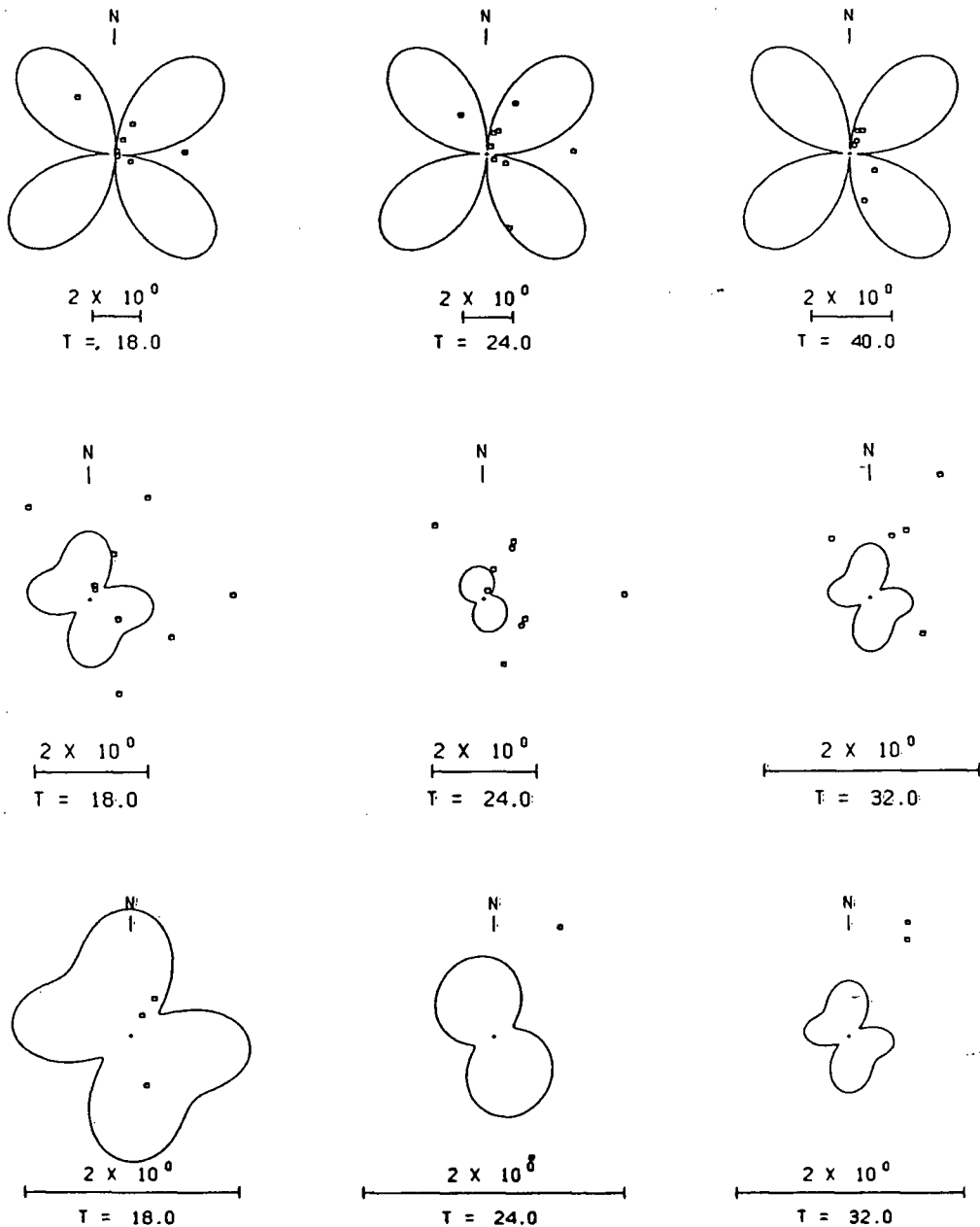


**Figure C.5.1** Theoretical radiation patterns (solid lines) of Love waves (top), horizontal Rayleigh waves (middle), and vertical Rayleigh waves (bottom) for the 1946 earthquake mechanism solution (see Figure 3). Each dot represents a spectral amplitude at a station for the 1918 earthquake. The azimuth of the dot represents the station azimuth, and the distance from the centre of the pattern is proportional to the spectral amplitude. The period, as well as a scale relating the plot size to units of dyne-cm is written below each plot.

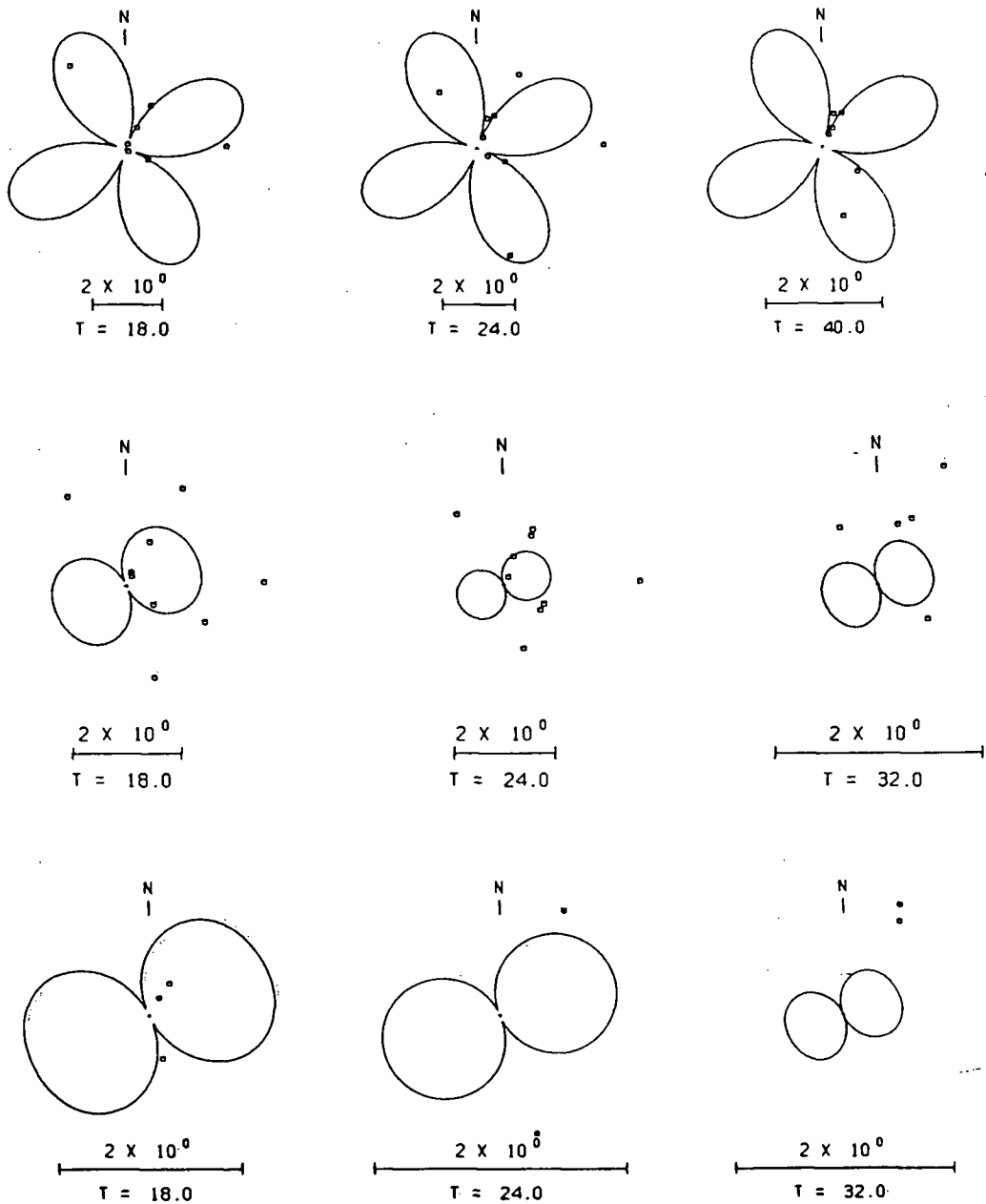


**Figure C.5.2** Theoretical radiation patterns (solid lines) of Love waves (top), horizontal Rayleigh waves (middle), and vertical Rayleigh waves (bottom) for the 1957 earthquake mechanism solution (see Figure 15). Each dot represents the spectral amplitude at a station for the 1918 earthquake. The azimuth of the dot represents the station azimuth, and the distance from the centre of the pattern is proportional to the spectral amplitude. The period, as well as a scale relating the plot size to units of dyne-cm is written below each plot.

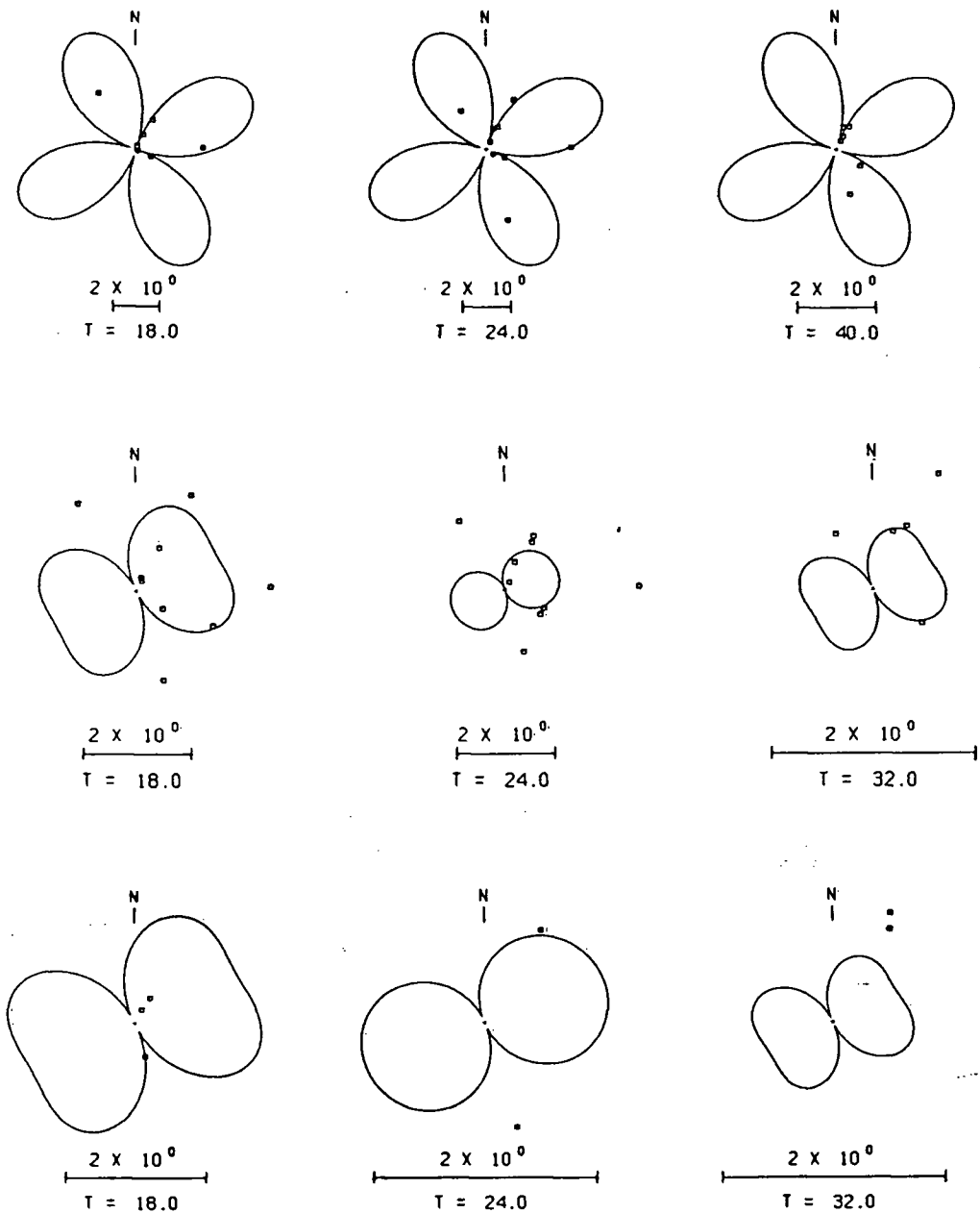


**Figure C.5.3** Theoretical radiation patterns (solid lines) of Love waves (top), horizontal Rayleigh waves (middle), and vertical Rayleigh waves (bottom) for the 1972 earthquake mechanism solution (see Figure 3). Each dot represents a spectral amplitude at a station for the 1918 earthquake. The azimuth of the dot represents the azimuth of the station, and the distance from the centre of the pattern is proportional to the spectral amplitude. The period, as well as a scale relating the plot size to units of dyne-cm is written below each plot.